Universidade Federal do Rio Grande – FURG

Instituto de Oceanografia

Programa de Pós-Graduação em Oceanologia

Ciclones Extratropicais no Sudoeste do Oceano Atlântico: Análise Temporal e Relações com Ondas de Calor Marinhas

Carina Klug Padilha Reinke

Tese apresentada ao Programa de Pós-Graduação em Oceanologia, como parte dos requisitos para a obtenção do Título de Doutor.

Orientador: *Prof. Dr.* Jeferson Prietsch Machado
Universidade Federal do Rio Grande (FURG), Brasil.

Co-orientadora: *Profa*. *Dra.* Regina Rodrigues Rodrigues
Universidade Federal de Santa Catarina (UFSC), Brasil.

Rio Grande, RS, Brasil

Outubro, 2024

Ciclones Extratropicais no Sudoeste do Oceano Atlântico: Análise Temporal e Relações com Ondas de Calor Marinhas

Tese apresentada ao Programa de Pós-Graduação em Oceanologia, como parte dos requisitos para a obtenção do Título de Doutor.

por

Carina Klug Padilha Reinke

Rio Grande, RS, Brasil

Outubro de 2024

© A cópia parcial e a citação de trechos desta tese são permitidas sobre a condição de que qualquer pessoa que a consulte reconheça os direitos autorais do autor. Nenhuma informação derivada direta ou indiretamente desta obra deve ser publicada sem o consentimento prévio e por escrito do autor.

Ficha Catalográfica

R372c Reinke, Carina Klug Padilha.
Ciclones extratropicais no sudoeste do Oceano Atlântico: análise temporal e relações com ondas de calor marinhas / Carina Klug Padilha Reinke. – 2024.
151 f.

Tese (doutorado) – Universidade Federal do Rio Grande – FURG, Programa de Pós-Graduação em Oceanologia, Rio Grande/RS, 2024.
Orientador: Dr. Jeferson Prietsch Machado.
Coorientadora: Dra. Regina Rodrigues Rodrigues.

1.Cciclones extratropicais 2. Ondas de calor marinhas 3. Tendência, 4. Variabilidade I. Machado, Jeferson Prietsch II. Rodrigues, Regina Rodrigues III. Título.

CDU 551.46

Catalogação na Fonte: Bibliotecário José Paulo dos Santos CRB 10/2344

UNIVERSIDADE FEDERAL DO RIO GRANDE - FURG
IO – INSTITUTO DE OCEANOGRAFIA
PROGRAMA DE PÓS-GRADUAÇÃO EM OCEANOLOGIA
E-mail: ccpofqg@furg.br – home-page: www.ppgo.furg.br

ATA ESPECIAL DE DEFESA DE TESE – 03/2024

Às nove horas e trinta minutos do dia vinte e nove de outubro do ano dois mil e vinte e quatro, por Video Conferência sala: https://conferenciaweb.rnp.br/conference/roons/jeferson-prietsch-machado/invite_userid, reuniu-se a Comissão Examinadora da Tese de **DOUTORADO** intitulada **"RELAÇÃO ENTRE CICLONES EXTRATROPICAIS E ONDAS DE CALOR MARINHAS NO SUDOESTE DO OCEANO ATLÂNTICO"**, da **Acad. Carina Klug Padilha Reinke**. A Comissão Examinadora foi composta pelos seguintes membros: Prof. Dr. Jeferson Prietsch Machado - Orientador – (IO/FURG); Prof. Dr. Ricardo de Camargo – (USP); Prof. Dr. Fabricio Sanguinetti Cruz de Oliveira – (IO/FURG), Prof. Dr. Mário Francisco Leal de Quadro – (IFSC) e Prof. Dr. Jorge Arigony Neto – (IO/FURG). Dando início à reunião, a Coordenadora do PPGO, Profa. Dra. Grasiela Lopes Leães Pinho, agradeceu a presença de todos e fez a apresentação da Comissão Examinadora. Logo após esclareceu que a candidata teria um tempo de 45 a 60 min para explanação do tema, e cada membro da Comissão Examinadora, um tempo máximo de 30 min para perguntas. A seguir, passou à palavra a candidata que apresentou o tema e respondeu às perguntas formuladas. Após ampla explanação, a Comissão Examinadora reuniu-se em reservado para discussão do conceito a ser atribuído a candidata. Foi estabelecido que as sugestões de todos os membros da Comissão Examinadora, que seguem em pareceres em anexo, foram aceitas pelo Orientador/Candidata para incorporação na versão final da Tese. Finalmente, a Comissão Examinadora considerou a candidata_APROVADA__, por maioria simples. Nada mais havendo a tratar, foi lavrada a presente ATA, por mim, Clabisnei Moura de Melo – Secretário PPGO, que após lida e aprovada, será assinada pela Comissão Examinadora, pela Candidata e pela Coordenadora do Programa de Pós-Graduacão em Oceanologia.

Documento assinado digitalmente
gov.br JEFERSON PRIETSCH MACHADO
Data: 29/10/2024 22:11:12-0300
Verifique em https://validar.iti.gov.br

Prof. Dr. Jeferson Prietsch Machado
Orientador

Prof. Dr. Ricardo de Camargo

Prof. Dr. Fabricio Sanguinetti Cruz de Oliveira

Prof. Dr. Mário Francisco Leal de Quadro

Documento assinado digitalmente
gov.br JORGE ARIGONY NETO
Data: 29/10/2024 20:13:38-0300
Verifique em https://validar.iti.gov.br

Prof. Dr. Jorge Arigony Neto

Acad. Carina Klug Padilha Reinke

Documento assinado digitalmente
gov.br GRASIELA LOPES LEAES PINHO
Data: 30/10/2024 11:23:56-0300
Verifique em https://validar.iti.gov.br

Profª. Drª Grasiela Lopes Leães Pinho
Coordenadora PPGO

Agradecimentos

Primeiramente agradeço a Deus, por me sustentar diariamente e me dar forças para concluir essa tese. Tudo o que sou hoje é por graça e bondade dEle.

Agradeço à minha família, Ricardo, Sofia, Alice e Ester, por todo o apoio nesta jornada, estando ao meu lado nos momentos fáceis e difíceis.

Agradeço a oportunidade de me afastar das atividades laborais do Centro de Pesquisas e Previsão Meteorológica da Universidade Federal de Pelotas (CPPMet/UFPel), com o objetivo de ter esse tempo de aprendizado. Essa condição me deu tranquilidade para aprofundar o conhecimento e concluir o meu trabalho com mais celeridade.

Agradeço ao Prof. Maurício que aceitou ser meu orientador, mesmo em um projeto desafiador, contribuindo com sua experiência nas atividades científicas. Agradeço ao Prof. Jeferson que aceitou me orientar na segunda metade do trabalho, muito obrigada pela confiança e pelo apoio.

Agradeço à banca de acompanhamento, Prof. Dr. José Luiz, Prof. Dr. Maurício Mata, Profa. Dra. Regina Rodrigues, que esteve presente principalmente me animando nas dificuldades relacionadas a publicação dos artigos.

Agradeço aos professores e colegas das disciplinas, que ajudaram a ampliar o meu conhecimento. Em especial, à Profa. Jaci pelo apoio nos artigos.

Agradeço ao Programa de Pós-Graduação em Oceanologia da FURG por perseguir a qualidade e as melhores experiências para o desenvolvimento de trabalhos pertinentes ao desenvolvimento da ciência no Brasil.

Índice

Agradecimentos.....iv

Lista de Figuras.....ix

Lista de Tabelas.....xii

Lista de Acrônimos, Abreviações e Símbolos.....xiii

Resumo.....xv

Abstract.....xvii

Capítulo I: Introdução.....19

1.1. Ciclones Extratropicais.....19

1.2. Evidências da Contribuição da Temperatura da Superfície do Mar para a Intensificação de Ciclones Extratropicais.....25

1.3. Ondas de Calor Marinhas.....26

1.4. Lacunas Científica.....29

1.5. Estrutura da Tese.....30

Capítulo II: Hipótese...31

Capítulo III: Objetivos.....32

3.1. Objetivo Geral.....32

3.2. Objetivos Específicos.....32

Capítulo IV: Dados e Métodos.....33

4.1. Dados.....33

4.1.1. Reanálise ERA5/ECMWF.....33

4.1.2. Análise de Alta Resolução NOAA OI SST V2.....34

4.1.3 Dados Auxiliares.....35

4.2. Área de Estudo.....35

4.3. Método de Identificação e Rastreamento de Ciclones Extratropicais.....37

4.4. Método de Identificação de MHW.....44

4.5. Métodos Estatísiticos.....46

Capítulo V: Algoritmo Objetivo para a Identificação e Rastreamento de Ciclones Extratropicais no Hemisfério Sul.....48

5.1. Introduction.....49

5.2. Material and Methods.....53

5.2.1. Data.....53

5.2.2. Methods.....54

5.2.2.1. Identifying Cyclones.....54

5.2.2.2. Tracking Cyclone Events.....56

5.2.2.3. Quantifying Cyclone Characteristics.....57

5.3. Results.....59

5.3.1. Sensitivity to the Smoothing Parameter for the Relative Vorticity Field.....59

5.3.2. Sensitivity to Threshold of Relative Vorticity.....61

5.3.3. Sensitivity to the Minimum Area of Relative Vorticity under the Threshold.....62

5.3.4. First Case Study: Extratropical Cyclone of 26–28 October 2016.....65

5.3.5. Second Case Study: Extratropical Cyclone of 15–17 August 2020.....67

5.3.6. Temporal Resolution.....68

5.3.7. Extratropical Cyclone Climatology.....72

5.4. Discussion and Conclusions.....74

Capítulo VI: Caracterização e Variabilidade de Ciclones Extratropicais no Sudoeste do Oceano Atlântico.....76

6.1. Introduction.....78

6.2. Data and Methods.....80

6.2.1. Data.....80

6.2.2. Methods.....81

6.3. Results and Discussion.....84

6.3.1. Spatial and Temporal Distribution.....84

6.3.2. Storm Characteristics.....86

6.3.3. Intense Events.....89

6.3.4. Interannual Variability.....91

6.3.5. Composite of Intense Events.....96

6.4. Summary and Conclusions.....99

Capítulo VII: Relação entre Ciclones e Ondas de Calor Marinhas.....104

7.1. Introduction.....105

7.2. Data and Methods.....108

7.2.1. Data.....108

7.2.2. Study Area.....109

6.2.3. Methods.....110
7.3. Results.....112
7.3.1. MHW characteristics in the Southwest Atlantic Ocean between 1982 and 2023.....112
7.3.2. Interannual Variability and Trends of MHW days per year in the Southwestern Atlantic Ocean.....116
7.3.3. Relationship between MHW and extratropical cyclones on the Southwestern Atlantic Ocean.....118
7.4. Conclusion.....120
Capítulo VIII: Síntese da Discussão.....122
Capítulo IX: Conclusões.....127
9.1. Perspectivas Futuras.....129
Referências Bibliográficas.....131

Lista de Figuras

Figura 1.1. Diagrama conceitual da estrutura dos ciclones extratropicais, (A) similar ao descrito por Bjerknes (1919) e (B) similar ao descrito por Shapiro e Keyser (1990), mas adaptado para o Hemisfério Sul.....21

Figura 1.2. Diagrama conceitual da estrutura vertical dos ciclones extratropicais no Hemisfério Norte (Fonte: Ahrens, 2001).....22

Figura 1.3. Áreas mais importantes para o estudo de MHWs (caixas cinzas) (a), intensidade (b), duração (c) e frequências de casos por ano (d) de MHW (Fonte: Holbrook et al., 2019).....27

Figura 1.4. Mecanismo de formação de MHWs, proposto por Rodrigues et al. (2019).....29

Figura 4.1. Área de estudo e batimetria (GEBCO), mostrando parte da América do Sul e do Oceano Atlântico Sudoeste.....37

Figura 4.2. Esquema explicativo da técnica de componentes conectados.....41

Figura 4.3. Exemplo de posições do centro de massa das áreas identificadas pela técnica de componentes conectados em uma sequência de horários.....42

Figura 4.4. Fluxograma das etapas do método de identificação, rastreio e caracterização de ciclones extratropicais desenvolvido no presente estudo.....43

Figure 5.1. Example of points center of mass of areas that match the relative vorticity threshold sequence of hourly data.....57

Figure 5.2. Mean sea level pressure and relative vorticity at 850 hPa under -10^{-4} s^{-1}, on 27 October 2016, 06 UTC. The green square is the “effective area” to search for the more intense characteristics of the cyclone.....58

Figure 5.3. Flowchart of the detection algorithm of extratropical cyclones proposed in this study.....59

Figure 5.4. Mean sea level pressure and relative vorticity at 850 hPa under -10^{-4} s^{-1}, on 1 July 2020, 12 UTC. (A) raw data and with different standard deviations of the Gaussian filter: (B) 0,5, (C) 1,0, and (D) 3,0.....60

Figure 5.5. Study of the features of cyclones for the three sensitivity tests of filter degree, computed from 2013 to 2022: (A) Frequency distribution of cyclone lifetime, (B) frequency distribution of cyclone mean speed and (C) time series of total annual number of extratropical cyclones.....61

Figure 5.6. Mean sea level pressure (contours) and relative vorticity at 850 hPa (shading) with thresholds of: (A) -10^{-5} s^{-1}; (B) $-0{,}5x10^{-4}$ s^{-1}; (C) -10^{-4} s^{-1} and (D) $-2x10^{-4}$ s^{-1}, on 1 July 2020, 12 UTC, using a Gaussian filter parameter of 0,5.....62

Figure 5.7. Mean Cyclone centers per month detected between 2013 and 2022, using a Gaussian filter parameter of 0,5, a threshold of relative vorticity of -10-4 s-1 and different sets of minimum area (number of pixels).....63

Figure 5.8. Study of the features of cyclones for four sensitivity tests of area criterion, computed between 2013 and 2022: (A) Frequency distribution of cyclone lifecycle, (B) frequency distribution of cyclone mean speed and (C) time series of total annual number of extratropical cyclones. 64

Figure 5.9. Extratropical cyclone during 26 to 28 October 2016.....66

Figure 5.10. Extratropical cyclone of 15 to 17 August 2020.....68

Figure 5.11. Study of the features of cyclones in the Southern Hemisphere using 1-hourly (blue) and 6-hourly (orange) temporal resolutions, for the period of 1982–2021.....70

Figure 5.12. Violin plot of extratropical cyclones tracking in the Southern Hemisphere using 1-hourly (blue) and 6-hourly (orange) temporal resolutions, for the period of 1982–2022….....71

Figure 5.13. The average number of cyclogenesis per month in the Southern Hemisphere, with a cap area of 10^6 km^2.....73

Figure 6.1. Study area showing the Southern Atlantic Ocean and part of South America.....83

Figure 6.2. Spatial distribution of Southwest Atlantic cyclogenesis per season for (A) winter (JJA), (B) spring (SON), (C) summer (DJF) and (D) autumn (MAM). The density unit is events per area, with a unit area of spherical cap of 10^6 km^2.....85

Figure 6.3. Spatial distribution of Southwest Atlantic on the position where relative vorticity on 850 hPa reach their more intense values per season for (A) winter (JJA), (B) spring (SON), (C) summer (DJF) and (D) autumn (MAM). The density unit is events per area, with a unit area of spherical cap of 10^6 km^2…….....86

Figure 6.4. Frequency distribution of (A) duration (days), (B) mean velocity (km/h), (C) minimum sea level pressure (hPa) and (D) maximum 10-meter winds (km/h) for each extratropical cyclone in the Southwest Atlantic Ocean…….....88

Figure 6.5. Tracks of intense events in the Southwest Atlantic Ocean based on: (A) sea level pressure below 966 hPa, (B) 10-meter wind above 84 km/h, (C) mean velocity above 78 km/h. The panel (D) shows intense events based on the three criteria, while the panel (E) shows intense events based on the criteria (A) and (B). Finally, the panel (F) is similar to (E), but for events generated just on the purple box…….....90

Figure 6.6. Positions where the extratropical cyclones of Southwest Atlantic Ocean reach the higher intensity.....91

Figure 6.7. Annual count of extratropical cyclones (blue), and respective linear regression (red) and cubic polynomial regression (purple). The upper panel shows the results for the Southwest Atlantic Ocean while the middle (lower) panel shows the same for the northern (southern) part of the whole area.....93

Figure 6.8. Annual count of intense extratropical cyclones in the Southwestern Atlantic Ocean based in minimum sea level pressure below 966 hPa (blue), maximum 10-meter winds above 84 km/h (red) and faster events (velocity greater than 78 km/h, purple) criteria.....94

Figure 6.9. The left (right) column shows the annual count of extratropical cyclones in blue, and respective linear regression in purple for the northern (southern) part of the study area. From top to bottom the results are presented for winter, spring, summer and autumn seasons.....95

Figure 6.10. Normalized power spectrum of extratropical cyclones count (blue) with 20 realizations, red-noise fit (red) and F-test confidence level of 95% (orange) and 99% (purple) for northern (left column) and southern (right column) parts of the study area.....97

Figure 6.11. Composites of the 14 intense events of Table 3 on 24 hours before (A, E, I and M), 12 hours before (B, F, J and N), the time (C, G, K and O) and 12 hours after (D, H, L and P) the cyclogenesis.....100

Figure 6.12. Composites of the 9 winter intense events of Table 3 on 24 hours before (A, E, I and M), 12 hours before (B, F, J and N), the time (C, G, K and O) and 12 hours after (D, H, L and P) the cyclogenesis.....101

Figure 7.1. Bathymetry map of the Southwestern Atlantic Ocean (GEBCO bathymetry dataset - www.gebco.net).....110

Figure 7.2. Spatial distribution of mean Southwestern Atlantic Ocean SST (°C) (A, C and E) and SST trends (°C/decade) (B, D and F) from 1982 to 2023 over the whole study period (A and B), winter (December, January and February) (C and D), and summer (June, July and August) (E and F).....114

Figure 7.3. Spatial distribution of mean Southwestern Atlantic Ocean MHWs characteristics between from 1982 to 2023: (A) frequency (events/year), (B) number of day with MHW (days/year), (C) mean intensity (°C), (D) maximum intensity (°C) and cumulative intensity (°C.day).....115

Figure 7.4. temporal evolution and trend of days with MHW per year in the whole study area between 1982 and 2023. In grey the year of the longest MHW, in red (yellow) the year of the event with the high maximum (mean) intensity.....117

Figure 7.5. Map of trend of days with MHW first period (A) and second period (B). Maps of trend of days with strong, severe and extreme MHW in the first period (C) and in the second period (D).....117

Figure 7.6. Correlation map of (A) days with cyclone and days with MHW in the study area and (B) last day of MHW and cyclone events, (C) days with intense MHW and cyclone and (D) last day of intense MHW and cyclone events.....118

Figure 7.7. Sea surface temperature anomaly (°C) during the first day of the 14 more intense events near coast of South Region of Brazil and Uruguay (purple box), selected by the study of Padilha Reinke et al. (2024). The greenlines are the tracks of these extratropical cyclones.....119

Lista de Tabelas

Tabela 4.1. Limite de intensidade máxima que categoriza localmente o evento de MHW.....45

Table 5.1. Relevant extratropical cyclone detecting and tracking methods.....51

Table 5.2. Statistics information of lifetime and mean speed of detected cyclones using different minimum area tests…….....64

Table 6.1. Statistical characteristics of extratropical cyclones in the Southwest Atlantic Ocean (red box of Figure 1).....89

Table 6.2. Slope of the linear trends in the 1982–2022 period, p-value according to the Mann–Kendal test and coefficient of determination (R^2) of extratropical cyclones of total, northern and southern parts of the study area.....92

Table 6.3. Extratropical cyclone events that reach the intense threshold of mean sea level pressure and 10-meter winds and with cyclogenesis under the coastal area (purple box of Figure 1)…….....98

Table 7.1. Threshold created by Hobday et al. (2018) to categorize a local event based on the long-term climatology…….....111

Lista de Acrônimos e Abreviações

A

AMO – Oscilação Multidecadal do Atlântico (*Atlantic Multidecadal Oscillation*).

AVHRR – *Advanced Very High-Resolution Radiometer imager*.

C

CCL – técnica de componentes conectados (*connected-component labeling technique*).

CM_a – centro de área da área que obedece o limite estabelecido.

CMIP6 – Projeto de Intercomparação de Modelos Acoplados Fase 6 (Coupled Model Intercomparison Project Phase 6).

E

ECMWF – Centro Europeu de Previsão do Tempo em Médio Prazo (*European Centre for Medium-Range Weather Forecasts*).

ENSO – El Niño Oscilação Sul (El-Nino South Oscillation).

ERA5 – Reanálise do Centro Europeu de Previsão de Tempo em Médio Prazo (*European Centre for Medium-Range Weather Forecasts Re-analysis 5*).

ERA-interim – Reanálise Interim do Centro Europeu de Previsão de Tempo em Médio Prazo (*European Centre for Medium-Range Weather Forecasts Interim Re-analysis*).

G

G(x,y) – filtro gaussiano na distância x,y até o ponto a ser suavizado.

GEBCO – modelo global de mapeamento da batimetria dos oceanos (*General Bathymetric Chart of the Oceans*).

I

I_{max} – intensidade máxima de uma MHW.

IMILAST – Projeto de Intercomparação de Diagnóstico de Tempestades de Latitude Média (*Intercomparison of Mid Latitude Storm Diagnostic Project).*

INMET – Instituto Nacional de Meteorologia (Brasil).

IPCC – Painel Intergovernamental em Mudanças Climáticas (*Intergovernmental Panel on Climate Change).*

M

MAL-JAPA – modelo regional da Agência Meteorológica do Japão (*Limited-area model-Japan Meteorological Agency*).

MHW – onda de calor marinha (Marine Heatwave).

N

NCEP/NCAR reanalysis – reanálise atmosférica do *National Centers for Environmental Prediction* e do *National Center for Atmospheric Research*.

NIIRS – *Visible Infrared Imaging Radiometer Suite*.

R

R^2 – coeficiente de determinação (*coefficient of determination*).

Rc – coeficiente de correlação.

RegCM4 – Modelo Climático Regional (*Regional Climate Model version 4*).

RN – ruído vermelho (red noise).

S

SAM – Modo Anular do Sul (*Southern Annular Mode*).

SST – temperatura da superfície do mar (sea surface temperature).

ζ_z – vorticidade relativa na direção vertical.

σ – desvio padrão.

T

TSM – temperatura de superfície do mar.

U

UOHC – conteúdo de calor do oceano superior (*Upper Ocean Heat Content*).

Resumo

Os ciclones extratropicais são responsáveis por precipitações intensas, ventos fortes e condições adversas em regiões costeiras, podendo também trazer perigo à navegação em latitudes médias. Seus impactos econômicos e sociais motivam a pesquisa sobre sua estrutura, climatologia e alterações ao longo dos anos. Em um ambiente de elevação da temperatura da superfície do mar (TSM), estudos indicam que os processos de troca na interface oceano-atmosfera podem ser alterados, modificando os fluxos de calor e influenciando na intensidade e na frequência de ciclones extratropicais localmente. Análises de eventos específicos confirmam que a TSM elevada pode intensificar ciclones extratropicais, pré-condicionando o ambiente para o seu desenvolvimento mais intenso. Além disso, as ondas de calor marinhas (MHW), que são prolongados períodos de TSM anomalamente elevada, tem sido relacionada a condições atmosféricas predominantes, principalmente a bloqueios atmosféricos. Esse trabalho analisa a tendência e variabilidade de ocorrência de ciclones extratropicais e as características e tendências de ocorrência de MHWs, estabelecendo uma relação estatística entre ambos, para compreender o papel das MHWs no desenvolvimento e intensificação de ciclones extratropicais. Para a compreensão da tendência e variabilidade dos ciclones extratropicais foi disponibilizado um programa de identificação e rastreamento de ciclones extratropicais, a partir da vorticidade relativa em 850 hPa, identificando os ciclones como áreas com valores abaixo do limite estabelecido. Pela análise da variabilidade, picos de energia em períodos de 2 a 3 anos, 5 anos, 8 e 10 anos foram encontrados. Com relação às características das MHWs no Sudoeste do Oceano Atlântico, foi encontrada uma área de eventos mais intensos e prolongados entre 37,5°S e 45°S de latitude e 50°W e 55°W de longitude, que pode estar relacionada com o deslocamento da Confluência Brasil-Malvinas. Além disso, a identificação do número de dias com MHWs por ano na área mostrou aumento, especialmente nos últimos 21 anos. Apenas 30% dos eventos de MHWs no Sudoeste do Oceano Atlântico terminaram com ciclones extratropicais e a relação entre os dias com MHW e dias com ciclone extratropical foi fraca nos 42 anos de estudo. Por outro lado, observando a TSM

durante o desenvolvimento dos eventos mais intensos de ciclones extratropicais da costa do sul do Brasil e Uruguai, a influência da TSM anomalamente elevada mostrou-se desnecessária para a intensificação, embora casos isolados podem ter uma contribuição mais significativa da TSM extrema para o seu desenvolvimento.

Palavras-Chave: ciclones extratropicais, ondas de calor marinhas, tendência, variabilidade.

Abstract

Extratropical cyclones are responsible for intense precipitation, strong winds and adverse conditions for coastal regions and navigation in mid-latitudes. Their economic and social impacts motivate research into their structure, climatology and change over the years. In an environment of rising sea surface temperature (SST), studies indicate that air-sea exchange processes may be altered, modifying heat fluxes and influencing the intensity and frequency of extratropical cyclones in various regions. Analyses of specific events confirm that high SST can intensify extratropical cyclones by pre-conditioning the environment for their more intense development. Additionally, marine heatwaves (MHWs), which are prolonged periods of anomalously high SST, have been linked to prevailing atmospheric conditions, particularly atmospheric blocking. This work analyzes the trends and variability of extratropical cyclone occurrence and the characteristics and trends of MHWs, establishing a statistical relationship between them to understand the role of MHWs in the development and intensification of extratropical cyclones. To understand the trends and variability of extratropical cyclones, a program for identifying and tracking extratropical cyclones based on relative vorticity at 850 hPa was implemented, identifying cyclones as areas with values below the established threshold. Analysis revealed energy peaks at periods of 2 to 3, 5, 8 and 10 years. Regarding the characteristics of MHWs in the southwestern Atlantic Ocean, an area with more intense and prolonged events was found between 37.5°S and 45°S latitude and 50°W and 55°W longitude, which may be related to the displacement of the Brazil-Malvinas Confluence. Additionally, the number of days with MHWs per year in the area showed an increase, especially in the past 21 years. Only 30% of MHW events in the southwestern Atlantic ended with extratropical cyclones and the relationship between MHW days and extratropical cyclone days was weak over 42 years of study. On the other hand, observing the SST during the development of the most intense extratropical cyclones events in the coastal area, the influence of the SST has been unnecessary to the intensification, although isolated cases

may have a greater contribution from anomalously high SST to their development.

Keywords: extratropical cyclones, marine heatwaves, trends, variability.

Capítulo I: Introdução

A variação na intensidade e na frequência dos ciclones extratropicais em áreas próximas à costa, especialmente em relação a condições de temperatura da superfície do mar acima da média, tem sido amplamente estudada nos últimos anos. A seguir, apresenta-se um resumo do conhecimento sobre ciclones extratropicais, o impacto das mudanças na temperatura da superfície do mar sobre sua dinâmica e o estado atual das pesquisas sobre ondas de calor marinhas, até a finalização deste trabalho. Por fim, são destacadas as lacunas científicas que este trabalho pretende abordar.

1.1. Ciclones Extratropicais

Ciclones extratropicais são sistemas meteorológicos migratórios de escala sinótica, com extensão horizontal geralmente entre 500 km e 2500 km e ventos horizontais que circulam na mesma direção da componente vertical local da rotação planetária [Haskim, 2015]. No Hemisfério Sul, a rotação ocorre no sentido horário, enquanto no Hemisfério Norte é no sentido anti-horário. Na vertical, os ciclones extratropicais podem, em alguns casos, abranger toda a troposfera, desde a superfície e até aproximadamente 10 km. Esses sistemas migratórios se formam a partir da interação e convergência entre uma massa de ar mais quente, originária das regiões tropicais, e uma massa de ar frio,

proveniente das regiões polares, juntamente com outros fatores atmosféricos [Bluestein, 1993].

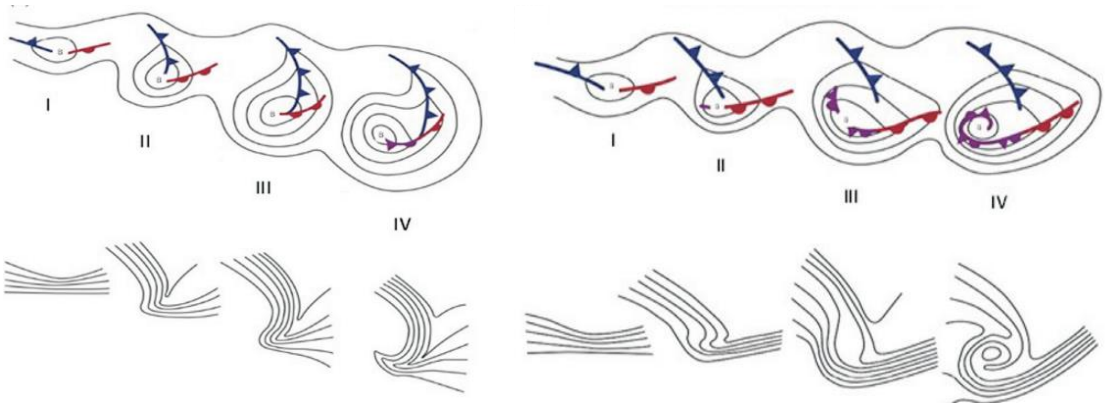
Grande parte das mudanças nas condições de tempo em latitudes médias está relacionada à ocorrência de ciclones extratropicais. Com o deslocamento e atuação desses sistemas meteorológicos a condição do tempo muda localmente, podendo ocorrer precipitação intensa, ventos fortes, além de episódios de neve, enchentes e marés de tempestade. Em alto mar, os ciclones extratropicais comumente causam condições severas, tornando a navegação perigosa na sua vizinhança. As mudanças das condições de tempo promovidas por esses importantes sistemas meteorológicos são responsáveis por grandes impactos sociais e econômicos, motivando várias pesquisas sobre a sua estrutura, climatologia e alterações esperadas em um ambiente de mudança climática [Shimkus et al, 2017; Catto et al, 2019].

Uma característica importante destes sistemas meteorológicos é a pressão mais baixa em seu centro, se comparado ao seu entorno e também os movimentos ascendentes no seu centro. Por serem zonas de maior gradiente de temperatura, pressão e umidade, estão associados a ventos moderados a fortes, muitas vezes persistentes, e precipitação intensa [Carlson, 1991]. O ar frio e mais denso tende a se direcionar para o centro do ciclone extratropical, criando um núcleo frio [Bluestein, 1993].

No aspecto global, os ciclones extratropicais desempenham um papel crucial no sistema climático do planeta, regulando os contrastes de temperatura entre o Equador e os Polos, estabilizando a estratificação da densidade e contribuindo na manutenção dos ventos de oeste em latitudes médias, contra o atrito com a superfície [Harvey, 1976; Peixoto e Oort, 1992].

A primeira descrição teórica da estrutura e evolução dos ciclones extratropicais foi realizada por Bjerknes [1919], com dados de várias localidades da Europa. O estudo descreveu as mudanças na pressão, na temperatura do ar e nos ventos em superfície, além de esquematizar a nebulosidade, precipitação e conceitos como frente fria e frente quente, importantes para a compreensão dos ciclones extratropicais.

Em trabalho subsequente de Bjerknes e Soldberg [1922], foi apresentada uma descrição do ciclo de vida de um ciclone extratropical. Assim, verificou-se que os ciclones passam pelos estágios de formação, intensificação e decaimento, até a sua dissipação. No estágio de formação, uma pequena ondulação ocorre na fronteira entre duas massas de ar distintas em superfície (frente), ocasionando um reajustamento no campo de pressão, em formato circular. Ao longo do estágio de desenvolvimento do ciclone, a fronteira onde a massa de ar frio desloca-se em direção à mais quente (frente fria) é mais veloz do que na fronteira em que a massa de ar quente atinge a área mais fria (frente quente), contribuindo para a aproximação das duas frentes. No estágio de dissipação, a diferença de temperatura entre as massas de ar em superfície não está mais presente, já que o ar mais quente se eleva (frente oclusa). A figura 1.1A mostra um diagrama conceitual similar ao apresentado no estudo de Bjerknes, porém adaptado para o Hemisfério Sul [Schultz et al.,1998; Reboita 2017].



(A) (B)

Figura 1.1. Diagrama conceitual da estrutura dos ciclones extratropicais, (A) similar ao descrito por Bjerknes (1919) e (B) similar ao descrito por Shapiro e Keyser (1990), mas adaptado para o Hemisfério Sul. As linhas cinzas na parte superior representam a altura geopotencial em 850 hPa, linhas azuis as frentes frias, linhas vermelhas as frentes quentes e linhas roxas as frentes oclusas. As linhas cinzas na parte inferior representam a temperatura potencial em 850 hPa (Fonte: Reboita, 2017, adaptado de Schultz et al., 1998).

A descrição apresentada por esse estudo inicial é válida até hoje, no entanto novos dados observacionais e desenvolvimentos teóricos têm expandido e enriquecido o conceito de ciclones extratropicais. Incorporou-se o conhecimento da estrutura vertical dos ciclones extratropicais ao diagrama conceitual inicial de Bjerknes, a partir de dados de balões meteorológicos [Pálmen, 1931], radiossondas [Bjerknes and Holmboe, 1944] e posteriormente

dados de satélites meteorológicos e radares. A Figura 1.2 resume algumas características desses sistemas meteorológicos em altitude [Ahrens, 2001]. A ondulação do escoamento de oeste em altos níveis da troposfera gera áreas propícias à convergência de massa e à divergência de massa, como mostra a parte superior da Figura 1.2. Como o ciclone extratropical está associado a convergência de ar em superfície e ar ascendente no seu centro (setas vermelhas na Figura 1.2), a região de divergência de ar em altitude deve estar alinhada com o centro de baixa pressão em superfície, para que o ciclone extratropical se intensifique. Assim, a região de baixo geopotencial em altitude (cavado) deve estar à oeste do ciclone em superfície. Na Figura 1.2, o cavado em altitude é representado pela letra L. Outro fator responsável pela intensificação de ciclones extratropicais é o jato em altos níveis da troposfera. O jato, que pode ser chamado de jato subtropical ou polar, dependendo da sua localização, é caracterizado por ventos intensos, comparado ao escoamento do seu entorno. Essa variação de intensidade do escoamento gera regiões propícias à convergência e divergência de massa em altitude em sua proximidade, influenciando a intensificação ou dissipação dos sistemas meteorológicos instáveis em superfície.

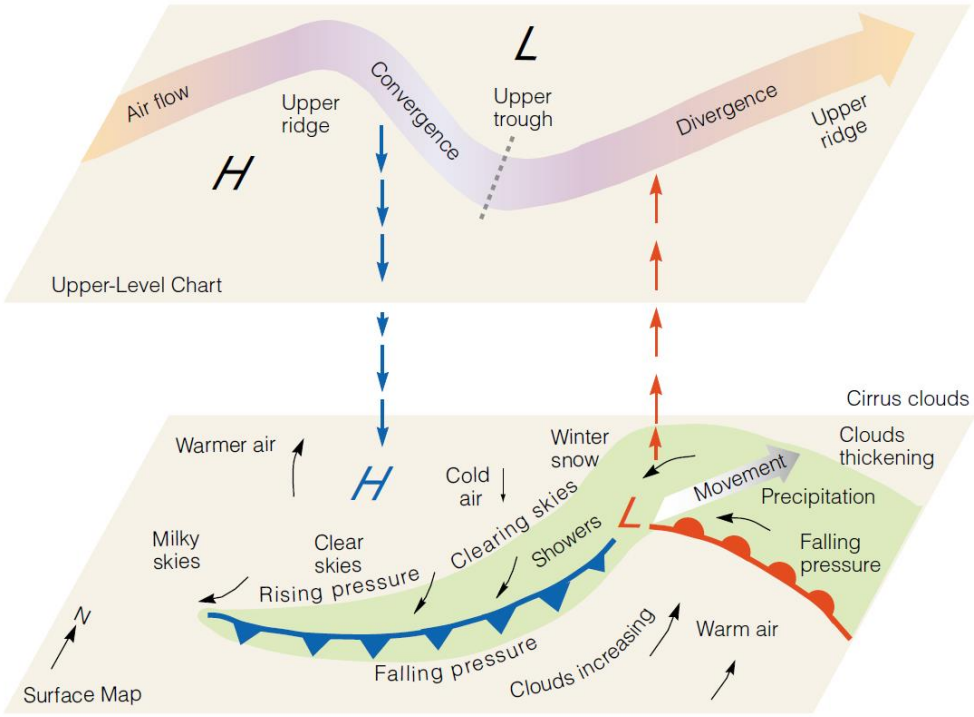


Figura 1.2. Diagrama conceitual da estrutura vertical dos ciclones extratropicais no Hemisfério Norte (Fonte: Ahrens, 2001). A parte superior da figura representa o escoamento em altos níveis

da troposfera; as setas em vermelho representam ar ascendente e em azul, ar descendente. A parte inferior da figura representa as condições nos baixos níveis da troposfera, em termos de condição do tempo, frentes fria (em azul) e quente (em vermelho); setas pretas representam a direção dos ventos em baixos níveis da troposfera em cada parte do ciclone extratropical.

Novas descobertas e um novo modelo conceitual foram propostos por Shapiro e Keyser [1990], que observaram que em muitos ciclones, principalmente aqueles chamados de explosivos, ocorre uma ruptura na frente fria, em vez de uma oclusão englobando a frente fria e a frente quente (Figura 1.1B). Em síntese, este trabalho demonstrou que um único modelo conceitual não inclui todo o espectro de estrutura e evolução dos ciclones extratropicais, indicando que ainda há muito a ser investigado [Dacre, 2020].

Nas últimas décadas, muitos estudos foram desenvolvidos para entender as regiões preferenciais de formação e atuação de ciclones extratropicais, tanto em uma abordagem para o hemisfério como em uma perspectiva local. Segundo Simmond e Keay [2000], a disposição espacial e temporal de ciclones é influenciada pela distribuição de continente e oceano, pelo gradiente de temperatura da superfície do mar e pelo posicionamento em relação às zonas baroclínicas. Diante do grande aumento do volume de dados, em resolução espacial e temporal cada vez maior, surgiu-se a necessidade de se aplicar métodos automáticos de identificação e rastreamento de ciclones, utilizando dados de reanálise ou modelos globais [Andrade et al., 2024]. Assim, realizaram-se vários estudos a partir de diferentes variáveis, conjunto de dados e metodologias. Para compreender o quanto a mudança da metodologia pode influenciar os resultados, várias instituições criaram o projeto de intercomparação chamado *Intercomparison of Mid Latitude Storm Diagnostic Project* (IMILAST) [Neu et al., 2013]. Utilizando o mesmo produto de reanálise (*European Centre for Medium-Range Weather Forecasts Interim Re-analysis* – ERA-interim), em uma resolução temporal de 6 horas, entre os mesmos anos (1989-2009), eles concluíram que a definição do algoritmo aplicado modifica a contagem, o tempo de vida e a intensidade dos ciclones. No entanto, ciclones profundos e mais longevos são consistentes ao longo das metodologias e existe congruência sobre a variabilidade e distribuição espacial dos ciclones, utilizando diferentes algoritmos.

Para o sudoeste do Oceano Atlântico, vários estudos comprovam uma significativa atividade ciclogenética, principalmente próximo à costa da América do Sul [Bitencourt et al., 2011; Reboita et al., 2012; Hoskins e Hodges, 2005; Gan e Rao, 1991]. Gramcianinov et al. [2019] verificaram que, no verão e nas áreas a norte de 35°S, as forçantes de baixos níveis são mais importantes para o processo de ciclogênese, principalmente devido ao transporte de umidade. Já no inverno, as forçantes em altos níveis da troposfera são mais importantes, por meio de instabilidades baroclínicas. Para os ciclones nas áreas a sul de 35°S, as forçantes em altos níveis são mais relevantes, em todas as épocas do ano.

Estudos recentes têm analisado a resposta dos ciclones extratropicais a um ambiente mais quente, com o objetivo de antecipar futuras mudanças de intensidade e áreas de atuação diante do aquecimento global. Como ciclones se desenvolvem em ambientes de instabilidade baroclínica, seu processo de formação é afetado pelo gradiente de temperatura entre o Equador e o Polo, como também pelo gradiente vertical de temperatura potencial, o que torna as mudanças destas variáveis cruciais para a determinação da frequência e intensidade dos ciclones extratropicais e o transporte de energia promovido por esses sistemas meteorológicos migratórios [Shaw et al., 2016]. Segundo Sinclair et al. [2020], em geral o ciclo de vida dos ciclones não é modificado por um ambiente mais quente, no entanto a quantidade de eventos por ano sofre um decréscimo de 3,3%. De acordo com Catto et al. [2019], o decréscimo na frequência de ciclones extratropicais projetada para o futuro pode estar relacionado a mudanças da baroclinia e a um deslocamento para os Polos do jato polar em altos níveis da troposfera. O relatório do Painel Intergovernamental sobre Mudanças Climáticas (*Intergovernmental Panel on Climate Change*) [IPCC, 2023] explica que ainda existe uma grande incerteza nas projeções de frequência e regiões preferenciais de formação de ciclones. No Oceano Atlântico Sudoeste, Reboita et al. [2018; 2020] encontraram uma diminuição na frequência de ciclones extratropicais, em simulações para o final do século.

1.2. Evidências da Contribuição da Temperatura da Superfície do Mar para a Intensificação de Ciclones Extratropicais

À medida que uma massa de ar se desloca do continente em direção ao oceano, a interação com a superfície gera processos de troca entre a atmosfera e o oceano. A magnitude da retirada de calor do oceano é fortemente dependente da temperatura e da umidade da massa de ar na camada mais próxima da superfície. Em ciclones extratropicais, mais de uma massa de ar com diferentes características chega até a área, produzindo uma variação importante no fluxo de calor sensível e latente em superfície [Wells, 2011]. Em um oceano com temperatura superficial mais elevada, os fluxos de calor podem ser intensificados, embora a quantificação das mudanças nestes processos seja um desafio ainda pouco explorado pela ciência [Sinclair et al., 2020]. Além disso, o fluxo de calor entre a atmosfera e o oceano pode apresentar mudanças bruscas em áreas de frentes oceânicas, as quais apresentam significativo gradiente de fluxo de calor, devido a temperatura do oceano superficial também apresentar um contraste horizontal intenso nestas áreas [Cronin et al., 2019].

Tentando compreender o papel dos processos de interação oceano-atmosfera para ciclones extratropicais, vários estudos de modelagem numérica foram desenvolvidos. Por exemplo, Dal Piva et al. [2008] estudaram o papel dos fluxos de calor latente e sensível em superfície associado a um caso de ciclogênese, cujo desenvolvimento foi rápido e intenso, na costa leste da América do Sul. Utilizando o modelo regional do Japão, chamado *Limited-area model-Japan Meteorological Agency* (MAL-JAPA), concluiu-se que os fluxos na interface ar-mar tiveram o papel de pré-condicionar o ambiente, tornando-o favorável ao desenvolvimento mais intenso do ciclone extratropical. Sutil et al. [2019] também buscaram analisar a interação ar-mar durante a ocorrência de um evento de ciclone extratropical no Oceano Atlântico sudoeste e tiveram resultados melhores com o modelo acoplado, mostrando maior habilidade para simular a intensidade e trajetória do ciclone com informações da TSM. Focando na evolução de perturbações ciclônicas em altos níveis da atmosfera na América do Sul subtropical, Vera et al. [2002] sugeriram que a presença de águas quentes da corrente do Brasil provê umidade e calor, reduzindo a estabilidade estática

em baixos níveis da atmosfera e assim contribuindo para a ciclogênese no oceano.

Outro exemplo muito importante foi o ciclone denominado *Catarina*, que atingiu a costa do sul do Brasil em março de 2004, que causou efeitos devastadores em áreas de Santa Catarina e Rio Grande do Sul. Esse evento merece destaque em relação à importância de incluir os processos oceânicos no prognóstico de ciclones [Glitzenhirn, 2015; Pezzi et al., 2016]. Conforme Vianna et al. [2010], o ciclone *Catarina* foi iniciado por um bloqueio atmosférico e a intensificação subsequente foi ativada via interação com os processos dinâmicos oceânicos.

Portanto, é reconhecido o papel da temperatura da superfície do mar elevada em intensificar ciclones extratropicais em uma visão teórica e por meio da análise de eventos individuais.

1.3. Ondas de Calor Marinhas (MHW)

As ondas de calor marinhas (*marine heatwaves* - MHW) são períodos em que a temperatura da superfície do mar é anomalamente elevada por um tempo prolongado [Hobday et al., 2016]. A definição dos eventos está intimamente ligada aos impactos que a alta TSM pode causar no ecossistema marinho, com base em um limite de anomalia de temperatura que pode ser fixo [Frölisher et al., 2018], variável conforme o período do ano [Hobday et al., 2016] ou cumulativo ao longo do evento [Eakin et al., 2010]. Estudos recentes mostraram que nos últimos anos estes eventos estão se tornando mais intensos, frequentes e longos globalmente [Oliver et al., 2018]. Utilizando modelos climáticos, Frölicher e Laufkötter [2018] também sugerem que as projeções futuras são de aumento ainda maior na intensidade, frequência e duração das MHWs no futuro.

Muitos estudos mostram o impacto que MHWs causam ao ecossistema marinho, como mudanças na distribuição de espécies [Werngerg, 2013; Salinger et al., 2019], aumento da mortalidade de cardumes [Gentemann et al., 2017] e prejuízos na indústria pesqueira [Pershing et al., 2013]. Principalmente na região tropical, onde o ambiente é pouco adaptado a variação de temperatura da água, existem impactos relacionados ao branqueamento de corais [Fordyce et al.,

2019]. Algumas MHWs persistem por dias enquanto outras por meses ou até anos, como no caso *Blob* do Pacífico Norte [Di Lorenzo e Mantua, 2016], que atuou entre os invernos boreais de 2013/2014 e 2014/2015. Esses eventos foram observados em diferentes áreas do oceano nas últimas décadas, mas apenas alguns casos foram documentados e bem analisados [Frölicher e Laufkötter, 2018].

Holbrook et al. [2019] combinaram o estudo de vários casos referidos na literatura para compreender os mecanismos importantes para a formação, persistência e decaimento das MHWs e identificaram que processos locais e forçantes remotas, como modos climáticos de grande escala e processos de teleconexões, podem ser importantes propulsores do desenvolvimento dos eventos. No estudo, foram mapeadas áreas onde existe maior predominância das MHWs (Figura 1.3) e foram discutidos os aspectos relevantes para cada região. O estudo sugeriu que no Oceano Atlântico Sudoeste os processos oceânicos e o modo de variabilidade climática do Niño do Atlântico Equatorial [Yang et al., 2022] podem ser promotores de MHW, porém a área necessita de estudos mais específicos.

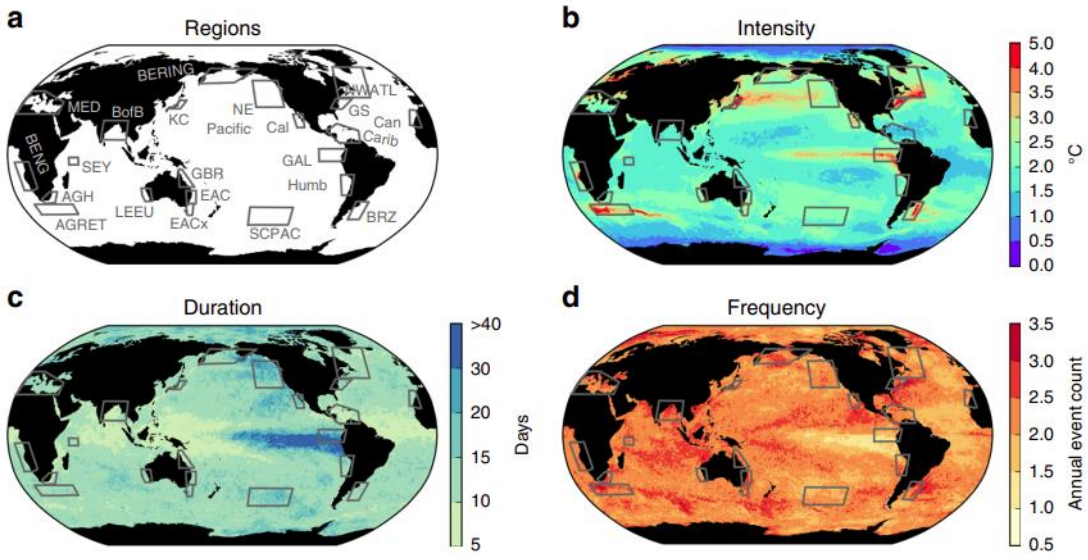


Figura 1.3. Áreas mais importantes para o estudo de MHWs (caixas cinzas) (a), intensidade (b), duração (c) e frequências de casos por ano (d) de MHW (Fonte: Holbrook et al., 2019).

Para o Atlântico Sudoeste, Manta et al. [2018] estudaram a ocorrência de MHW na plataforma continental próxima à pluma do Rio de La Plata entre 1988 e 2017, e verificaram um aumento no número de dias com MHW por ano a partir

de 2014. Um evento extremo ocorrido no verão austral de 2017, responsável pela mortalidade em massa de algumas espécies de peixes, foi analisado. O evento ocorreu de forma simultânea a um bloqueio atmosférico, quando predominaram ventos fracos e pouca nebulosidade, possibilitando o desenvolvimento da MHW. A configuração em escala planetária da Oscilação Madden-Julian possibilitou a persistência da condição de estabilidade na região por um longo período.

Rodrigues et al. [2019], analisando a área próxima à costa de Santa Catarina (SC), identificaram um aumento na intensidade, frequência e duração das MHWs para o período de 1982 a 2016. As análises mostraram também que a maior parte das MHWs nessa região é favorecida por bloqueios atmosféricos com circulação anticiclônica persistente que, por sua vez, causam secas severas no sul e sudeste do Brasil. A redução da nebulosidade leva ao aumento da energia solar no oceano e ao enfraquecimento dos ventos, o que leva à diminuição do resfriamento evaporativo. Ambos os fatores contribuem para o desenvolvimento das MHWs nesta região. Como efeito remoto das condições atmosféricas e oceânicas, o estudo apontou a propagação do trem de onda estacionária de Rossby, gerada a partir de convecção profunda no Oceano Índico, associada à Oscilação Madden-Julian [Zhang, 2005] (Figura 1.4). Neste período, destaca-se o evento de bloqueio atmosférico de 2013/2014, que favoreceu a onda de calor marinha durante praticamente todo o verão.

Costa e Rodrigues [2021] usaram observações e simulações do conjunto de modelos globais *Coupled Model Intercomparison Project Phase 6* (CMIP6) [Eyring et al., 2016] em dois diferentes cenários, para analisar as mudanças em MHW no Sudoeste do Oceano Atlântico em um ambiente de aquecimento global e encontraram um aumento na frequência de casos por ano durante o século 21. Além disso confirmaram a associação entre bloqueios atmosféricos e MHW nesta área. Oliver et al. [2019] fez um estudo de projeções do cenário futuro de MHW e destacou o impacto maior em um cenário de maior emissão de poluentes, discutindo sobre as implicações ecológicas de uma condição de MHW permanente, devido ao aquecimento global.

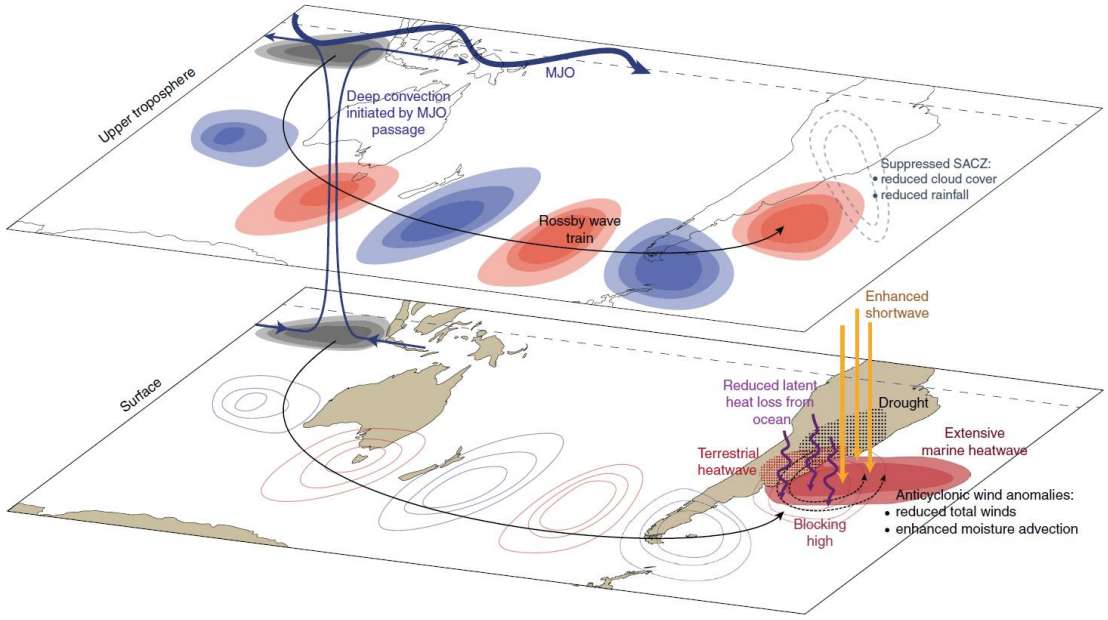


Figura 1.4. Mecanismo de formação de MHWs, proposto por Rodrigues et al. [2019].

1.4. Lacunas Científicas

Nos trabalhos acima citados, nota-se a grande ligação entre a dinâmica dos sistemas meteorológicos instáveis, como é o caso dos ciclones extratropicais, e as áreas com TSM extremamente elevada.

Apesar de muitos estudos reconhecerem o Oceano Atlântico sudoeste como uma área propícia à formação e intensificação de ciclones extratropicais, os seguintes aspectos do tema necessitam de esclarecimentos:

- Como é a variabilidade da contagem de ciclones de acordo com sua estação do ano?
- Como é a variabilidade da contagem de ciclones de acordo com sua posição de formação?
- Quais características precursoras podem ser destacadas em ciclones extratropicais intensos, formados na costa do sul do Brasil e Uruguai?

Considerando que poucos estudos abordam de forma detalhada as características das MHWs e a ligação destas com ciclones extratropicais, os seguintes aspectos são pertinentes ao estudo:

- Quais são as principais características das MHWs no Sudoeste do Oceano Atlântico?

- Existe ligação estatística entre ciclones extratropicais e MHWs no Sudoeste do Oceano Atlântico?

1.5. Estrutura da Tese

No capítulo seguinte a este, apresento a hipótese testada e no capítulo 3 são apresentados os objetivos da tese, trabalhados durante todo o documento. No capítulo 4, é realizada uma descrição dos dados e metodologias, além de uma exposição da área de estudo.

No capítulo 5, o artigo "*Objective Algorithm for Detection and Tracking of Extratropical Cyclones in the Southern Hemisphere*", publicado na revista *Atmosphere* mostra os detalhes e testes realizados para a metodologia de detecção e rastreamento de ciclones extratropicais desenvolvida neste trabalho, cumprindo o objetivo específico 1. Além disso, mostra exemplos de casos específicos e uma apresentação dos resultados para o Hemisfério Sul, para quatro décadas de dados, comparando com outros estudos.

No capítulo 6, o artigo "*Characterization and Variability of Extratropical Cyclones in the Southwest Atlantic Ocean*", submetido na revista *Advances in Meteorology* mostra os resultados científicos para os objetivos específicos 2 e 3. Os resultados abrangem uma caracterização e análise da variabilidade dos eventos de ciclone extratropical na área de estudo, focando em aspectos como posição de formação, estação do ano e intensidade.

No capítulo 7, o artigo "*Marine Heatwaves in the Southwest Atlantic Ocean and their Relationships with Extratropical Cyclones*", submetido à revista *Atmospheric Research* mostra os resultados científicos para o objetivo específico 4, discutindo assim a relação entre os ciclones extratropicais e MHWs no Sudoeste do Oceano Atlântico.

Por fim, o capítulo 8 descreve uma síntese abrangente das discussões abordadas e o capítulo 9 apresenta as conclusões e oferece sugestões para trabalhos futuros. As referências bibliográficas utilizadas em todo o documento estão compiladas no capítulo 10.

Capítulo II: Hipótese

Considerando que períodos prolongados de anomalia positiva extrema de temperatura da superfície do mar podem desencadear uma intensificação dos processos de troca de calor e umidade, infere-se que sistemas meteorológicos instáveis, como ciclones extratropicais, têm potencial para tornarem-se mais intensos na área, quando a temperatura da superfície do mar está extremamente elevada.

De forma alternativa, os ciclones extratropicais podem ser responsáveis por diminuição de TSM, já que estão associados à ventos intensos, que promovem mistura da água, e precipitação, adicionando água mais fria ao ambiente superficial. Dessa forma, pode-se esperar que a finalização das MHWs tipicamente ocorra devido a chegada de ciclones extratropicais à área. Assim, a primeira hipótese testada neste trabalho foi de que há uma relação significativa entre a presença de MHWs e a intensificação de ciclones extratropicais na área de estudo. Uma segunda hipótese a se considerar é de que eventos de MHWs geralmente terminem com a chegada de um ciclone extratropical à região.

Capítulo III: Objetivos

3.1. Objetivo Geral

O objetivo geral do trabalho é desenvolver uma metodologia de identificação de ciclone extratropicais e aplicar na análise da variabilidade e características dos ciclones extratropicais no Oceano Atlântico Sudoeste e explorar suas interações com eventos de MHWs ao longo das últimas décadas.

3.2. Objetivos Específicos

Pretende-se:

(i) Desenvolver um programa de identificação e rastreamento de ciclones extratropicais ajustado para dados de alta resolução temporal e espacial;

(ii) Analisar as principais características dos eventos de ciclone extratropicais no Oceano Atlântico Sudoeste;

(iii) Investigar a variabilidade dos ciclones extratropicais no Oceano Atlântico Sudoeste ao longo das últimas décadas, quanto à intensidade e posição de formação;

(iv) Analisar as características os eventos de MHWs e estabelecer sua relação com a ocorrência de ciclones extratropicais no Oceano Atlântico Sudoeste.

Capítulo IV: Dados e Métodos

4.1. Dados

Neste trabalho, foram utilizados dados de reanálise atmosférica do projeto *European Centre for Medium-Range Weather Forecasts Re-analysis 5* (ERA5), produzido pelo *European Centre for Medium-Range Weather Forecasts* (ECMWF) e o conjunto de dados de temperatura da superfície do mar global em alta resolução da *National Oceanic and Atmospheric Administration Optimum Interpolation Sea Surface Temperature Version 2 High-Resolution Blended Analisys (*NOAA OI SST V2*)*. Os dois conjuntos de dados serão descritos nos itens seguintes.

4.1.1 Reanálise ERA5/ECMWF

O conjunto de dados ERA5/ECMWF abrange o período desde 1979 e continua a ser atualizado ao menos até a finalização do presente trabalho [Hersbach et al., 2020]. A resolução horizontal do modelo é de 31 km em uma grade gaussiana reduzida, com 137 níveis verticais, da superfície da Terra até 0,01 hPa, com dados horários. De acordo com Hersbach et al. [2020], os principais pontos fortes destes dados de reanálise são suas resoluções temporal e espacial, além da melhora da assimilação dos conjuntos de dados reprocessados, se comparado aos produtos anteriores. A reanálise ERA5/ECMWF apresenta um ajuste mais

preciso da temperatura, ventos e umidade da troposfera do que versões passadas, utilizando dados de mais de 200 instrumentos de satélite ou tipos de dados convencionais. Para compor os campos em grade regular em altitude, são assimilados dados de radiossondas, dropsondas e aeronaves, além de ventos derivados do rastreamento de nuvens e características do vapor d´água em sequências de imagens de satélites geoestacionários ou em pares de imagens de satélites em órbita polar.

O presente estudo envolveu dados horários do ERA5 entre 1982 e 2023, para as variáveis: vorticidade relativa em 850 hPa, pressão ao nível médio do mar e vento (meridional e zonal) em 10 metros. Para a análise de períodos específicos de ciclones extratropicais intensos, também foram utilizadas as seguintes variáveis: vento (meridional e zonal) em 300 hPa, 700 hPa, 850 hPa, altura geopotencial e temperatura de ar em 500 hPa, 700 hPa e 850 hPa, umidade relativa do ar em 700 hPa e 850 hPa. A teoria clássica [por exemplo, Holton, 2004] apresenta a vorticidade relativa como a medida microscópica da rotação em um fluído, matematicamente definido como o rotacional da velocidade do fluído. Em uma análise de escala, somente a componente vertical da vorticidade relativa é utilizada (ζ_z), obtendo-se assim, a Equação (4.1).

$$\zeta_{Z=} \frac{\partial v}{\partial x} - \frac{\partial u}{\partial y} \qquad (4.1)$$

Considerando a mesma equação em coordenadas esféricas, a Equação (4.2) é obtida, em que *u* e *v* são as velocidades zonal e meridional, respectivamente, *r* é o raio da Terra, θ e λ são a latitude e longitude do local.

$$\zeta_Z = \frac{1}{r\cos\theta}\left(\frac{\partial v}{\partial \lambda} - \frac{\partial u\cos\theta}{\partial \theta}\right) \qquad (4.2)$$

4.1.2 Análise de Alta Resolução NOAA OI SST V2

Para o estudo das condições oceânicas, este trabalho utilizou dados de alta resolução da NOAA OI SST V2. Os dados diários de temperatura da superfície do mar estão disponíveis a partir de setembro de 1981 até ao menos a finalização deste documento, em uma grade global de 1/4 de grau (0,25°) latitude/longitude [Reynolds, 2007]. O conjunto de dados incorpora observações

de plataformas como satélites, navios, boias e sondas do sistema Argo. Com isso, um mapa de temperatura da superfície do mar espacialmente regular é criado, utilizando interpolação para preencher lacunas. Dados de satélite e de navios são calibrados em relação às boias, para corrigir discrepâncias entre os diferentes tipos de sensores observacionais das múltiplas plataformas.

Uma atualização no cálculo da estimativa de temperatura da superfície do mar no conjunto de dados foi realizada em 2016 [Huang et al., 2021], impactando principalmente as condições em altas latitudes. Para o presente estudo, os dados diários entre 1982 e 2023 foram utilizados na identificação das MHWs.

4.1.3 Dados Auxiliares

Ilustrando as condições em um evento de ciclone extratropical em outubro de 2016, responsável por mudanças significativas na morfologia costeira na praia do Hermenegildo, no extremo sul do Rio Grande do Sul, foram utilizados dados de rajadas de vento e pressão ao nível médio do mar da estação automática de superfície do Instituto Nacional de Meteorologia (INMET) localizado em 33,74°S e 53,37°W, identificada como A899 no banco de dados do INMET (Figura 4.1).

Além disso, para ilustrar as condições da área de estudo, foram utilizados dados de batimetria obtidos pelo conjunto de dados *General Bathymetric Chart of the Oceans* (GEBCO). GEBCO é um modelo global de mapeamento oceânico e terrestre desenvolvido por várias instituições ao redor do mundo, que fornece dados de elevação em metros em uma grade de 15'' (arco-segundos). Os dados de entrada deste modelo global são heterogêneos, principalmente utilizando sistemas de medida acústica, como ecossondas multifeixe [Hell and Jakobsson, 2011].

4.2. Área de Estudo

A região foco do presente estudo abrange o Oceano Atlântico Sudoeste, entre as latitudes 20°S e 50°S e longitudes 30°W a 65°W. Neste setor, ocorre o encontro entre a Corrente do Brasil, que escoa para sul com águas salgadas e quentes, e a Corrente das Malvinas, que se direciona para norte com águas subantárticas mais frias, mais doces e ricas em nutrientes. Esse encontro,

próximo à foz do Rio De La Plata, é chamado Confluência Brasil-Malvinas. Essa descontinuidade é caracterizada por um intenso gradiente de temperatura e pelo favorecimento de perturbações de meso-escala ao longo da frente termohalina, como meandros, vórtices e filamentos [Matano et al., 2010; Telesca et al., 2017; Piola et al., 2018].

A batimetria no Oceano Atlântico Sudoeste é mostrada na Figura 4.1. A profundidade máxima ocorre na parte sul da área, chegando a aproximadamente 6500 m. A plataforma continental é mais larga na parte sul e mais estreita na parte norte, apresentando vários golfos. Em alto mar, a área de menor profundidade entre 25°S e 35°S é chamada de Elevação de Rio Grande, com fendas profundas e picos, formando um relevo acidentado (Castello e Krug, 2017).

Vários estudos destacam a importância desta área para a formação de ciclones extratropicais [Simmonds e Keay, 2000; Vera et al., 2002; Hoskins e Hodges, 2005; Reboita et al., 2010, 2018; Gramcianinov et al., 2020]. No primeiro artigo (Capítulo V), a metodologia de rastreio de ciclones extratropicais foi aplicada para todo o Hemisfério Sul. Já no segundo artigo (Capítulo VI), são utilizados os eventos que estiveram na região entre 20°S e 50°S de latitude e 30°W e 65°W de longitude, em algum momento de seu ciclo de vida (caixa vermelha da Figura 4.1). Além disso, no desenvolvimento do artigo, foram separados os eventos formados a norte e a sul de 35° S de latitude (linha rosa da Figura 4.1) e eventos intensos que atingiram a área costeira entre 30°S e 40°S de latitude e entre 45°W e 60°W de longitude (caixa lilás da Figura 4.1). No terceiro artigo (Capítulo VII), a área de estudo compreende 25°S a 45°S de latitude e 40°W a 65°W de longitude (caixa verde da Figura 4.1), abordando também as diferenças entre eventos que ocorrem a norte e a sul de 35°S de latitude.

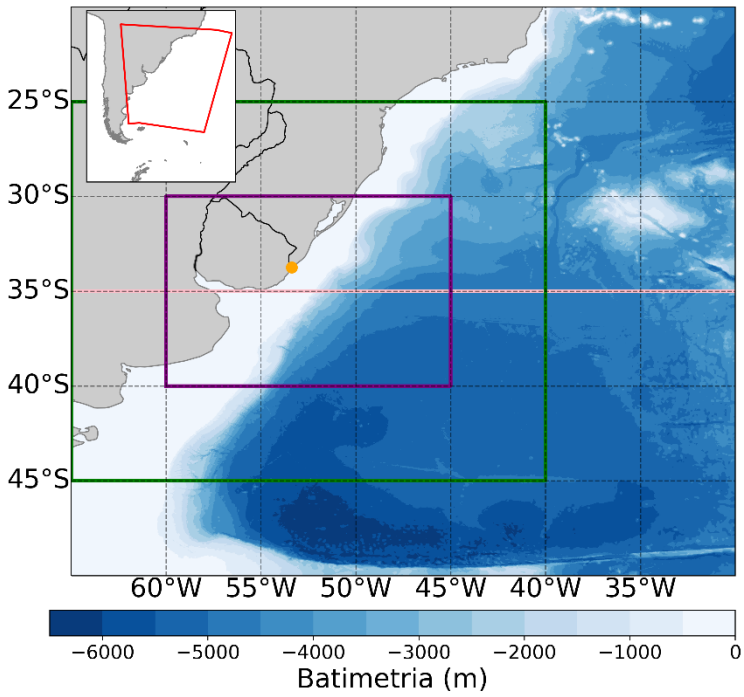


Figura 4.1. Área de estudo e batimetria (GEBCO), mostrando parte da América do Sul e do Oceano Atlântico Sudoeste. A caixa vermelha delimita a área de estudo do artigo 2 e a caixa verde delimita a área de estudo do artigo 3. Para estes dois artigos, foram comparados eventos formados a norte e ao sul de 35°S de latitude (linha rosa). A caixa roxa delimita a região de formação dos eventos intensos analisados no artigo 2. O marcador em laranja mostra a posição da estação meteorológica automática de superfície da Barra do Chuí (A899), utilizada no artigo 1.

4.3. Método de Identificação e Rastreamento de Ciclones Extratropicais

Vários algoritmos foram propostos em estudos prévios para a identificação objetiva dos ciclones extratropicais. Esses estudos utilizam diferentes técnicas, tipos de dados e séries temporais para a identificação objetiva, trajetória e estimativa de intensidade de ciclones em superfície.

Um primeiro esforço de identificação automática de ciclones extratropicais foi publicado por Williamson [1981]. Posteriormente, Lambert [1988] utilizou a identificação de mínimos de altura geopotencial em 1000 hPa para a detecção objetiva de ciclones, enquanto que Murray e Simmonds [1991] sugeriram a utilização de mínimos de pressão ao nível médio do mar. Estudos como de Hodges [1994; 1995] e Sinclair [1997] descreveram um procedimento para uso em análises numéricas em que ciclones foram identificados como um máximo de vorticidade ciclônica, para a eliminação de algum viés que favorecesse eventos mais lentos ou mais intensos, como quando é usada a pressão mínima.

Sinclair [1994] pontuou que a vantagem em utilizar o campo de vorticidade relativa para a identificação de ciclones extratropicais é que esta representa melhor um sistema em rotação do que a pressão ao nível médio do mar. Além disso, em alguns casos, os ciclones extratropicais não apresentam isóbaras fechadas, portanto não seriam selecionados com a utilização do mínimo da pressão ao nível médio do mar.

Em relação à altitude em que os dados são utilizados, muitos estudos apresentam metodologias diferentes, embora grande parte destes foquem nos baixos níveis da troposfera. Por exemplo, nos estudos de Hodges [1994; 1995], foi descrita a metodologia para a identificação e trajetória de ciclones usando o campo de vorticidade relativa em 850 hPa, computado a partir da variável vento (meridional e zonal). Já no estudo de Sinclair e Watterson [1999], o máximo local de vorticidade ciclônica do gradiente do vento foi calculado em 1000 hPa para a identificação dos ciclones, enquanto Reboita et al. [2010], mais recentemente, utilizaram um esquema automático que identifica mínimos de vorticidade relativa no vento em 10 metros.

Diante desta grande variedade de métodos para a identificação de ciclones extratropicais, os estudos de Trigo [2006], Raible et al. [2008] e Ulbrich et al. [2009] compararam diretamente algoritmos de identificação e trajetória de ciclones extratropicais e mostraram que, mesmo utilizando a mesma base de dados, diferentes métodos podem levar a diferentes conclusões e até sinais opostos para uma mesma tendência. Em 2009, foi conduzido um projeto de intercomparação, chamado de *Intercomparison of Mid-Latitude Storm Diagnostics* (IMILAST) [Neu et al., 2013], com o objetivo de avaliar as incertezas relacionadas aos vários tipos de métodos para a identificação e trajetória de ciclones extratropicais, com a participação de pesquisadores de 20 grupos no mundo. Os resultados mostraram que o tempo de atuação, número de eventos e posição dos eventos varia dependendo do método. Por outro lado, eventos mais profundos em seus períodos mais intensos foram identificados em todos os métodos. A comparação foi realizada com os dados do ERA-interim em uma resolução temporal de 6 horas. Os autores pontuaram a expectativa por uma análise mais precisa, com a utilização do ERA5 [Hewson e Neu, 2015].

No presente estudo, um conjunto de dados mais refinado em termos de resolução temporal e espacial motivou a utilização de ajustes inovadores para a identificação, rastreio e caracterização dos ciclones extratropicais. A metodologia utilizou a técnica de componentes conectados, implementada para a identificação de ciclones inicialmente por Inatsu [2009] e por Inatsu e Amada [2013]. Como no presente estudo a variável meteorológica para a identificação apresenta um campo ruidoso, principalmente em baixos níveis da troposfera (vorticidade relativa em 850 hPa), optou-se por iniciar o processo de identificação com a utilização do filtro gaussiano. Outros autores optaram por diferentes filtros, como β-*spline* [Hodges, 1995], 1-2-1 [Satake et al., 2013], 1-1-1 [Flaounas et al., 2014]. No entanto, o filtro gaussiano permite uma suavização mais delicada dos efeitos orográficos e de costa, também suavizando os máximos locais de vorticidade aninhados ao campo ruidoso [Gonzales e Woods, 1992]. O grau de suavização precisa ser escolhido, conforme o desvio padrão da gaussiana (σ). O cálculo do filtro gaussiano é dado pela equação 4.3, em que *x* e *y* são as distâncias zonal e meridional do ponto para o qual a suavização é calculada.

$$G(x,y) = \frac{1}{2\pi\sigma^2} e^{-\frac{x^2+y^2}{2\sigma^2}} \qquad (4.3)$$

A Figura 4.2A mostra um campo de vorticidade relativa em 850 hPa na data em que ocorreu um ciclone extratropical intenso e de rápido desenvolvimento, também chamado de ciclone bomba (1° de julho de 2020, às 18 UTC). Na Figura 4.2B o campo foi suavizado com a utilização do filtro gaussiano. Após a aplicação deste filtro no campo de vorticidade relativa em 850 hPa do ERA5/ECMWF, é realizada binarização, ou seja, o campo é transformado em dados binários, a partir de um valor limite. A discussão sobre o melhor valor limite para a aplicação desta etapa é parte do artigo 1 (Capítulo V). Dessa forma, cada horário corresponde a um campo, onde o valor abaixo do limite L recebe o valor 1 e na condição contrária recebe o valor 0. Um exemplo desta etapa é mostrado na Figura 4.2C, em que a área preta recebeu o valor zero, enquanto que a área branca recebeu o valor 1.

Em sequência, o campo binarizado é submetido à técnica de rotulagem de componentes conectados. Essa técnica consiste em reunir em conjuntos os

pontos que estão conectados uns com os outros. Dessa forma, todos os pontos que recebem valor 1 e são vizinhos dentro do campo, pertencem ao mesmo componente. Para exemplificar essa técnica, a Figura 4.2D apresenta o campo para a mesma área e data da Figura 4.2C. O fundo escuro representa as partes do campo em que a vorticidade relativa em 850 hPa não atingiu o limiar L estabelecido, enquanto cada cor representa o grupo de pontos separados por uma rotulagem. Os grupos pequenos em termos de número de pontos são removido, ou porque são ruídos que não foram suavizados pelo filtro, ou porque seus pontos não estavam unidos com os demais pontos do ciclone. Assim, conjuntos menores do que um limiar C são removidos, como uma forma de se retirar aqueles que não representam ciclones extratropicais. A discussão sobre a escolha do limiar C e teste de sensibilidade é parte do artigo 1 (Capítulo V). Na Figura 4.2D, existem dois ciclones extratropicais, devido à retirada dos componentes que são mostrados na Figura 4.2C à esquerda, por ser menores do que o limiar C.

Cada um dos conjuntos de posições restantes é identificado por uma posição, que é calculada pelo centro de massa simples (CM_a), conforme a equação 4.4, em que (m,R) é a massa e posição de cada ponto do conjunto e N é o número de pontos das superfícies independentes fechadas (a). A massa é calculada pelo valor de vorticidade relativa em 850 hPa do ponto e a posição é gravada como uma posição geográfica (latitude/longitude).

$$CM_a = \frac{\sum_{i=N}^{i=1} m_i R_i}{\Sigma m_i} \qquad (4.4)$$

Assim, o desempenho do algoritmo de identificação de ciclones extratropicais é influenciado até essa etapa pela escolha do desvio padrão do filtro gaussiano (durante o estágio de pré-processamento), do limiar L da vorticidade relativa em 850 hPa e da exclusão de conjuntos menores que o limite C. A Figura 4.2E exemplifica os pontos de componentes, identificadas em uma posição geográfica pelo cálculo do centro de massa, para a mesma data da Figura 4.2A.

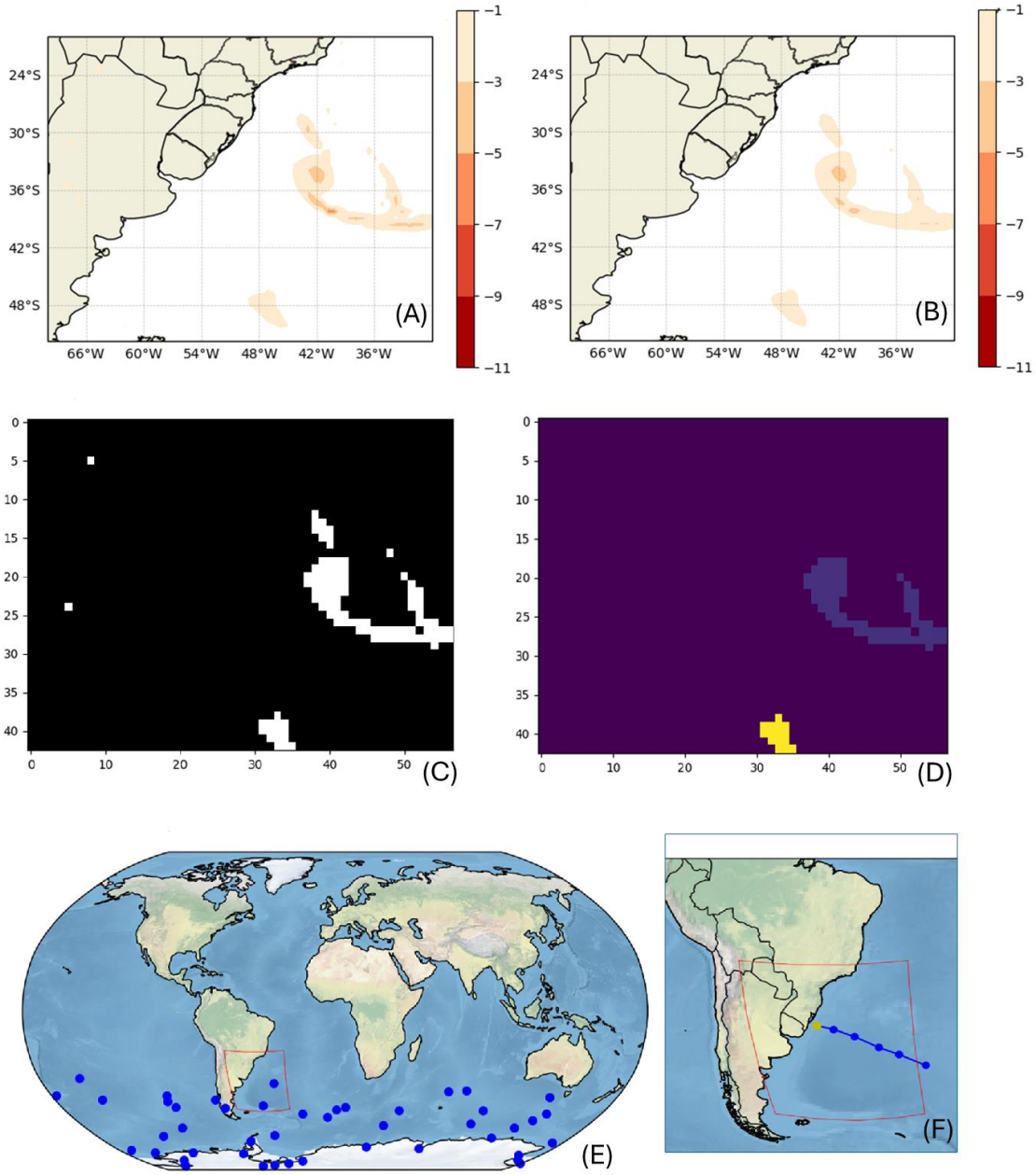


Figura 4.2. Esquema explicativo da aplicação da técnica de componentes conectados. (A) Campo de vorticidade relativa em 850 hPa (ERA5/ECMWF), em 1° de julho de 2020, às 18 UTC, com um fator de multiplicação de 10^4, em um recorte em parte da América do Sul e Oceano Atlântico; (B) o mesmo campo após a aplicação do filtro gaussiano em 0,5; (C) binarização do campo pelo limiar L de 10^{-4} s^{-1}; (D) aplicação da técnica de componentes conectados (cada cor representa um componente) e retirada de componentes menores do que 15 pontos; (E) posições de possíveis ciclones na mesma data das letras (A) e (B) no Hemisfério Sul; (F) identificação das posições do ciclone ocorrido entre 1 e 2 de julho de 2020, após a aplicação do critério de tempo de vida mínimo e deslocamento máximo entre horários. Os eixos nas figuras (C) e (D) representam os pontos de grade de espaçamento regular para o recorte do dado ERA5/ECMWF.

Para o rastreamento dos eventos, uma ligação foi encadeada entre os horários subsequentes e, assim, foi definido um deslocamento máximo na velocidade de 150 km/h, similar ao estudo de Crawford et al. [2021]. O tempo de

vida mínimo utilizado para a identificação dos eventos é de 12 horas. A Figura 4.2F mostra a posição do ciclone bomba entre os dias 1° e 2 de julho de 2020, gerada pelo método apresentado neste trabalho. A Figura 4.3 mostra um segundo exemplo de posições de centros de massa que atingiram todos os limiares para a identificação do evento, em uma sequência de horários.

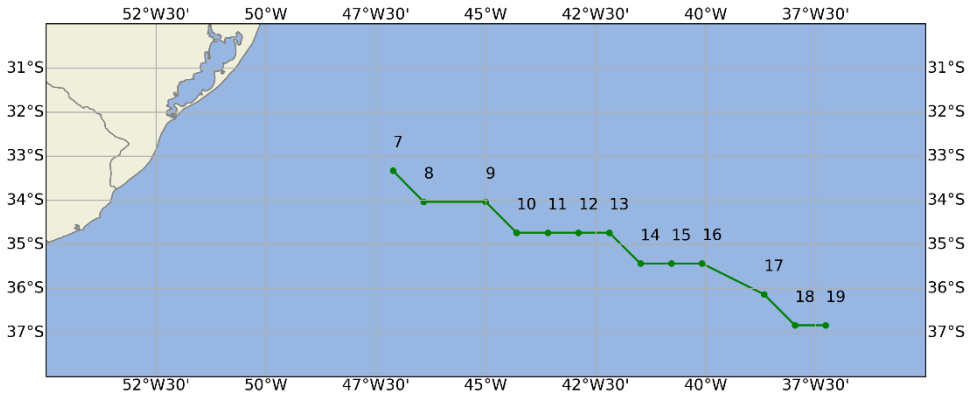


Figura 4.3. Exemplo de posições do centro de massa das áreas identificadas pela técnica de componentes conectados em uma sequência de horários.

A partir desta etapa, uma lista de eventos é registrada, contendo a latitude, longitude, vorticidade relativa em 850 hPa mais intensa e tamanho da área de abrangência de cada evento, para cada horário. Para identificar eventos mais intensos em relação à menor pressão ao nível médio do mar e ao maior vento em 10 metros, uma nova etapa foi realizada, que consiste em adicionar a menor pressão ao nível médio do mar e o maior vento em 10 metros em uma área de atuação do ciclone extratropical. Em alguns estudos, a área de atuação é calculada para cada horário do evento (por exemplo, Lu [2017]) e em outros, é definido um limite constante de atuação por simplificação (por exemplo, Murray e Simmonds [1991]). No presente estudo, optou-se por investigar os valores mais intensos de pressão ao nível médio do mar e de vento em 10 metros em um limite constante do dado de ERA5/ECMWF, que corresponde à aproximadamente 3,6 graus de latitude/longitude ao redor da posição de cada horário dos ciclones extratropicais. Assim, a caracterização dos eventos foi completada com essa etapa. Embora alguns desvios entre a posição da menor pressão ao nível médio do mar e do centro de massa da vorticidade relativa sejam esperados, o resultado deste algoritmo é satisfatório para a análise

climatológica de ciclones extratropicais. A Figura 4.4 apresenta o fluxograma das etapas do método de identificação, rastreio e caracterização dos ciclones extratropicais utilizado no presente trabalho.

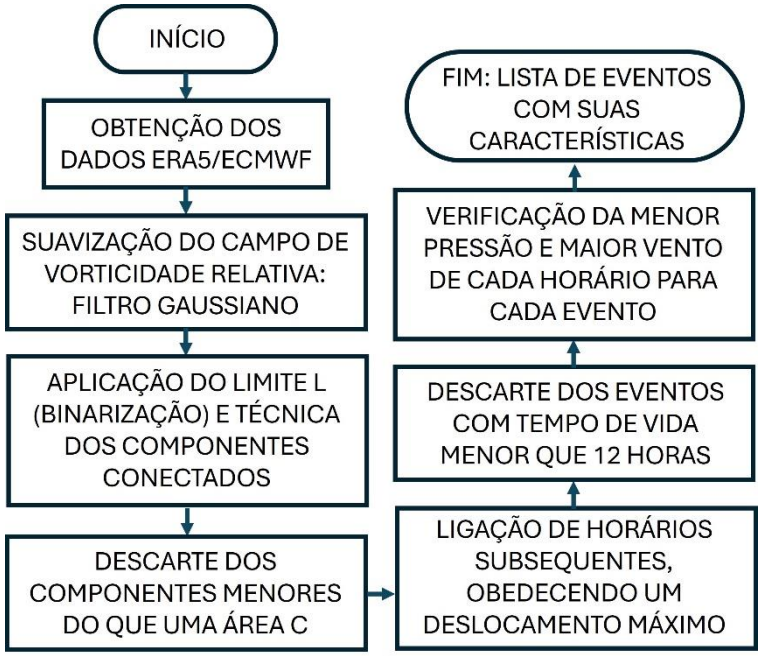


Figura 4.4. Fluxograma das etapas do método de identificação, rastreio e caracterização de ciclones extratropicais desenvolvido no presente estudo.

No artigo 1, buscou-se analisar os melhores parâmetros para aplicar no algoritmo. Nos artigos 2 e 3, foram utilizados os seguintes parâmetros: desvio padrão do filtro gaussiano de 0,5, limiar L de vorticidade relativa de -10^{-4} s^{-1} e descarte de áreas menores que 15 pontos de grade.

No artigo 2, a avaliação dos eventos intensos e rápidos foi conduzida a partir do limiar do percentil 90% (10%) considerando os eventos encontrados na área de estudo (caixa vermelha da Figura 4.1), durante os anos de 1982 a 2022. Os eventos intensos com relação à menor pressão ao nível do mar foram definidos como aqueles com valores menores que 966 hPa, o que corresponde ao percentil 10% dos ciclones extratropicais da área. Lambert e Fyfe [2006] rodaram testes de sensibilidade para diferentes limites e encontraram que os resultados para eventos intensos não são particularmente sensíveis ao valor de limite de pressão ao nível médio do mar utilizado. Além disso, o limite escolhido por eles foi de 960 hPa para o Hemisfério Sul, o que é próximo do valor deste trabalho.

Uma segunda avaliação dos casos intensos é baseada nos maiores ventos em 10 metros relacionados ao ciclone extratropical. Foi utilizado o limiar do percentil 90% dos eventos encontrados na área de estudo, em torno de 84 km/h. Esta definição não possibilita a conclusão de que esses eventos causaram maiores danos relacionados aos ventos fortes, porque em algumas situações os danos estão relacionados à proximidade a áreas costeiras ou mesmo à persistência ou direção dos ventos associados ao ciclone extratropical. Contudo, o limite de vorticidade relativa rigoroso e a utilização do percentil 90% permitem a restrição de casos pouco intensos e a seleção daqueles mais destacados. Para separar os casos mais rápidos, foi realizada a média da velocidade de deslocamento ao longo do tempo de vida completo dos ciclones extratropicais. O percentil 90% da velocidade dos eventos na área de estudo foi de aproximadamente 78 km/h, valor este que foi utilizado para a obtenção dos eventos mais rápidos.

4.4. Método de Identificação de MHW

Neste trabalho, a identificação das MHW segue o método documentado por Hobday et al. [2016], uma metodologia amplamente aceita na literatura, baseada nas definições prévias de onda de calor atmosférica. O evento de MHW é obtido para cada ponto do oceano e é definido qualitativamente como um evento discreto e prolongado de águas anomalamente quentes. De forma quantitativa, a MHW é definida com base na anomalia de temperatura da água, relacionando a temperatura do dia em questão com a climatologia. Seguindo o método desenvolvido por Hobday et al. [2016], esta condição climática foi construída para cada dia do ano a partir de uma média em janelas de 11 dias, centrada em cada dia do ano, utilizando os dados entre 1982 e 2023. O limite para que a anomalia de temperatura da água seja considerada extrema é o percentil 90% da série temporal do ponto no oceano. Semelhante a Hobday et al. [2016], o tempo mínimo para a definição de uma MHW no presente estudo é de 5 dias consecutivos com a temperatura do mar excedendo o limite, baseado no percentil 90%. Eventos separados por até 2 dias, são consideradas parte de uma mesma MHW.

Para desenvolver mapas que representam a frequência, o número de dias e as características médias das MHW em uma determinada área, o método foi aplicado a séries temporais de dados de cada ponto do oceano na área de estudo. Assim, a resolução da grade do mapa resultante é similar àquela dos dados de temperatura da superfície do mar, nos dados do NOAA OI SST V2.

Para identificar as características de cada evento, um grupo de propriedades pode ser destacadas [Hobday et al., 2018]: duração em dias, intensidade média, intensidade cumulativa e intensidade máxima. Essas características representam o quão significativos podem ser os impactos sociais e ecológicos do evento. Enquanto a intensidade média é definida como a média da anomalia de temperatura da água durante os dias da MHW, em °C, a intensidade máxima é obtida pelo maior valor de anomalia de temperatura da água durante os dias da MHW, em °C. Por outro lado, a intensidade cumulativa mede a soma da anomalia de temperatura da água durante todos os dias da MHW, em °C.dia, tornando esse parâmetro mais sensível a eventos longos.

Os eventos foram categorizados, conforme os critérios estabelecidos por Hobday et al. [2018]. As categorias são obtidas em relação a intensidade máxima do evento, calculada conforme a Equação 4.5, definidas como “Moderado”, “Forte”, “Severo” e “Extremo”. Nesta equação, $SST_{d,lat,lon}$ representa a temperatura da superfície do mar em um dia específico, na posição de latitude e longitude indicadas. Já $SST_{cld,lat,lon}$ representa a média climatológica da temperatura da superfície do mar para o mesmo dia, na mesma posição de latitude e longitude. Essas categorias estão explicadas na Tabela 4.1.

$$I_{max} = \max\left(SST_{d,lat,lon} - SST_{cld,lat,lon}\right) \qquad (4.5)$$

Tabela 4.1. O limite criado por Hobday et al. (2018) para categorizar um evento local, baseado na climatologia. DBH90 é a diferença de temperatura entre a climatologia e o percentil 90%.

Categoria	Limite
Moderado (categoria I)	I_{max} > DBH90
Forte (categoria II)	I_{max} > Duas vezes DBH90
Severo (categoria III)	I_{max} > Três vezes DBH90
Extremo (categoria IV)	I_{max} > Quatro vezes DBH90

4.5. Métodos Estatísticos

Neste estudo, uma série temporal de ciclones extratropicais formados dentro no Sudoeste do Atlântico (Figura 4.1, caixa vermelha) para cada ano e a separação de eventos formados na faixa norte e sul, de acordo com 35°S (linha rosa da Figura 4.1) foram examinados. As tendências foram calculadas aplicando modelos de regressão linear e cúbica para a série temporal. Muitos estudos focam somente na regressão linear, porém um modelo mais complexo foi capaz de mostrar resultados mais refinados. A significância estatística foi performada pelo teste-T, porém o teste Mann-Kendall [Kendall, 1975] avaliou a significância da tendência.

No artigo 2 (Capítulo VII), foi conduzida a análise de Fourier, para identificar de forma adequada oscilações periódicas na série de ciclones extratropicais [Emery e Thomson, 2001]. A significância dos picos foi aferida pelo ruído vermelho (RN), com uma técnica formulada matematicamente por Gilman et al. [1963] (Equação 4.6) e pelo teste F de significância, relacionado ao ruído vermelho. Na Equação 4.6, ρ é a autocorrelação lag-1, *N* é o tamanho da série de dados e *h* varia de forma unitária de 1 até a metade de *N*. Seguindo Prieto [2007], vinte realizações do espectro de potência foram computadas, para melhorar a visualização dos picos mais importantes e remover ruídos.

$$RN = \frac{1-\rho^2}{1-2\rho\cos\left(\frac{h\pi}{\frac{N}{2}}\right)+\rho^2} \qquad (4.6)$$

A tendência do número de dias por ano com MHWs foi analisada no artigo 3 (Capítulo VIII). A média do número de dias com MHWs foi realizada dentro da área total de estudo (área dentro da caixa verde na Figura 4.1). Para identificar a tendência de dias com MHW por ano dos eventos de categoria “Forte”, “Severo” e “Extremo”, obteve-se a série temporal média destes eventos. Observando o comportamento destas séries temporais, performou-se uma regressão linear para dois períodos distintos de 21 anos. A significância estatística da tendência foi avaliada pelo teste Mann-Kendall [Kendall, 1975].

Quatro abordagens da medida da correlação linear, por mapas de coeficiente de correlação de Pearson, foram utilizadas para relacionar os ciclones extratropicais com as MHWs. Esse coeficiente mede a intensidade e direção de relações lineares, conforme a Equação 4.7, em que *Rc* é o coeficiente de correlação, σ_1 e σ_2 representam os desvios padrão das variáveis 1 e 2 e *N* é o tamanho da série de dados [Everitt e Hothorn, 2011]. Em primeira abordagem, a correlação foi realizada entre os dias com ciclone e dias com MHW, considerando dados diários dos 42 anos. Como segunda abordagem, a correlação foi realizada para dias com ciclone extratropical e dias de término das MHW. A terceira e a quarta abordagem consistem em considerar apenas os eventos “Fortes”, “Severos” e “Extremos” de MHW, para correlações de todos os dias com MHW e dos últimos dias dos eventos. A relação foi realizada para cada posição do Oceano Atlântico Sudoeste, em uma grade equivalente aos dados de temperatura da superfície do mar do NOAA OI SST V2. Para isso, foi construída uma série diária com a soma de todas as posições dos ciclones extratropicais ao longo do dia, com abrangência de 4° de latitude/longitude de raio.

$$Rc = \frac{\sum \sigma_1 \sigma_2}{N} \qquad (4.7)$$

Capítulo V: Algoritmo Objetivo para a Identificação e Rastreamento de Ciclones Extratropicais no Hemisfério Sul

O manuscrito apresentado neste capítulo, em síntese, apresenta a implementação de um programa de identificação, rastreamento e caracterização de ciclones extratropicais, identificando seus pontos fortes e fracos. Este estudo contribuiu para a geração de um banco de dados, necessário para a obtenção dos objetivos da presente tese. O manuscrito apresenta a descrição detalhada da metodologia, testes de sensibilidade e o seu desempenho para eventos individuais. Além disso, o artigo mostrou a comparação dos resultados para a resolução temporal de 1 hora e de 6 horas e mostrou a frequência de ciclogênese para cada estação do ano em todo o Hemisfério Sul, comparando com os resultados obtidos com outras metodologias, em estudos anteriores.

De autoria de Carina K. Padilha Reinke, Jeferson P. Machado, Maurício M. Mata, José Luiz L. de Azevedo, Jaci M. B. Saraiva e Regina R. Rodrigues, intitulado "***Objective Algorithm for Detection and Tracking of Extratropical Cyclones in the Southern Hemisphere***", foi publicado na revista "***Atmosphere***", disponível em https://www.mdpi.com/2073-4433/15/2/230.

Abstract

In this study, we propose an easy and robust algorithm to identify and track extratropical cyclone events using 850 hPa relative vorticity data, gaussian filter and connected-component labeling technique, which recognize the cyclone as areas under a threshold. Before selecting the events, the algorithm can include essential characteristics that are good metrics of intensity, like minimum mean sea level pressure and maximum 10-m winds. We implemented the algorithm in the Southern Hemisphere, using a 41-year high resolution dataset. Sensitivity tests were performed to determine the best parameters for detection and tracking, such as degree of smoothing, thresholds of relative vorticity at 850 hPa and the minimum area within the threshold. Two case studies were used to assess the positive and negative points of the methodology. The results showed that it is efficient in obtaining the position of extratropical cyclones in their most intense stage, but it does not always perform well during cyclolysis. We compare the methodology using 1-h temporal resolution to that using a 6-hours temporal resolution, and their reproducibility regarding the literature. The extratropical cyclone climatology in the Southern Hemisphere is provided and discussed. The algorithm developed here can be applied to datasets with good spatial and temporal resolution, providing a better inventory of extratropical cyclones.

Keywords: extratropical cyclones; cyclone detection and tracking algorithm; sensitivity studies; cyclone frequency.

5.1. Introduction

Extratropical cyclones are responsible for transporting a large amount of heat, moisture, and momentum, playing a fundamental role in atmospheric circulation [Wallace, 2006; Peixoto and Oort, 1992]. Typically, extratropical cyclones cause damages and natural hazards because they are associated with strong winds, intense precipitation and extreme waves. Understanding how these meteorological systems change over the years and their climatological features over a region can help in predicting local weather, mainly with respect to precipitation, wind, and wave intensity [Ulbrich et al., 2009; Catto et al., 2019; Sinclair et al., 2020].

The first efforts to identify extratropical cyclones from digital data were reported more than three decades ago (e.g., [Lambert, 1988; Murray and Simmonds, 1991]). The increase in the amount of information obtained by reanalysis data over a long period of time provides the challenge of organizing an automatic method for identifying and tracking extratropical cyclones on a gridded map, connecting the path of events [Ulbrich et al.,2009]. Methods use different input parameters like mean sea level pressure (e.g., [Lionello et al, 2002, Rudeva and Gulev, 2007; Hanley and Caballero, 2012]), minimum low-pressure level geopotential height [Sinclair, 1994], or low pressure level relative vorticity (e.g., [Catto et al., 2019; Inatsu, 2009; Hodges, 1994; Reboita et al., 2018]). Ulbrich et al. [2009] pointed out that schemes that detect extratropical cyclones using mean sea level pressure may produce unreliable results over high ground due to the effects of vertical extrapolation and the real orography in reanalysis datasets. Moreover, Hodges et al. [2003] explained that vorticity data is more focused on the wind field, giving more information on the high-frequency synoptic scale, while sea level pressure data is linked to the mass field and represents the low-frequency scale better.

In addition to choosing the best meteorological variable that identifies the position of the cyclones, other restrictions must be considered. One of the challenges is to track the events when several grid points can be considered the next location of a cyclone. There are methods that apply an across-time “nearest neighborhood” approach to connect the identified cyclone centers of two consecutive time step with the nearest neighbors [Blender and Shubert, 2000; Trigo, 2006], other studies apply algorithms based on displacement speed [Murray and Simmonds, 1991; Hanley and Caballero, 2012] and, innovating, Inatsu [2009] uses connected-component label technique (CCL) to connect cyclone as areas that overlap in consecutive time steps. Another step to improve the selection of centers of cyclones is applying spatial filters, usually a mean filter. Flauonas et al. [2014] tested three degrees of spatial filtering, in order to capture the physical characteristics of cyclones. Also, in order to remove spurious or very short-lived systems in cyclone identification schemes, the minimum lifetime of events can be selected, with values of 12 h [Hanley and Caballero, 2012], 18 h [Rudeva and Gulev, 2007] or 24 h [Trigo, 2006; Flauonas et al., 2014; Lim and

Simmonds, 2007; Wang et al., 2006; Pinto et al., 2005]. Table 5.1 shows a list of relevant extratropical cyclones detecting and tracking methods, all based on objective criteria. Some of these methods were designed upon a coarser spatial and temporal resolution dataset, compared to those available today. Furthermore, the difference between the methods reflects the multiple understandings of what best characterizes a cyclone.

Table 5.1. Relevant extratropical cyclone detecting and tracking methods.

References	Variable Used to Identify	Main Characteristics
Blender and Schubert, 2000; Trigo, 2006	Local minimum of the geopotential height of the 1000-hPa surface	Nearest-neighbor search method
Crawford and Serreze, 2016; Crawford et al., 2021; Hanley and Caballero, 2012; Lionello et al., 2002	Minimum mean sea level pressure	Nearest-neighbor search method
Murray and Simmods, 1991; Simmons and Keay, 2000, Lim and Simmonds, 2007; Pinto et al., 2005; Rudeva and Gulev, 2007	Minimum mean sea level pressure	Estimate the subsequent displacement and pressure change
Reboita et al., 2010; Reboita, 2017	Relative vorticity of the 925 hPa surface	Nearest-neighbor search method
Inatsu, 2009	Relative vorticity of the 850 hPa surface	Area under a threshold
Flauonas et al., 2014	Relative vorticity of the 850 hPa surface	Most natural evolution of relative vorticity field
Hewson and Titley, 2009	Mean sea level pressure and relative vorticity	Graphical processing

Cyclone detection and tracking are highly complex [Neu et al., 2013], and differences in results can occur depending on the methodology or the dataset. The first efforts to intercompare tracking and detection methods of extratropical cyclones and reanalysis datasets were from Trigo et al. [2006], who compared results from ERA-40 and NCEP/NCAR reanalysis and Raible et al. [2008], who compare three different cyclone detection and tracking schemes with different

reanalysis datasets. They identify differences in terms of the number of cyclones and cyclone intensity. However, their interannual variability and number of more intense events agreed. A project named Intercomparison of Mid-Latitude Storm Diagnostics (IMLAST) was created to identify uncertainties related to the choice of method [Neu et al., 2013]. Using the same input dataset, a minimum life cycle of 24 h and 6-h intervals, they concluded that the consistency across the methods is generally higher for deep cyclones. The periods of development and cyclolysis diverge over the methods; however, the most intense part of the life cycle is similar. The number of cyclone centers differs, but overall they agree in terms of interannual variability and geographical distribution, with some exceptions, such as in the Mediterranean. Comparing the hemispheres, the distribution of cyclone density is more zonally symmetric in the Southern Hemisphere than in the Northern Hemisphere, because of the larger land mass and the topographic features in the latter [Simmond and Keay, 2000]. Recently, Reale et al. [2019] compared the identification of cyclones of explosive activity by a group of methods and found that the area of greatest activity of these explosive cyclones agreed with previous studies, despite the huge spread in the number of explosive cyclones identified. Gramcianinov et al. [2020] compared the results of Atlantic extratropical cyclones characteristics using two different datasets and showed small differences in cyclone number and characteristics and divergences in the intensity distributions.

The objective of this study is thus to implement an easy way to identify, track and characterize extratropical cyclones, using a gaussian filter, which provides a more delicate filtering of the contours. Moreover, the technique identifies events with CCL, which is recognized as a good method in the literature. An important contribution of this work is to generate a cyclone identification and track database to understand the modifications of cyclone frequency and intensity over the last decades. This paper provides a description of the methodology as well as tests of sensitivity and performance of individual events to evaluate the algorithm. Also, we compare the results using 1-h resolution and 6-h resolution, extracted from the same dataset and for the same period. To understand the differences with other methodologies, we present the Southern Hemisphere climatology of extratropical cyclones using 40-yr high-resolution ERA5 reanalysis

dataset from the European Centre for Medium-Range Weather Forecasts (ECMWF).

5.2. Materials and Methods

5.1.1. Data

In this study, we use meteorological data from ERA5/ECMWF reanalysis, the fifth generation ECMWF reanalysis for the global climate and weather. According to Hersbach [2021], a major strength of this new reanalysis is the much higher temporal and spatial resolutions than those of previous reanalysis. The horizontal resolution is 31 km, and it has 137 vertical levels, spanning the surface of the Earth to 0.01 hPa, in hourly output, in a regular Gaussian grid (F128). In addition to that, it has improved the assimilation of the reprocessed dataset, with respect to previous products.

We use the relative vorticity data available from ERA5/ECMWF reanalysis to find maximum values of cyclonic vorticity, in vorticity fields at 850 hPa level. The parameter is a measure of the rotation of air in the horizontal, around a vertical axis, relative to a fixed point on the surface of the Earth. In the classical theory (e.g., [Holton, 2004]), the microscopic measure of rotation in a fluid is a vector field, defined as the curl of the velocity of the fluid, resulting its relative vorticity (ζ). From a scale analysis, only the vertical component (ζz) is used, leading to the Equation (1).

$$\zeta_{Z=}\frac{\partial v}{\partial x}-\frac{\partial u}{\partial y} \qquad (1)$$

The corresponding expression in spherical coordinates can be written as Equation (2) form, where u and v are the local zonal and meridional velocities (m/s) respectively, r is the earth's radius, θ is the latitude and λ is the longitude.

$$\zeta_Z = \frac{1}{r\cos\theta}\left(\frac{\partial v}{\partial \lambda}-\frac{\partial u\cos\theta}{\partial \theta}\right) \qquad (2)$$

This study applies the program of identification and tracking of cyclones in the Southern Hemisphere, therefore clockwise rotation (negative relative vorticity) is associated with cyclones. Mean sea level pressure data and 10-m

winds data at grid points (ERA5/ECMWF) are used to characterize the most intense events.

5.2.2. Methods

Basically, three independent steps compose the algorithm: detection of the position of the potential cyclones, linkage of the events and addition of mean sea level pressure and 10-m wind data, to identify the intensity of the events. These three steps are detailed distinctly in the following.

5.2.2.1. Identifying Cyclones

The relative vorticity field is usually very noisy, mainly in low levels of the troposphere. One way to improve the noisy characteristic of the field is applying a preprocessing stage by a spatial filter. Other studies used the B-spline technique [Hodges, 1995], time band-pass filtering [Inatsu, 2009; Hoskins and Hodges, 2002], 1-2-1 filter [Satake et al., 2013] or 1-1-1 filter [Flauonas et al., 2014]. In the present study, we use a multidimensional Gaussian filter (G(x,y)) implemented by scipy.ndimage python package. This filter allows a more delicate smoothing of the orographic and coastal effects and also smooths the maximum local vorticity that is nested with the noisy fields, compared to the medium filter [Gonzales and Woods, 1992]. The degree of smoothing is determined by the standard deviation of the Gaussian (σ). The Gaussian filter is calculated by the Equation (3):

$$G(x,y) = \frac{1}{2\pi\sigma^2} e^{-\frac{x^2+y^2}{2\sigma^2}} \qquad (3)$$

where x and y are the zonal and meridional distances from the point for which the smoothed is calculated. As this parameter increases, the smoothing operation on the relative vorticity field becomes stronger.

After this preprocessing stage, the connected-component labeling technique (CCL) is used. CCL is explained by Samet [1989] and used for extratropical cyclones by Inatsu [2009] and Inatsu and Amada [2013]. In the relative vorticity field, the group of data that satisfies a pre-set threshold is selected for a single time frame. This group represents an area big enough to

attempt the recognized characteristics of extratropical cyclones. At this point, a binary matrix of the relative vorticity field is constructed, with areas that satisfy the threshold. These enclosed independent surfaces are considered possible positions of extratropical cyclones at that time frame. The center of mass (CMa) of each area is calculated (Equation (4)) in a simplified form [Bai and Breen, 2008] to identify the location of the enclosed independent surfaces (a),

$$CM_a = \frac{\sum_{i=N}^{i=1} m_i R_i}{\Sigma m_i} \qquad (4)$$

where (m,R) is the mass and position, respectively, of singles grid points and N is the number of grid points of the enclosed independent surfaces (a). The center of mass from the relative vorticity field indicates that the latitude/longitude position of the area is influenced by the position within the area captured by CCL technique where the relative vorticity is greatest. To further explain, if we imagine a circular area in which the southwest sector has the highest vorticity, the identification position of this area will not be at the central point of the circular area, but will be shifted southwest.

The center of mass will be labeled and treated as a unique possible cyclone position at that time frame. The higher resolution of ERA5 data exposes the noisy characteristic of the relative vorticity field, labeling some enclosed independent surfaces that clearly are not cyclones. To reduce this resolution problem, we simply discarded areas of less than a given limit of grid points.

Therefore, the algorithm's performance up to this step is influenced by the choice of the standard deviation of the Gaussian filter (during the preprocessing stage), the threshold of relative vorticity at 850 hPa and the minimum area attending the threshold that characterizes an extratropical cyclone. In this study, we show the following tests: gaussian standard deviation of 0.5, 1.0, 1.5 and 3.0; threshold of relative vorticity of -10^{-5} s^{-1}, -5×10^{-5} s^{-1}, -10^{-4} s^{-1} and -2×10^{-4} s^{-1} and minimum area of 9, 12, 15 and 18 grid points. The tests of Gaussian standard deviation and different thresholds of relative vorticity at 850 hPa are applied to the relative vorticity field of 1 July 2020, 12 UTC, when strong winds associated with an extratropical cyclone at 35°S and 46°W caused damage on the coast of Southern Brazil. A weaker event was at the Atlantic Ocean, at 50°S and 48°W.

For the minimum area test, the algorithm is applied to 10 years, from 2013 to 2022, and some differences of the choices are discussed.

From these tests, we chose the standard deviation of the Gaussian filter of 0.5, threshold of relative vorticity of -10^{-4} s^{-1} and masked areas less than 15 grid points, at the relative vorticity of ERA5/ECMWF. This step was applied to the Southern Hemisphere, for the whole study period generating a file of possible positions of each extratropical cyclone.

5.2.2.2. Tracking Cyclone Events

Following this step, a link between the time frames is chained. The first independent enclosed area is searched at the following time frame around a defined displacement maximum, that can be adjusted. For this study, we adjust the maximum displacement in 150 km/h, similar to the algorithm of Crawford and Serreze [2016]. Lifetime condition is another typical criterion of extratropical cyclone tracking algorithms. Like in many studies (e.g., [Inatsu and Amada, 2013]), we consider a minimum lifetime of 12 h. It is obvious that a shorter lifetime condition would increase the number of cyclones considerably and a longer one would decrease it. However, we use a minimum lifetime of 12 h to be comparable to other methodologies in the literature.

Cyclogenesis refers to the first-time frame of the emerged event identification. If there is no identification that corresponds to the displacement and lifetime criteria at the next time frame, the label identification is discarded. If it attends the two criteria, the algorithm moves to the next time frame until no identification corresponds to the criteria. Then, the event is selected, and the last time frame indicates the event's end or cyclolysis. Figure 5.1 shows an example of sequence of hourly points center of mass of detected areas that match the relative vorticity threshold. The points of the southwest Atlantic can be selected and connected as an event, because it continues under the maximum displacement for at least 12 h.

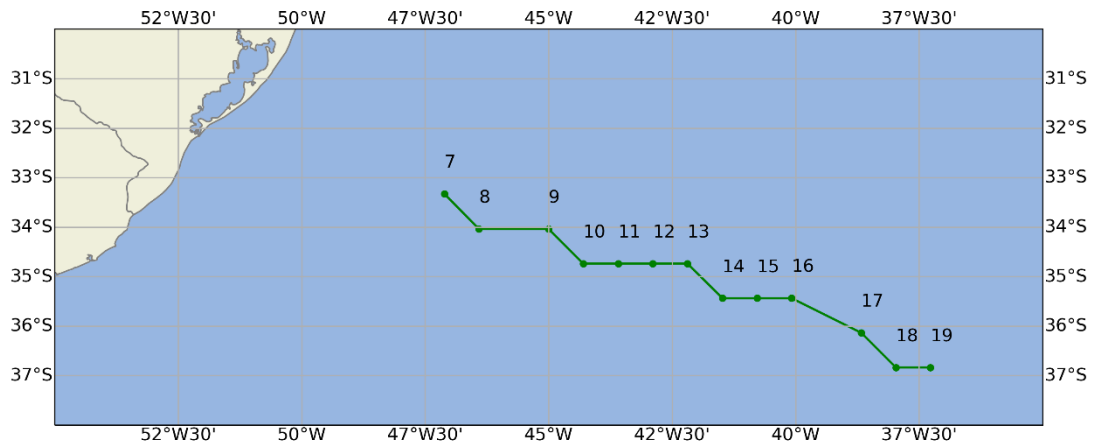


Figure 5.1. Example of points center of mass of areas that match the relative vorticity threshold sequence of hourly data.

These stages generate a list of events with the latitude/longitude of cyclogenesis, position during the following time frame and the latitude/longitude of cyclolysis, with the more intense relative vorticity and the area in grid points, captured by the CCL. This database may be used to understand the frequency of cyclones over a region, areas of cyclogenesis and cyclolisis, the growth rate, as well as select the more intense events of an area.

5.2.2.3. Quantifying Cyclone Characteristics

The minimum mean sea level pressure and maximum 10-m wind associated with all time frames of the events are investigated to characterize each event in terms of intensity. To do this, an “effective area” for each time the cyclone is scanned, centered at the cyclone vorticity center of mass of the area selected by the connected-component labeling technique. It was stipulated that 12 grid points, corresponding to approximately 3.6 latitude/longitude degrees at temperate regions, is a good effective area to characterize the maximum intensity of the events. Figure 5.2 shows, as an example, the effective area of an intense event of 27 October 2016, 6 UTC. The minimum sea level pressure detected was 986.5 hPa, and the maximum 10-m wind was 71.3 km/h. Thus, with this identifying and tracking extratropical cyclone method, the events can be selected by their characteristics, in a subsequent study.

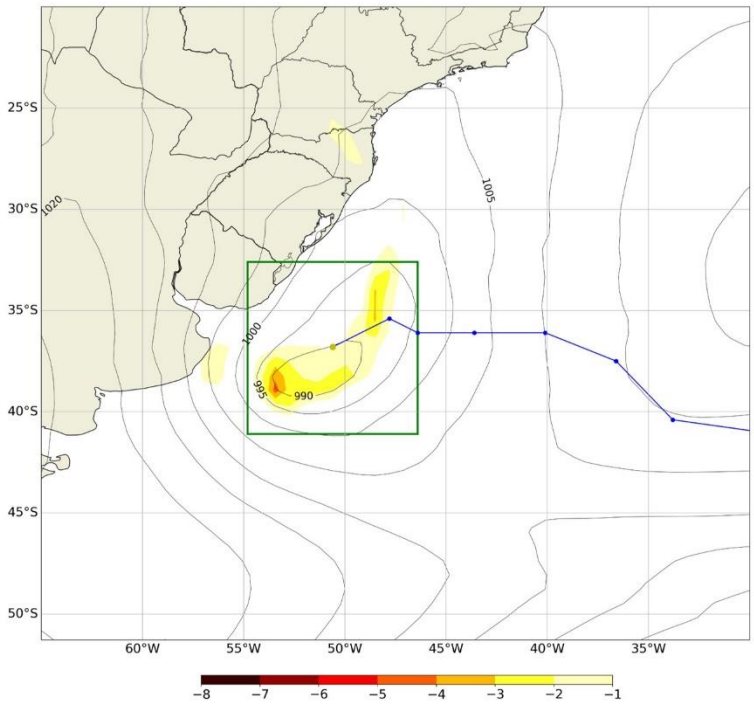


Figure 5.2. Mean sea level pressure and relative vorticity at 850 hPa under -10^{-4} s^{-1}, on 27 October 2016, 06 UTC. The green square is the “effective area” to search for the more intense characteristics of the cyclone. The yellow point is the center of mass identified by the algorithm and the blue line and points are the following time frames of the event.

Part of the area of relative vorticity above the threshold can be out of the effective area. In addition, the center of mass of the area can have a relative vorticity lower than the threshold because of the shape of the area. Other studies have developed different ways to characterize cyclone events in terms of minimum sea level pressure and maximum 10-m winds, considering a circular disk around the maximum vorticity [Flauonas et al., 2014] or the minimum pressure center [Lim and Simmonds, 2007]. However, a fixed area is the simplest choice and an effective alternative for our algorithm.

Figure 5.3 shows the flowchart of the program of identification of extratropical cyclones proposed in this study. In the next section, we present the tests of different levels of filtering, different values of threshold and a sensitivity test of minimum area criteria.

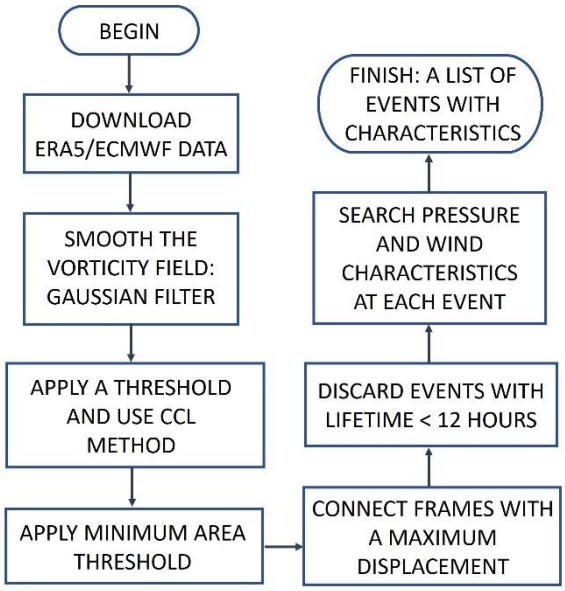


Figure 5.3. Flowchart of the detection algorithm of extratropical cyclones proposed in this study.

5.3. Results

5.3.1. Sensitivity to the Smoothing Parameter for the Relative Vorticity Field

Figure 5.4A shows the mean sea level (contours) and relative vorticity field (shading) obtained directly from ERA5/ECMWF for 1 July 2020, 12 UTC, when an intense extratropical cyclone was near the coast of Uruguay and southern Brazil (35°S/46°W) and another weak cyclone was positioned at 50°S and 48°W. Using standard deviation of Gaussian filter of 0.5 to the same time frame (Figure 5.4B), intense characteristic of coastal cyclone and weak characteristic of the southeast cyclone are preserved. However, tests of sigma equal to 1 (Figure 5.4C) and 3 (Figure 5.4D) over-smoothed the relative vorticity field, to the extent of nullifying the weak event or reducing its area. A test of sigma equal to 5 underestimates the number of cyclones for 2020 (not shown) giving unrealistic results.

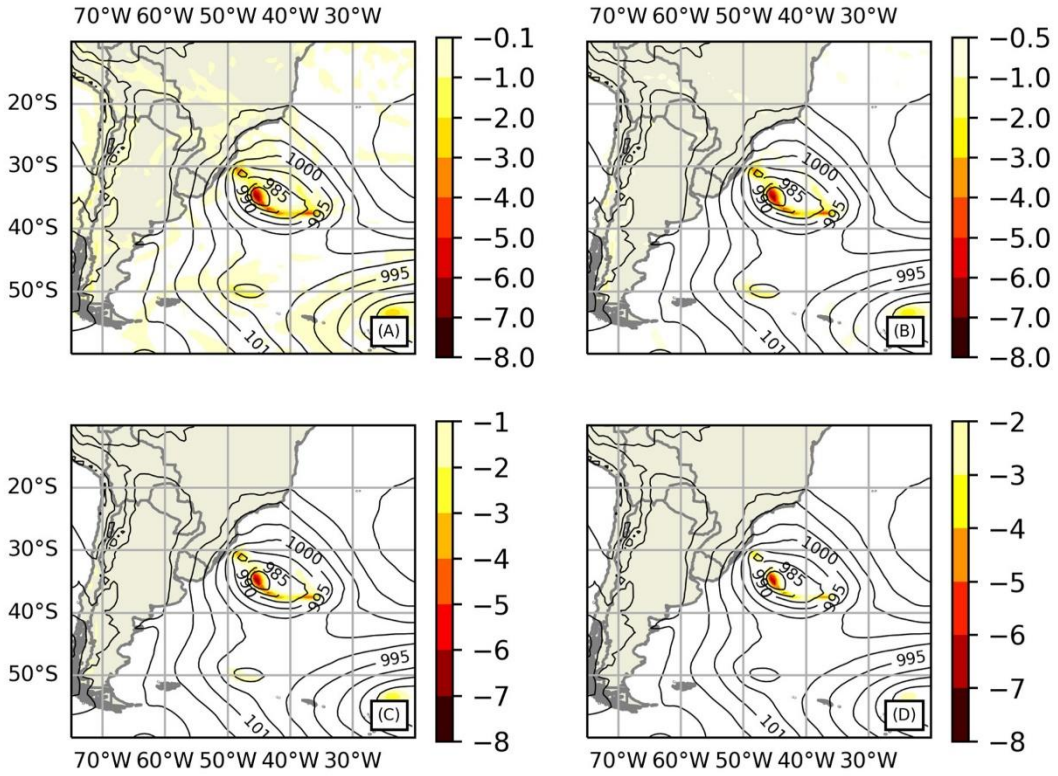


Figure 5.4. Mean sea level pressure and relative vorticity at 850 hPa under -10^{-4} s^{-1}, on 1 July 2020, 12 UTC. (A) raw data and with different standard deviations of the Gaussian filter: (B) 0,5, (C) 1,0, and (D) 3,0.

According to analysis of the relative vorticity field of this known event, it can be seen that weak events are detected just in low level of smoothing, then a more detailed study of the extratropical cyclone features is shown just to 0.5, 1.0 and 1.5 degree of smoothing, applied to 10 years in Figure 5.5. As expected, the number of events depends on the filtering strength, with more events using lower degree of smoothing. Figure 5.5A shows that there are more events of less than two days and Figure 5.5B shows that the mean speed of the events are between 40 km/h and 60 km/h using the three levels of smoothing. These are expected features of cyclones in Southern Hemisphere. The mean count of extratropical cyclones is 2430, 2258 and 1693 using 0.5, 1.0 and 1.5 respectively. Thus, the suppression of events was on average 25%, comparing smoothing level from 1.0 to 1.5, and 7% comparing 0.5 to 1.0. For the following steps, we used a smoothing parameter of 0.5.

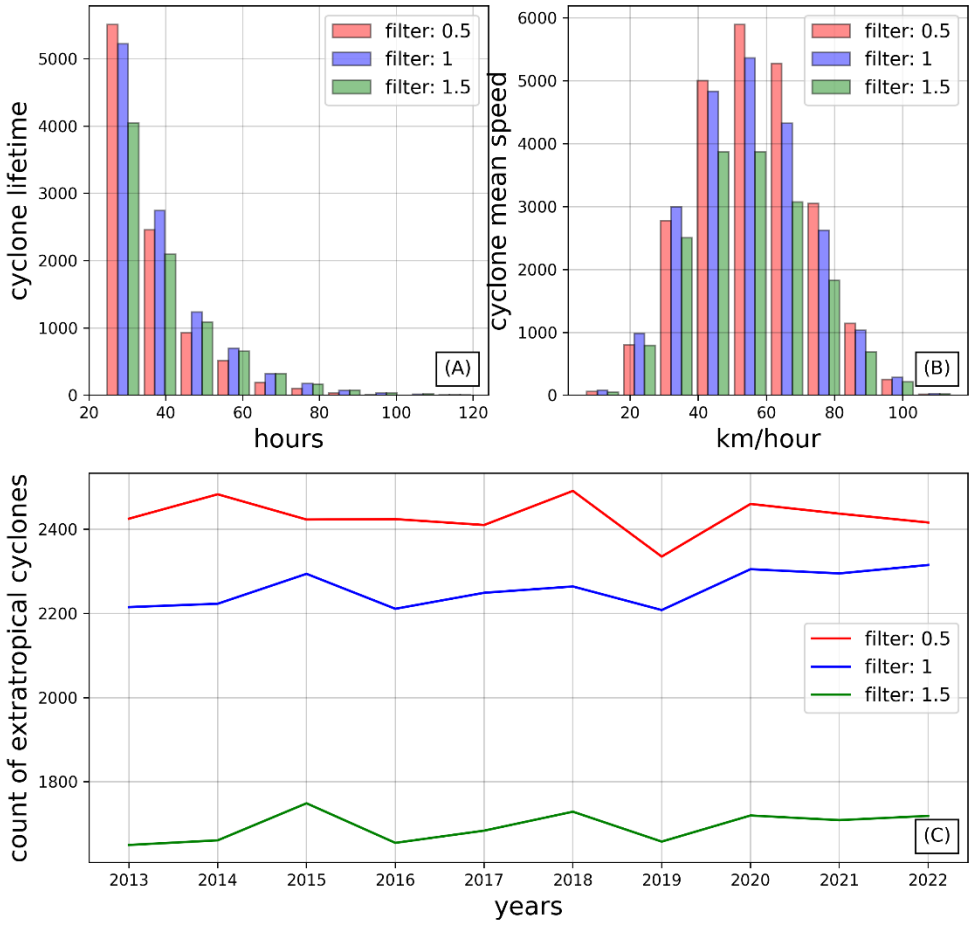


Figure 5.5. Study of the features of cyclones for the three sensitivity tests of filter degree, computed from 2013 to 2022: (A) Frequency distribution of cyclone lifetime, (B) frequency distribution of cyclone mean speed and (C) time series of total annual number of extratropical cyclones.

5.3.2. Sensitivity to Threshold of Relative Vorticity

The choice of the threshold of relative vorticity will calibrate the number of possible cyclone centers and remove signals that are not related to these systems. Figure 5.6 shows the relative vorticity field from ERA5/ECMWF on 1 July 2020, 12 UTC, with the standard deviation of Gaussian filter of 0.5, for four different thresholds of relative vorticity. Figure 5.6A shows a noisy field with a threshold of -10^{-5} s^{-1}. A threshold of -0.5×10^{-4} s^{-1} generates a spurious signal mainly at the Andes (Figure 5.6B). On the other hand, the threshold of 2×10^{-4} s^{-1} (Figure 5.6D) cannot identify the cyclone centers in the region. Then, from the visual analysis of the relative vorticity field, we conclude that a good threshold to identify the events and suppress the spurious signals in our tests is 10^{-4} s^{-1} (Figure 5.6C).

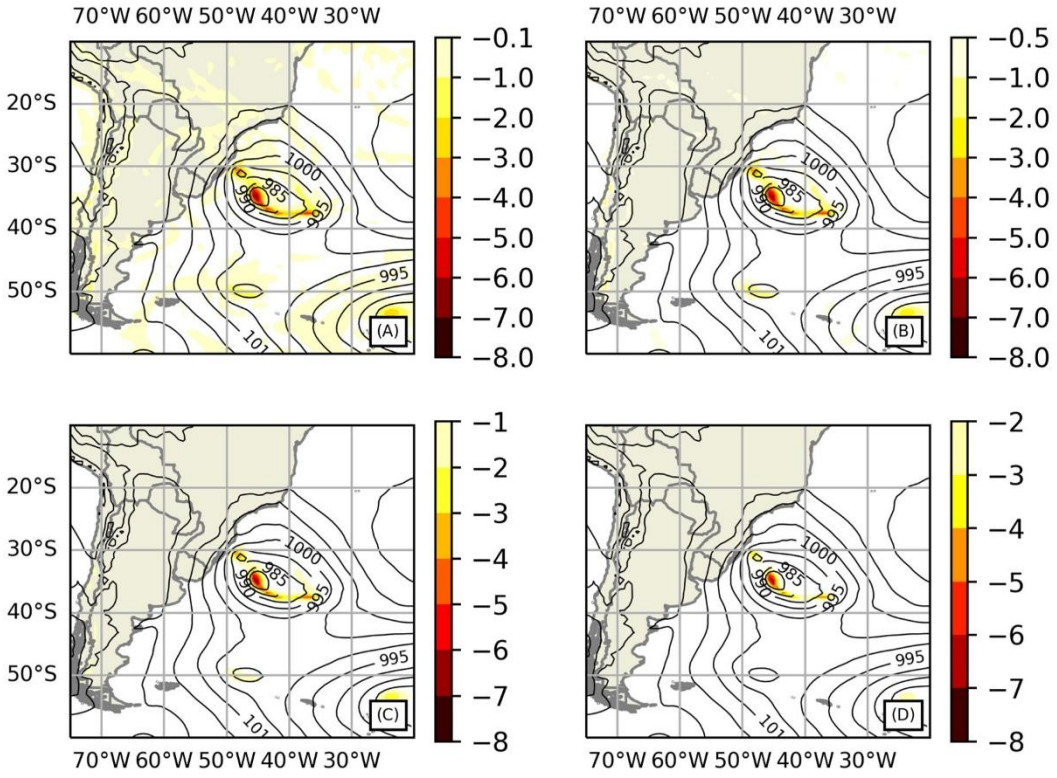


Figure 5.6. Mean sea level pressure (contours) and relative vorticity at 850 hPa (shading) with thresholds of: (A) -10^{-5} s^{-1}; (B) $-0{,}5x10^{-4}$ s^{-1}; (C) -10^{-4} s^{-1} and (D) $-2x10^{-4}$ s^{-1}, on 1 July 2020, 12 UTC, using a Gaussian filter parameter of 0.5.

5.3.3. Sensitivity to the Minimum Area of Relative Vorticity under the Threshold

Figure 5.7 presents the mean monthly cyclone centers detected between 2013 and 2022 using 0.5 of filter parameter, threshold of relative vorticity of 10^{-4} s^{-1} and with different thresholds of minimum area of relative vorticity labels. As expected, the number of cyclone centers per day depends on the choice of the minimum area size. This criterion should be neither so strict as to remove real small cyclones, nor so lenient as to include spurious cyclones. Furthermore, there is an expectation that more events will take place in the winter than in the summer because the large-scale temperature gradients are higher in the winter [Ulbrich et al., 2009]. Using a minimum area of less than 9 points (not shown) yields an unrealistic number of cyclones (more than 1000 per month). It can be an indication that persistent signals are counted as different cyclone events, like those generated by orography. However, Figure 5.7 shows minimum area tests of 9, 12, 15 and 18 points and the expected increase in the number of cyclones in winter is obtained. Moreover, correlation of monthly number of cyclones

between the 9 and 12 tests are 0.983, between 12 and 15 tests are 0.987 and between 15 and 18 are 0.985, suggesting that the results converge around test of minimum area equal to 15.

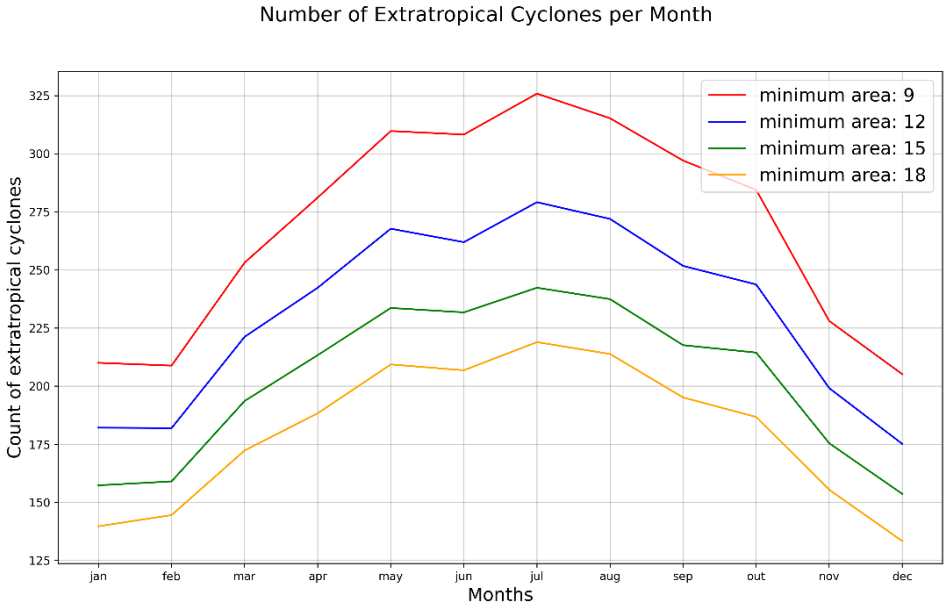


Figure 5.7. Mean Cyclone centers per month detected between 2013 and 2022, using a Gaussian filter parameter of 0.5, a threshold of relative vorticity of -10^{-4} s^{-1} and different sets of minimum area (number of pixels).

Figure 5.8 shows the frequency distribution of cyclone lifetime (A), frequency distribution of cyclone mean speed (B) and the time series of total annual number of extratropical cyclones between 2013 and 2022 (C). Although the number of cyclones detected using the different tests are clearly dependent on the choice of the minimum area criterion, cyclone lifetime and mean speed distribution are similar using the four tests. Table 5.2 shows the mean lifetime and standard deviation in hours and the mean speed mean and standard deviation for the four tests and they have no significant changes on the results. This means that these characteristics of cyclones are not sensitive to the area criteria within this range of values. For the rest of the study, we selected the 15 minimum area criteria as a good choice.

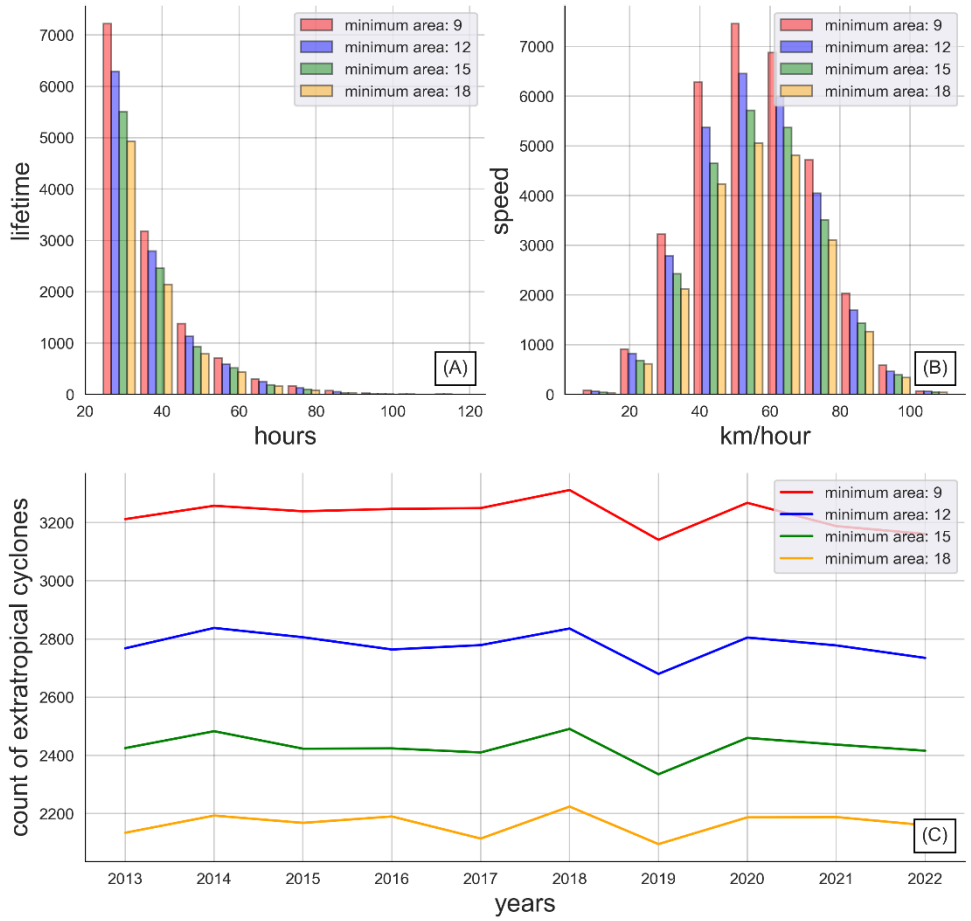


Figure 5.8. Study of the features of cyclones for four sensitivity tests of area criterion, computed between 2013 and 2022: (A) Frequency distribution of cyclone lifecycle, (B) frequency distribution of cyclone mean speed and (C) time series of total annual number of extratropical cyclones.

Table 5.2. Statistics information of lifetime and mean speed of detected cyclones using different minimum area tests.

Minimum Area Test	Lifetime Mean	Lifetime Stadard Deviation	Mean Speed Mean	Mean Speed Standard Deviation
9	24.9	12.6	56.4	16.5
12	24.8	12.2	56.3	16.4
15	24.6	12.0	56.3	16.2
18	24.4	11.7	56.3	16.1

5.3.4. First Case Study: Extratropical Cyclone of 26–28 October 2016

An intense extratropical event in southern Brazil was documented by Albuquerque et al. [2018] and Oliveira et al. [2019], with impacts at Hermenegildo beach (33.7°S, 53.4°W, Figure 5.9A). It was an event of high wave energy, with significant shifts in coastal morphology. The automatic station of Santa Vitoria do Palmar (identified by A899), at 33.74°S/53.37°W (Figure 9A), recorded a maximum wind gust of 111.2 km/h at 17 UTC of 27 October 2016 and a minimum mean sea level pressure of 997.4 hPa at 15 UTC and 16 UTC of 27 October 2016. The cyclone started to develop on 26 October, with lower mean sea level pressure over Uruguay and southern Brazil. Figure 5.9B shows the storm track identified by the algorithm (blue line) and identified by a visual inspection of the pressure field (green line). The evolution of the cyclone track from the algorithm agrees relatively well with that from the visual detection. Figure 5.9C, 5.9D show the similarity of the visual field inspection and the algorithm results (green point) and the location of the extratropical cyclone at the initial frame (20 UTC 27 October) and during the more intense stage (16 UTC on 27 October) respectively. Figure 5.9E, 5.9F show the evolution of cyclone intensity by the maximum 10-m winds, minimum mean sea level pressure, maximum relative vorticity detection and the size of vorticity above the threshold at each time frame. All the parameters show the intense period between 12 UTC on 27 October and 03 UTC on 28 October. The last time frame has strong winds, low mean sea level pressure and intense relative vorticity, which may be associated with a loss of the cyclolysis process. These results suggest that our algorithm had the best accuracy at the initial stage and during the intense period of the cyclone for the case study.

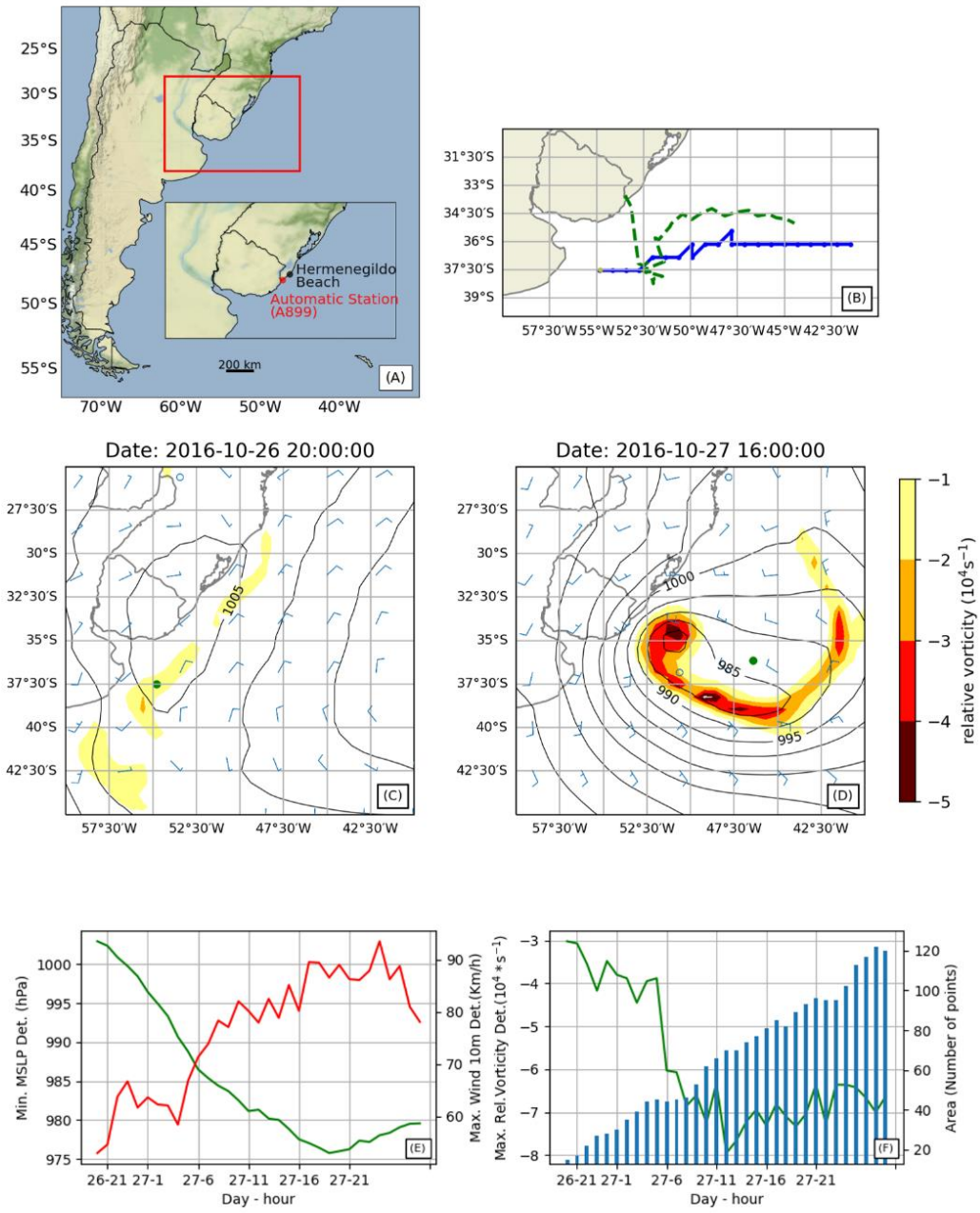


Figure 5.9. Extratropical cyclone during 26 to 28 October 2016. (A) Location of Hermenegildo Beach and automatic station of Chui (A899). (B) Cyclone track from 26 October 2016, 20 UTC to 28 October 2016, 6 UTC obtained from the program (blue line) and visual inspection (green line). (C) Mean sea level pressure and relative vorticity at 850 hPa, on 26 October 2016, 20 UTC, the green point is the position obtained from the algorithm. (D) Same as (C) except for: 27 October 2016, 16 UTC. (E) Minimum mean sea level pressure (green line) and maximum 10-m wind (red line) detected by the algorithm during the event. (F) Minimum relative vorticity (green line) and total area under the threshold (blue histograms) detected by the algorithm during the event.

5.3.5. Second Case Study: Extratropical Cyclone of 15–17 August 2020

The second case study has the important feature of merging with another low-pressure center. When two or more neighbouring cyclones merge or split, the recognition of the cyclone trajectory becomes more difficult [Lu, 2017]. There is an improvement in recognizing merging or splitting extratropical cyclones by using techniques such as connected-component label (e.g., [Hanley and Caballero, 2012; Inatsu, 2009; Hewson and Titley, 2009; Lu, 2017]). Figure 5.10A shows the storm track identified by the algorithm (blue line) and that identified by a visual inspection (green line), using sea level pressure field. Both tracks converge over all stages of the cyclone lifecycle. The extratropical cyclone developed over the southwest Atlantic at 20 UTC on 15 August 2020 (Figure 5.10B). Figure 5.10C shows the event in the more intense stage, with a maximum relative vorticity of $-8.6\ -10^{-4}\ s^{-1}$. Along the southeastward displacement, it started to merge at 00 UTC on 17 August 2020. Figure 5.10D shows the event on the merged stage.

Figure 5.10E, F present the evolution of minimum sea level pressure, maximum 10-m winds, maximum relative vorticity at 850 hPa and total area above the threshold over the cyclone time frames. A minimum mean sea level pressure and a maximum area above the threshold occurred during the last hours of 16 August. However, the maximum winds and more intense relative vorticity was during the early hours of the event. This can be a consequence of the merging process just before the weakening that is observed during cyclolysis. In the subsequent time frame, the algorithm maximum displacement part promoted the end of the event. Possibly part of the decay process of the event was not included by the program, due to the increase in area within the threshold, which displaces the calculated center of mass, making the dissolution phase shorter. These two events highlight the ability of the method to track the cyclogenesis process and the more intense stage of the events and a possible suppression of part of the cyclolysis stage.

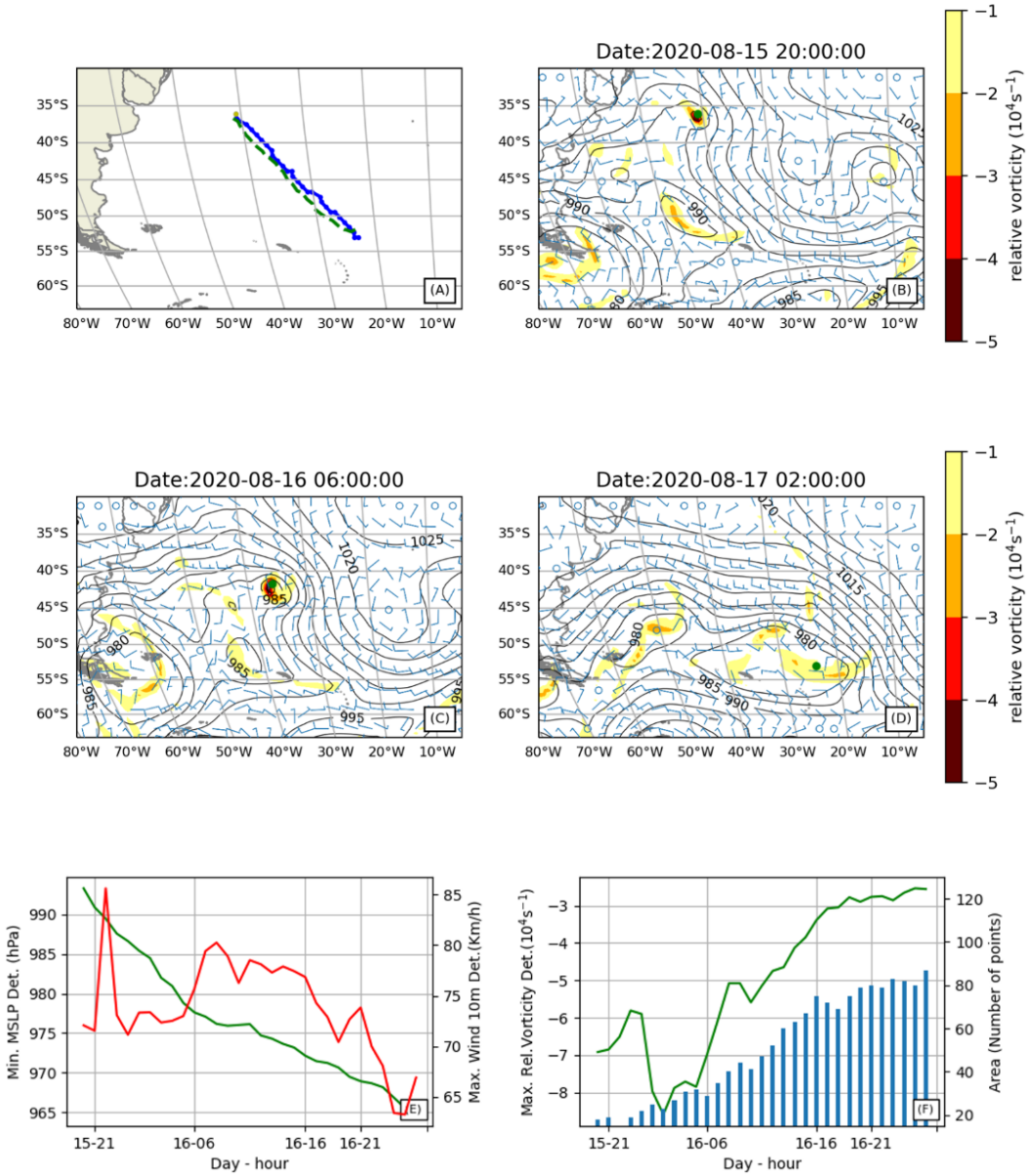


Figure 5.10. Extratropical cyclone of 15 to 17 August 2020. (A) Cyclone track from 15 August 2020, 20 UTC to 17 August 2020, 06 UTC, obtained from the algorithm (blue line) and from visual inspection (green line). (B) Mean sea level pressure and relative vorticity at 850 hPa, 15 August 2020, 20 UTC, the green point is the position obtained from the algorithm. (C) Same as (B) except for: 16 August 2020, 06 UTC. (D) Same as (B) except for: 17 August 2020, 02 UTC. (E) Minimum mean sea level pressure (green line) and maximum 10-m wind (red line) detected by the algorithm during the event. (F) Minimum relative vorticity (green line) and total area under the threshold (blue histograms) detected by the algorithm during the event.

5.3.6. Temporal Resolution

We expect that the finer the temporal resolution, the better the tracking process because the search in the following time step is done within a shorter time gap, and a shorter radius of searching if the propagation speed does not

change [Blender and Shubert, 2000]. Another implication of using higher time resolution data is that the cyclones are weaker on the average, because weaker systems with shorter tracks are not identified in coarser time resolution data [Pinto et al., 2005]. However, Crawford et al. [2021] examined the sensitivity of cyclone detection and tracking for the Northern Hemisphere and showed that refining beyond 3 h does not necessarily lead to more accurate detection and tracking, using the algorithm explained by Crawford and Serreze [2016] applied to finer temporal resolution dataset.

In addition to this, most climatology is constructed based on 6-hourly atmospheric fields. Gramcianinov et al. [2020] compared the 6-hourly and 1-hourly tracking using the same tracking method and thresholds. The results showed a higher genesis density in Uruguay and a smaller density in southern Brazil, using 1-hourly data. According to the authors, this difference can be associated with the identification of the cyclonic systems at earlier stages of development using 1-hourly data.

Our study compares the cyclone tracking performance using 6-hourly and 1-hourly datasets. Figure 5.11 shows the frequency distribution of cyclone lifetime, cyclone mean speed and the count of extratropical cyclones per year from 1982 to 2022, with 1-hourly and 6-hourly temporal resolution. Crawford et al. [2020] detached that changing from 6-hourly to 1-hourly resolution shorter events are more inclined to late detection or early termination and explained that this leads to a grow of short-lived events. The same influence was observed in ours results, that is more events of less than two days using 1-hourly resolution. In terms of mean speed, although the mean values are similar, the frequency distribution is more dispersed using 1-hourly resolution, with a standard deviation of 21.2 km/h to 1-hourly and 15.3 km/h to 6-hourly resolution. The time series of total annual number of extratropical cyclones for the two resolutions, applied to 41 years (Figure 5.11C) show an increasing tendency. The coefficient of determination is of 0.56 and 0.77 for 6-hourly and 1-hourly resolution, respectively.

Violin plot of extratropical cyclone tracking in Southern Hemisphere for the period of 1982–2022 (Figure 5.12A) highlights that 1-hourly temporal resolutions

has more events per year than 6-hourly resolution, with an average of 2314 for the 1-hourly dataset and 1750 for the 6-hourly dataset.

Considering the period of 1982 to 2022, the duration of the events using 1-hourly and 6-hourly datasets has analogous difference to the frequency distribution of lifetime, with an average of 24 h from the former and 49 h for the latter (Figure 5.12B). One explanation to this difference could be a premature termination of tracks and/or split of two tracks in situations that would be continued if analyzed manually by a meteorologist. These issues can be addressed in a future improvement of the program. Heading of Figure 5.12C, track length in km tends to be shorter using the finer temporal resolution dataset, because the search of the next frame has a shorter time gap, and this implies more details along the cyclone track, with more events of short lifetime and short distance traveled included in the group of events. The track distance averages from 1355 km using the 1-hourly dataset to 2224 km using 6-hourly dataset. The third quartile also shows a difference, with 1628 km and 2917 km using 1-hourly and 6-hourly dataset resolution, respectively.

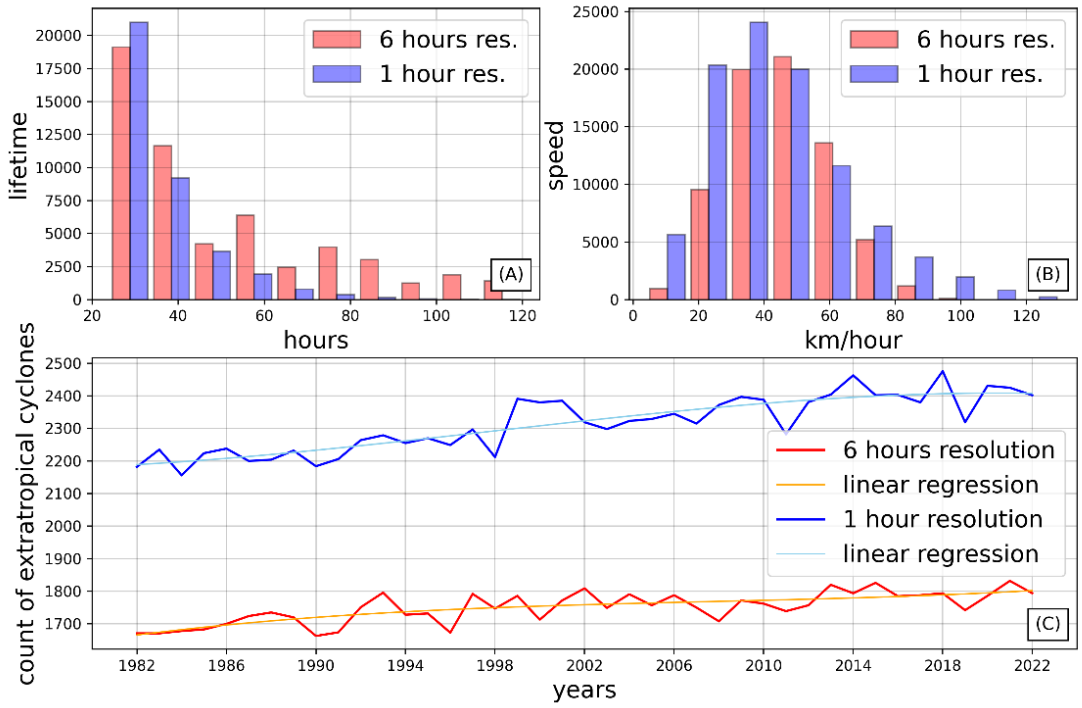


Figure 5.11. Study of the features of cyclones in the Southern Hemisphere using 1-hourly (blue) and 6-hourly (orange) temporal resolutions, for the period of 1982–2021: (**A**) Frequency distribution of cyclone lifecicle, (**B**) Frequency distribution of cyclone mean speed and (**C**) time series of total annual number of extratropical cyclones.

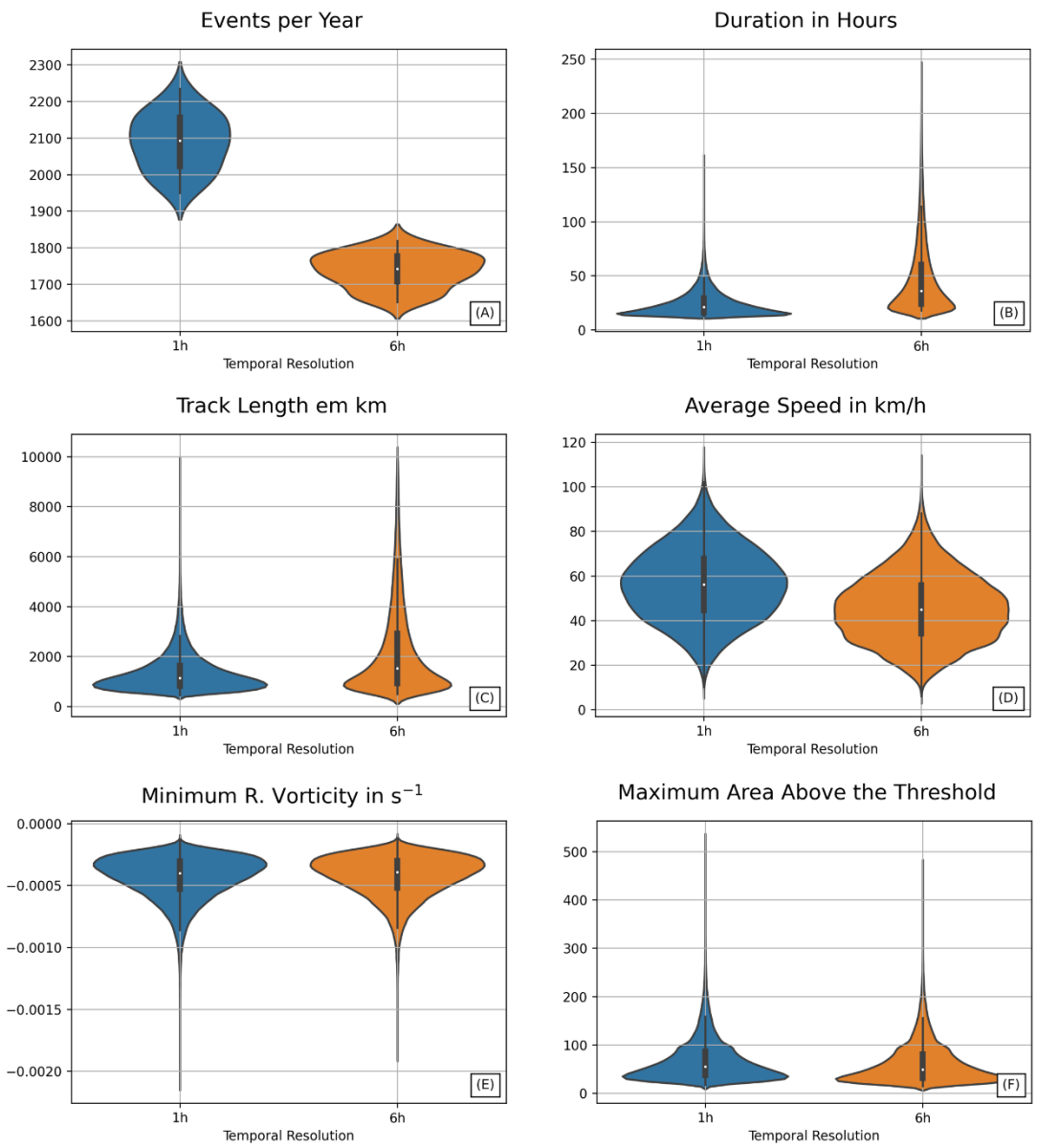


Figure 5.12. Violin plot of extratropical cyclones tracking in the Southern Hemisphere using 1-hourly (blue) and 6-hourly (orange) temporal resolutions, for the period of 1982–2022. (**A**) Events per year. (**B**) Duration in hours. (**C**) Track length in km. (**D**) Average speed in km/h. (**E**) Minimum relative vorticity of events in s^{-1}. (**F**) Maximum area with relative vorticity under the threshold.

The evaluation of cyclone speed (Figure 5.12D) shows similar average values using the 6-hourly dataset comparing to those obtained by IMILAST intercomparison project. However, the average speed 56 km/h using the 1-hourly dataset is slightly higher than that from the 6-hourly dataset (46 km/h) and IMILAST intercomparison project. This can be explained by the inclusion of faster

cases, with finer temporal resolution and the more disperse distribution shown in Figure 5.11B.

Focusing on the intensity of the events, Figure 5.12E shows the relative vorticity minimum at 850 hPa, identified using the two temporal resolutions. The averages are -4.4×10^{-4} s^{-1} and -4.3×10^{-4} s^{-1} for the 1-hourly and 6-hourly datasets, respectively. As expected, using the 1-hourly resolution, the algorithm is more efficient in finding the most intense events, indicated by the elongated range of values in the violin plot. In terms of the average of the area with relative vorticity above the threshold (Figure 5.12F), the two temporal resolutions are similar, 106 and 95 for the 1-hourly and 6-hourly dataset, respectively. When using the finer resolution, the algorithm captures slightly larger areas.

5.3.7. Extratropical Cyclone Climatology

Generally, studies using different methodologies of detecting and tracking of extratropical cyclones present the number of cyclone centers, either by month or season, and per unit area over a hemisphere. This is called system density by Simmonds and Keay [2000]. When these results are presented as a percentage of the total time, it is usually called cyclone frequency or cyclone density [Neu et al., 2013]. Most of the previous studies use different 6-hourly reanalysis datasets. To determine the robust features among the different methodologies, the IMILAST project compiled climatologies of cyclone frequency over the same period (20-yr period), with the same time resolution (6 hourly), and the same dataset (ERA Interim/ECMWF dataset, with 1.5° spatial resolution), with the same minimum lifetime of 24h [Neu et al., 2013], for both hemispheres. Here, we compare the results obtained from our algorithm with those from the IMILAST project and other studies, taking into consideration that our study uses a different dataset, with higher temporal and spatial resolution, for a longer period. So, we intend to present the similarities and differences with these assumptions in mind.

Figure 5.13 shows the mean number of cyclogeneses per month, with a cap area of 10^6 km^2 in the Southern Hemisphere for the four seasons. It is evident that the greatest number of cyclogeneses occurs along the 70°S–50°S latitude band, which agrees with Simmonds and Keay [2000]. Consistent with previous studies and as expected, the frequency and spatial extent of cyclogenesis are

higher during winter. Our methodology also reproduces the absence of cyclogenesis west of the Andes and an intensification of cyclogenesis along the southeastern coast of South America [Gan and Rao, 1994; Vera et al., 2002]. As the perturbation crosses the Andes at middle latitudes, the lower-level perturbation advances following the orography and propagates on the lee side of the Andes, detached from the upper-level perturbation and suppressing the instability. Approaching the southeastern coast of South America, the perturbation encounters a more favorable baroclinic structure, promoting cyclogenesis. The strong region of cyclogenesis observed in the coastal area of Antarctica was also observed by Treut and Kalnay [1990], Murray and Simmonds [1991], Hodges [1995], Simmonds and Keay [2000], Hoskings and Hodges [2005] and Valsangkar et al. [2019].

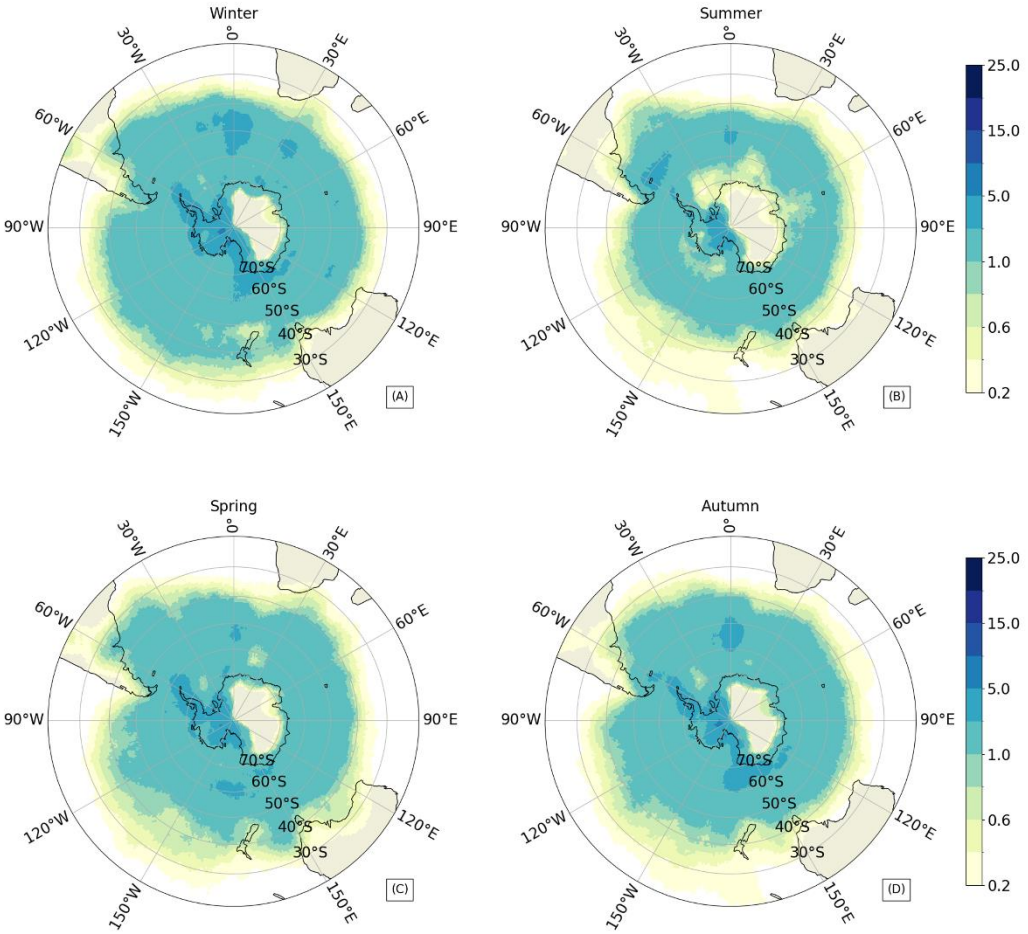


Figure 5.13. The average number of cyclogeneses per month in the Southern Hemisphere, with a cap area of 10^6 km^2. (**A**)Winter: June, July and August, (**B**) Summer: December, January and February, (**C**) Spring: September, October and November, (**D**) Autumn: March, April and May.

5.4. Discussion and Conclusions

In this article, we presented an algorithm to detect and track extratropical cyclones, studying the choice of parameters for the ERA5 reanalysis, in the Southern Hemisphere. To identify cyclonic centers, we use relative vorticity at 850 hPa and connected-component labeling, which tracks cyclones as areas rather than local minimums. We tested the use of three degrees of filtering smoothing of gaussian filter to determine the ideal level of filtering for the best detection of cyclones. Also, we showed an example of relative vorticity field at 850 hPa, using different thresholds for relative vorticity and tested four different values of minimum area criteria. With these analyses, we adjusted within the algorithm to improve its performance. We use standard deviation of the gaussian filter of 0.5 grid points, threshold of relative vorticity of -10^{-4} s^{-1}, and area criteria of 15 pixels. The maximum displacement in one hour was fixed to 150 km.

The two case studies presented here highlighted the good performance to detect cyclogenesis and the more intense periods of the cyclones and identify cyclones that merge/split along their lifetime. However, the position of the cyclone center during the cyclolysis can be inaccurate, because of the increase in the area within the threshold, possible suppressing part of the dissipation process, as shown by the second case study. Despite these findings, we believe that the algorithm is useful for studying extratropical cyclones and exploring the different characteristics of the events.

Comparing the results using 1-hourly and 6-hourly temporal resolution, we find a greater average number of events per year using 1-hourly temporal resolution. This can be explained by the greater precision in identifying the time frame of cyclogenesis and cyclolysis with a finer resolution, and by the inclusion of some shorter events that would have been removed by the minimum lifetime threshold. Using 41 years of data, the annual count of extratropical cyclones of Southern Hemisphere displayed a slowly increasing trend in both temporal resolution. The duration of the cyclones of around 2 days is slightly larger using 6-hourly temporal resolutions, but it is in agreement with Neu et al. [2013], which compares various methodologies using 6-hourly resolution dataset. The distance traveled by the cyclones was a little longer using the 6-h temporal resolution due

to the removal of shorter cases. The cyclones captured by 1-h temporal resolution are in average faster than those by the 6-h temporal resolution. Our 6-h temporal resolution results agreed with IMILAST in term of average speed, mainly ranging from 20 km/h to 60 km/h.

The spatial distribution of cyclogenesis frequency from our algorithm is very similar to those from other studies, in particular with regard to the most favorable areas of development of extratropical cyclones. In general, the number of events is consistent with previous studies, although there is no consensus on this among the various methods, as shown by the IMILAST project. In terms of areas of suppression and intensification of cyclogenesis in the Southern Hemisphere, our results are consistent with previous studies. Further improvements to the algorithm can be made, such as including different parameter thresholds at different altitude levels. The algorithm was implemented in Python, and its source code is freely available from the authors upon request.

Future research using the methodology developed in this study includes understanding the interannual variability of the characteristics of extratropical cyclones along the southeastern coast of South America and potential links to extreme events of ocean temperature, known as marine heatwaves.

Capítulo VI: Caracterização e Variabilidade de Ciclones Extratropicais no Sudoeste do Oceano Atlântico

Em síntese, esse capítulo apresenta as características gerais dos ciclones extratropicais atuantes no Sudoeste do Oceano Atlântico. Além disso, analisa a variabilidade interanual da frequência de ocorrência de ciclones extratropicais, para cada estação do ano e dividindo a área em dois segmentos, de acordo com a latitude de 35°S. Foi investigada a tendência dos eventos, tanto na perspectiva anual como por estação do ano. A análise da variabilidade revelou os períodos de maior significância para a série de dados, para cada estação do ano e região de formação, de acordo com a latitude de 35°S.

Os eventos mais intensos com respeito a pressão ao nível do mar mínima e ao vento em 10-metros máximo e os eventos mais rápidos foram estudados. Uma análise mais aprofundada dos campos meteorológicos precursores dos 14 eventos que atingiram simultaneamente os dois parâmetros de intensidade e se formaram próximo à costa do Uruguai e sul do Brasil foi realizada.

Esse estudo ofereceu uma nova perspectiva dos ciclones extratropicais que atuam no sudoeste do Oceano Atlântico, contribuindo para melhorar a compreensão da variabilidade e características distintas destes eventos nas últimas décadas.

O manuscrito é de autoria de Carina K. Padilha Reinke, Jeferson P. Machado, André L. Brum, José Luiz L. de Azevedo, Maurício M. Mata e Jaci M. B. Saraiva, intitulado **"Characterization and Variability of Extratropical Cyclones in the Southwest Atlantic Ocean**". Foi submetido no periódico **"Advances in Meteorology"** e está em fase de revisão.

Abstract

Extratropical cyclones are key features that contribute to changes in precipitation, wind and temperature in midlatitudes, sometimes causing extreme conditions. Despite the southwest Atlantic Ocean being recognized for cyclone formation and intensification, several aspects of the spatial and temporal variability remain unclear. Hence, in this study, the overall characteristics of cyclones that form within the southwest Atlantic Ocean are investigated. We also analyze the interannual variability in the frequency of cyclone occurrences across each season. To accomplish this, we use dataset from hourly ERA5/ECMWF reanalysis spanning in 41 years. The results showed an enhanced interannual variability, which fit with a cubic regression for the whole study area, as well as for the northern and southern part of the area, according to the 35° S of latitude. Seasonally, we found a positive trend of 1.7 per decade in cyclone occurrences for the southern part of the area, during summer, with a statistical significance of 95%. The Fourier analysis revealed an energy peak at 2-3 years in the northern part during winter, as well as in the whole area during spring, summer, and autumn. Additionally, important peaks at 5-year, 6-year and 8-10-year periods were observed. Moreover, we investigated extreme events and found that those selected by the minimum sea level pressure are more concentrated south of intense events by 10- meter winds. The composites of meteorological fields during intense cyclones that formed near the coastal area suggested that the equatorial entrance of the upper-level jet stream is a preferential condition for develop intense events. In addition, our analysis revealed the importance of a wide-ranging meridional moving trough in the upper and middle-levels troposphere, and the relevance of the moisture transport via northwest low-level jet from the tropics to the coastal area inducing the intense cyclones in the southwestern Atlantic region.

Keywords: extratropical cyclones; interannual variability; Southwest Atlantic Ocean.

6.1. Introduction

In the midlatitudes, weather changes are often controlled by the migration of extratropical cyclones and fronts [Kunkel et al., 2012]. These events induce heavy precipitation eventually causing floods, strong surface winds, wind gusts, storm surges and marine storminess (e.g. [Parise et al., 2009]). Regarding to coastal area, intense extratropical cyclones can cause large amplitude waves and abrupt changes in the coastal landscape (e.g. [Almeida et al., 2011; Albuquerque et al., 2018; Gramcianinov et al., 2018]). On the global scale, extratropical cyclones are a key factor in midlatitude atmospheric circulation, due to its capability to transport heat, moisture, and momentum (e.g., [Eichler and Gottschalck, 2018; Sinclair et al. 2020]). Several studies have focused on understanding climate characteristics, trends, and variability of cyclones in a local perspective (e.g., [Laurila et al, 2021; Zhang et al., 2019]). Moreover, recent studies analyze the cyclones' response to a warmer environment, seeking to anticipate future changes in extratropical cyclones frequency (e.g., [Sinclair et al., 2020; Zhang et al, 2019; Fyfe, 2003; Shaw et al., 2016]).

To objectively identify extratropical cyclones in large datasets, many studies developed automatic detection and tracking schemes on a gridded map by using reanalysis and global model data. Thus, a spread of results was found due to the different datasets and different measures of cyclone activity [Ulbrich et al., 2009; Pérez-Alarcón et al., 2024; Andrade et al, 2024]. Raible et al. [2008] applied three different algorithms to the same dataset and highlighted that a trend analysis of cyclone characteristics can be sensitive to the choice of cyclone detection and tracking schemes. To address the main results of different methods in a unique set-up, several institutions created the Intercomparison of Mid Latitude Storm Diagnostics project (IMILAST) [Neu et al, 2013; Hewson and Neu, 2015]. They concluded that the definition of the algorithm applied will set the count, lifetime and intensity of the cyclones. However, deep cyclones and the largest life cycle are consistent among the different methodologies, and there is a good agreement of interannual variability and geographical distribution.

Many authors have focused on extratropical cyclones formed in the Southwest Atlantic Ocean, especially on the impacts over the southeast America population and environment. It is well known that southeastern South America is a main cyclogenesis area (e.g., [Simmonds and Keay, 2000; Reboita et al., 2010]). The baroclinicity, defined as the slope in constant pressure surfaces with respect to surfaces of constant density [Peixoto and Oort, 1992], is the main source of energy that develop synoptic scale disturbances at midlatitudes [Holton, 2004]. Vera et al. [2002] analyzed synoptic-scale waves over the cold season and discovered that cyclonic perturbations display significant modifications over South America midlatitude, with lower-level perturbations following the shape of the Andes Mountains and upper-level perturbations mostly unaffected when moving eastward. From this misalignment, the cyclone formation is suppressed in the vicinity of the orography and favored on the lee side, where the perturbations acquire a typical baroclinic wave structure [Gan and Rao, 1991; 1994]. Mendes et al. [2009] found that winter events have a total displacement frequency better distributed than the other seasons. Crespo et al. [2020] analyzed the cyclogenesis conditions in the central-eastern South America and highlighted the importance of upper-level potential vorticity streamers and cutoff for a better understanding of cyclogenesis. Dalanhese et al. [2023] identified a low-frequency decade-to-decade seesaw of lee and coastal cyclogenesis and related the occurrence of variations to anomalies of ocean temperature.

The impacts of extratropical cyclones over the coastal area have been examined by Parise et al. [2009] and Simões et al. [2022]. These studies highlight the correlation between meteorological tides and coastal erosion in the southern regions of Brazil with the proximity of extratropical cyclones to the coastline. The strong winds generated by these cyclones can induce significant alterations to the coastline, contributing to events of coastal erosion and meteorological tides.

Sinclair et al. [2020] utilized Aquaplanet [Medeiros, 2016] simulations to analyze changes in cyclone patterns in a warmer environment finding that the cyclone lifetime did not change in this condition and that the count of events per year decreased about 3.3%. According to the latest IPCC report [IPCC, 2023] there is a large uncertainty in projected frequencies and preferred locations of

extratropical cyclones. As outlined by Catto et al. [2019], a decrease in cyclone frequency could be related to changes in baroclinicity and a pole ward shift of the upper-level polar stream jet, which can contribute to intensified precipitation patterns. Nevertheless, it is imperative to conduct more thorough regional assessments of these changes. Reboita et al. [2018;2021], using the Regional Climate Model version 4 (RegCM4) [Giorgi et al., 2012], identified a statistically significant decrease in cyclone frequency towards the end of the century across the southwestern Atlantic Ocean.

The aim of this study is to provide a comprehensive characterization of extratropical cyclones within the southwest Atlantic Ocean, with a specific focus on investigating their interannual variability in terms of frequency and seasonal patterns. To understand the dynamics of intense cyclonic events, we analyze annual cyclone counts during four decades spanning from 1982 to 2022. Additionally, we present composite fields of various pressure levels during the pre- and post-cyclogenesis phases of intense events originating in a coastal area. Our primary contribution lies in advancing understanding of extratropical cyclones in the southwest Atlantic Ocean, with particular emphasis on the coastal zone where their impact is most pronounced, notably through flooding and strong winds. These findings serve to enhance the knowledge base for scientists and decision makers, facilitating a deeper comprehension of the development and implications of intense extratropical cyclones within the southwest Atlantic Ocean. The paper is organized as follows: Section 2 describes the data and methodology. Section 3 presents the results and discussion, and finally, Section 4 presents our summary and conclusions.

6.2. Data and Methods

6.2.1. Data

Data from ERA5 reanalysis dataset produced by the European Centre for Medium Range Weather Forecasts (ECMWF) [Hersbach et al., 2020] were used in this study. The dataset has a horizontal resolution of 31 km and 137 vertical levels from the surface up to approximately 80 km. In addition to the increased spatial and temporal resolution, ERA5 has improved the assimilation of reprocessed dataset and core dynamics, comparing to previous generations of

ECMWF reanalysis, which benefited our analysis. We used hourly data of mean sea level pressure, 850 hPa relative vorticity and 10-meter wind from 1982 to 2022. For the construction of extreme event composites, we additionally incorporated zonal and meridional winds, geopotential height, air temperature, and relative humidity from the 300 hPa, 500 hPa, 700 hPa, and 850 hPa pressure levels.

Campos et al. [2022] investigated the performance of the ERA5 reanalysis for representing wind patterns in the Atlantic Ocean. Their findings revealed that ERA5 is highly reliable for weak wind conditions. However, as wind intensity increases, the accuracy of the dataset decreases. Despite this, they concluded that extreme winds are reasonably well represented in ERA5 in extratropical regions of the South Atlantic Ocean, suggesting that the reanalysis is a valuable tool for studying extratropical cyclones in the area. Moreover, Erlich et al. [2023] compared ERA5 reanalysis to WindSat polarimetric microwave radiometer measurements for Southern Hemisphere midlatitude to high-latitude cyclones and suggested that ERA5 is adequately determining cyclone structure along the life stages and is valuable for use in cyclone compositing analysis.

6.2.2. Methods

This study uses a recent Lagrangian approach technique that unifies the cyclones identification and tracking process by joining enclosed surfaces areas that satisfy a threshold of -10^{-4} s^{-1} at the 850 hPa relative vorticity, described by Padilha Reinke et al. [2024]. Several studies have employed other thresholds for this parameter. For instance, Hoskins and Hodges [2005] utilized a threshold of -10^{-5} s^{-1}, while Reboita et al. [2018] opted for $-1.5x10^{-5}$ s^{-1} to identify cyclones. However, a sensitivity test conducted by Padilha Reinke et al. [2024] demonstrated that our threshold proves to be adequate for the present study. The identification method was based on Inatsu [2009] that applied the connected component labeling technique [Samet,1989] to join the surfaces areas that satisfy the threshold of relative vorticity and treat them as a unique labeled field. The labeled field is identified by a geographic point (longitude, latitude) using a simple center of mass [Bai and Breen, 2008]. This labeled surface area is recorded with its number of grid points and its minimum 850 hPa relative vorticity. The

advantage of the method is the easy adjustment of the parameters and more plentiful outputs than conventional neighbor point tracking [Inatsu and Amada, 2013]. The cyclone tracking method searches the enclosed independent areas at the following time frame around a maximum displacement of 150 km/h, similar to Crawford et al. [2021]. We consider a minimum lifetime of 12 hours, similar to Gramcianinov [2020] and Padilha Reinke et al. [2024]. At this stage, a list of cyclones with the respective position is generated. The minimum mean sea level pressure and 10-meter wind, associated with all time frames of each event are investigated in a 3.6 latitude/longitude degree radius, to characterize the cyclone of interest, and further separate intense events.

The intense events related to mean sea level pressure were defined as the mean sea level pressure lower than the 10th percentile of the events in the area, which results in around 966 hPa. Lambert and Fyfe [2006] ran sensitivity tests of different threshold to identify intense events and found that qualitatively results are not particularly sensitive to the used value. Furthermore, they used the threshold of 960 hPa to the Southern Hemisphere, a lower value compared to the Northern Hemisphere, because there are more intense cyclones in the former hemisphere.

Additional evaluation of the intense events is based on 10-meter winds stronger than 84 km/h, which are approximately the 90th percentile of the maximum winds associated with the cyclones of the area. Certainly, defining a threshold at which extreme winds are causing damages in a region is not straightforward [Laurila et al., 2021]. Furthermore, there are situations in which the direction of persistent winds can be more important to the coastal environmental modification than its intensity. Besides our method naturally restricts weak events, because of the strict 850 hPa relative vorticity threshold the 90th percentile is a common parameter for identifying extreme events.

In a first stage, the identification and tracking of the cyclones were made to the whole Southern Hemisphere, and secondly it was selected events with at least one point of their track located within the interest area of the southwest Atlantic Ocean. Figure 6.1 shows the domain of this study, covering latitudes of 20°S-50°S and longitudes of 295°E-330°E (red box). We separated the events

formed north of 35°S from those formed south of this latitude, to verify the variability of count of cyclones related to the formation position (the green line in Figure 1 at 35°S latitude makes this division).

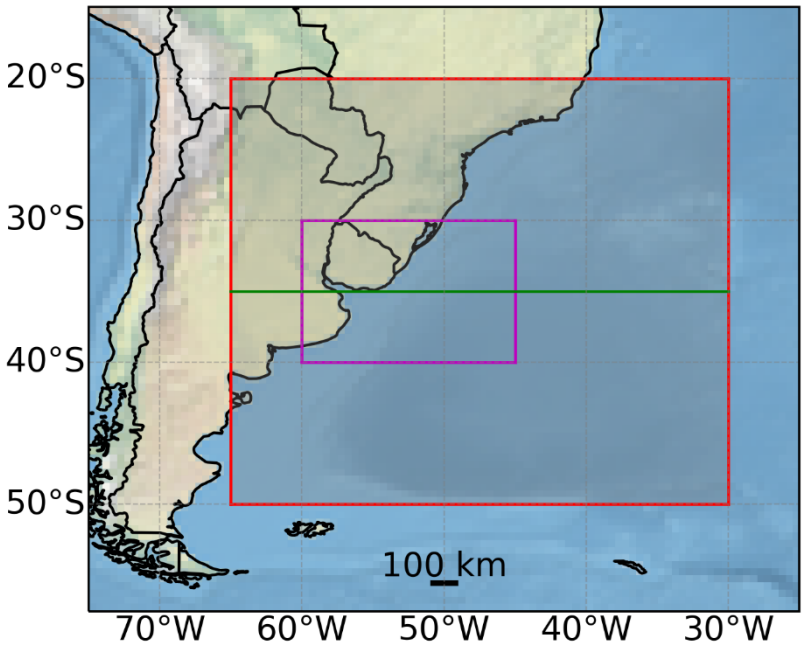


Figure 6.1. Study area showing the Southern Atlantic Ocean and part of South America. The boundaries of the red box (gray area) are 20°-50° S and 65°-30° W. The purple box (indicating the coastal area) has boundaries of 30° -40° S and 45°-60° W. The green line at 35° S divides the red box into two bands.

We examined the interannual variability across the entire study area, as well as its northern and southern segments. Trends were calculated by applying linear and cubic regression models to the time series. Some studies utilize solely linear regression; however, the rationale for employing a more complex model to fit the data is to find a more refined adjustment. The statistical significance was performed by a T test and the Mann-Kendall test [Kendall, 1975] was implemented in both northern and southern regions for each season, to assess the significance of the trends [Yue and Pilon, 2019]. To accurately identify periodic oscillations in the time series, we conducted Fourier analysis (e.g. [Emery and Thomson, 2001]). To ascertain the significance of power spectrum peaks, we utilized a red noise analysis, with a technique mathematically formulated by Gilman et al. [1963] and F-test of significance distribution related to the red noise. Twenty realizations of the power spectrum were performed in order to enhance the major peaks and remove noise [Prieto, 2007].

We also examined the characteristics of the streamlines, geopotential height, air temperature and relative humidity at 300 hPa, 500 hPa, 700 hPa and 850 hPa, representing the upper, middle and low-levels of the troposphere, by creating spatial-temporal evolution of composites of the intense extratropical cyclones that were generated in the coastal area indicated by the purple box in Figure 1. The maps are presented from 24 hours before the cyclogenesis to 12 hours after it. These maps contribute to a better understanding of the preconditions of formation of intense coastal extratropical cyclones with respect of pressure and 10-meter winds, and their first hour's evolution in the vicinity of the coastal area.

6.3. Results and Discussion

6.3.1. Spatial and Temporal Distribution

Firstly, this section provides an overview of the cyclones of southwest Atlantic Ocean. The horizontal distribution cyclogenesis frequency for each season is presented in Figure 6.2. It is well known that the largest frequency of cyclogenesis and cyclone tracks in the Southern Hemisphere is between 50°S and 70°S, due to the large baroclinicity in that region (e.g., [Eichler and Gottschalck, 2018; Hoskins and Hodges, 2005; Murray and Simmonds, 1991]). However, the region between 30°S and 50°S presented the largest seasonal variation in cyclogenesis frequency, with more events per season on the winter than on the summer, at the coast of South America. Autumn and spring have intermediate values within this area, with slightly more events on spring. The almost absence of cyclogenesis over the western part of South America is explained by the modification of the low-level perturbations related to the Andes Mountains range (e.g. [Vera et al., 2002; Gan and Rao, 1991]). Mendes et al. [2007] studied the precondition for the formation of extratropical cyclones in South America and found that the Andes Mountains seem to play a dual role: on one hand channeling warm and moist air from the tropics into the mid-latitudes, and on other hand, interacting with the upper-levels undulations leading to intensification of the cyclogenesis due to the downstream flow lee the mountain range.

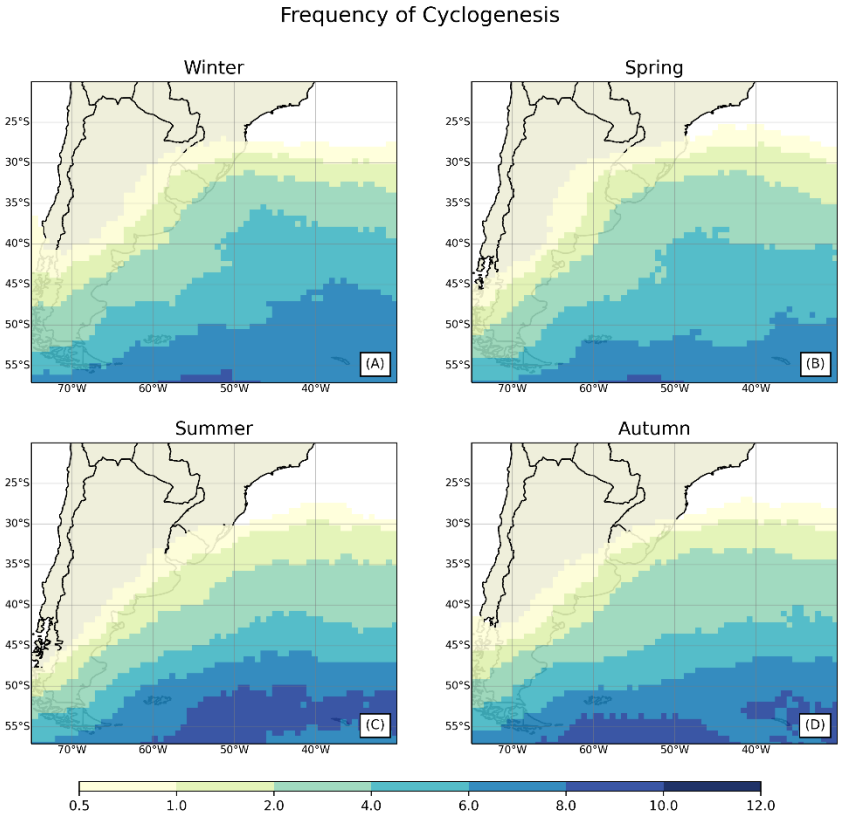


Figure 6.2. Spatial distribution of Southwest Atlantic cyclogenesis per season for (A) winter (JJA), (B) spring (SON), (C) summer (DJF) and (D) autumn (MAM). The density unit is events per area, with a unit area of spherical cap of 10^6 km^2.

Following the maximum relative vorticity at 850 hPa for each extratropical cyclone, we obtained the more intense time frame and position of each cyclone. Figure 6.3 shows the horizontal distribution of the events in the more intense position, with respect to 850 hPa relative vorticity. Comparing with the panels of cyclogenesis, the position is shifted further away from the coast. To assess this, we computed the mean frequency of cyclone genesis within a defined coastal region, delineated by latitudes 25°S and 40°S, and longitudes 50°W and 65°W. The frequency of cyclogenesis exceeded that of the more intense period by 59%, 62%, 54%, and 57% during the summer, autumn, winter, and spring seasons, respectively. The maximum position in the open ocean is associated with strong baroclinicity in the higher latitudes, which agrees with the results of Lim and Simmonds [2007]. Dos Santos et al. [2023] in recent study provided an overview of baroclinic instability in the Southern Atlantic Ocean to characterize the storm track region in the Southwestern Atlantic. They found higher values mainly between 40°S and 50°S, similar to our results. According to Wells [2011], this

preferential zone is called baroclinic zone and it is influenced by the large meridional topographic barriers, like Andes Mountains, and the distribution of continents and oceans, which are regions of heat sources or sinks, driven by the cycle of solar radiation over a year. The large horizontal gradient of temperature produced by this distribution is crucial to explain the favorable regions of intensification of extratropical cyclones. This baroclinic zones can be seen most clearly in mean fields over a great number of years, like it is shown in Figure 6.3. Together, Figures 6.2 and 6.3 provide a comprehensive depiction of the storm-track distribution in the southwest Atlantic Ocean, as well as their seasonal differences.

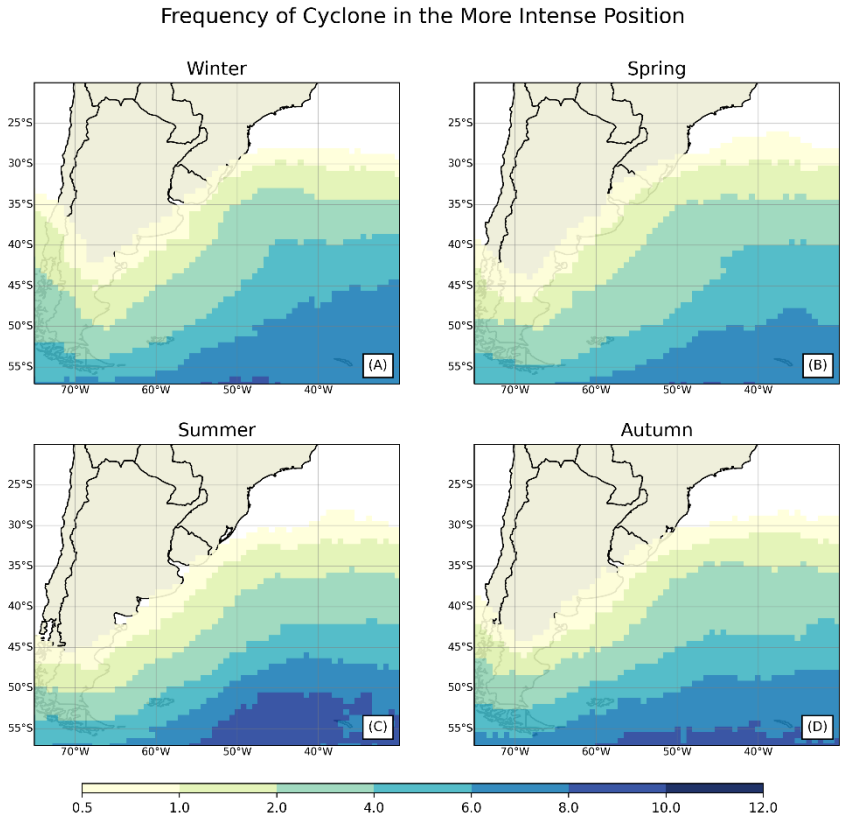


Figure 6.3. Spatial distribution of Southwest Atlantic on the position where relative vorticity on 850 hPa reach their more intense values per season for (A) winter (JJA), (B) spring (SON), (C) summer (DJF) and (D) autumn (MAM). The density unit is events per area, with a unit area of spherical cap of 10^6 km^2.

6.3.2. Storm Characteristics

To address the characteristics of extratropical cyclones in the Southwestern Atlantic Ocean, Figure 6.4 shows the histograms of lifetime (Figure 6.4A), mean velocity of displacement (Figure 6.4B) and maximum intensity of extratropical

cyclones measured by the minimum sea level pressure (Figure 6.4C) and the maximum 10-meter winds (Figure 6.4D). Approximately 49% of the extratropical cyclones persisted for one day, while 40% endured for two days. Our methodology employs a stringent threshold for relative vorticity at 850 hPa (-10^{-4} s^{-1}), potentially leading to the exclusion of certain cyclolysis processes. Consequently, our findings indicate a higher prevalence of short-lived events compared to other studies, such as Gramcianinov [2020-2]. However, we are focused on events that could result in higher impacts for the coastal area, and for marine navigation and hence this criterion restricts weak cyclones that cannot produce extreme precipitation and strong winds. The lifetime of cyclones of the Southern Hemisphere produced with the same methodology has a similar feature, with a large number of short-life events [Padilha Reinke et al., 2024]. With respect to the mean velocity, 50% of the extratropical cyclones of the study region are in the range between 50 km/h and 70 km/h. On average, these results were faster than the velocity presented by Padilha Reinke et al. [2024] to the Southern Hemisphere, with the same methodology. The minimum sea level pressure and the maximum 10-meter winds of the cyclones were effective parameters to evaluate the intensity of the extratropical cyclones. They are indirectly related, because low pressure is usually associated with increase of pressure gradient, which is associated with stronger winds in the low-level troposphere [Laurila et al., 2021]. Both frequency distributions are skewed towards the most intense events, with more weight in the right tail of maximum 10-meter winds and in the left tail of minimum sea level pressure.

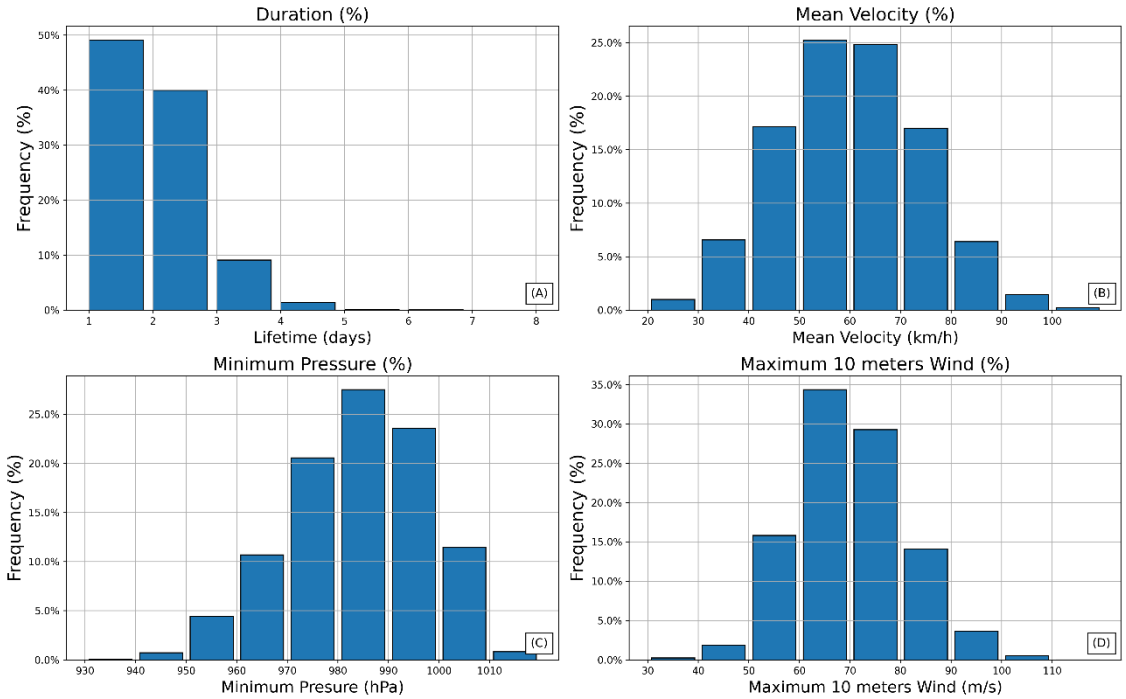


Figure 6.4. Frequency distribution of (A) duration (days), (B) mean velocity (km/h), (C) minimum sea level pressure (hPa) and (D) maximum 10-meter winds (km/h) for each extratropical cyclone in the Southwest Atlantic Ocean.

Table 6.1 shows the statistics of extratropical cyclones in the study area, spanning from 1982 to 2022. On average, 97.1 cyclones were observed yearly, with a standard deviation of 9.9 and 90th percentile of 111.0. The mean velocity of the extratropical cyclones is 60.1 km/h, with a 90th percentile of 78.3 km/h. The fastest event occurred between 12th and 14th of December of 2022, with a maximum 10-meter wind of 82.0 km/h and minimum sea level pressure of 977.5 hPa, far from the continent but within the study area. Minimum sea level pressure mean is 984.0 hPa, and the maximum 10-meter wind mean is 70.0 km/h. The 90th percentile of the maximum 10-meter wind (84.4 km/h) and the 10th percentile of the minimum mean sea level pressure (965.9 hPa) shown in the last column of Table 6.1 serve as benchmarks for assessing more intense events in the subsequent subsection.

Table 6.1. Statistical characteristics of extratropical cyclones in the Southwest Atlantic Ocean (red box of Figure 1).

	Mean	Median	Standard Deviation	Percentile of intensity (10%/90%)
Count per year	97.1	97.0	9.9	111.0 (90%)
Mean Velocity (km/h)	60.1	59.9	14.0	78.3 (90%)
Minimum sea level pressure (hPa)	984.0	985.3	13.6	965.9 (10%)
Maximum 10-meter winds (km/h)	70.0	69.3	10.9	84.4 (90%)

6.3.3. Intense events

The intensity of an extratropical cyclone can be defined by a wide broad variety of meteorological variables. Figure 6.5A, 6.5B and 6.5C show the tracks of intense extratropical cyclones based on minimum sea level pressure (A), maximum 10-meter winds (B) and the faster cyclones (C), respectively, according to the percentile shown in Table 6.1. Cyclones generated north (south) of 35° S are depicted in green (blue). A total of 407 intense events based on mean sea level pressure criteria, 425 based on 10-meter wind thresholds, and 417 fast events were identified. Intense events based on sea level pressure are shifted to south and some events of the extreme south of South America are included. Overall, faster events in the area tend to form slightly away from the continent, indicating that occurrences of rapid events are less common near the coastline. The tracks of events meeting all three criteria display a notable southward and away-from-the-continent shift, totaling 56 occurrences (Figure 5D). There were 166 intense events based simultaneously on sea level pressure and 10-meter winds criteria (Figure 6.5E). To understand the behavior of intense cyclones that develop near the coast, we selected events between 30° S and 40° S latitudes and 45° W and 60° W longitudes (purple box on Figure 5F) and created composites with some similar characteristics of these extratropical cyclones (see subsection 3.5).

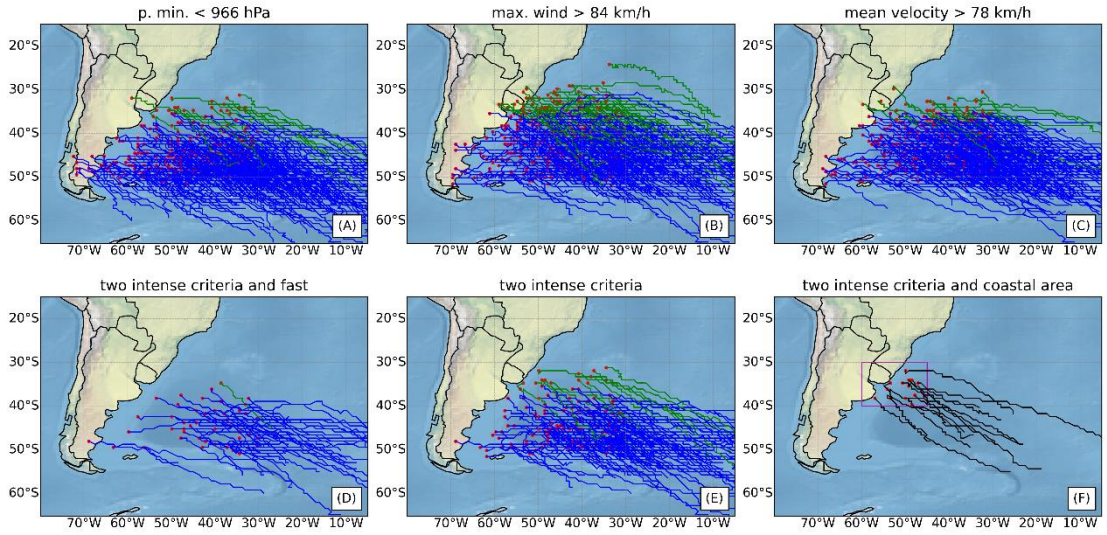


Figure 6.5. Tracks of intense events in the Southwest Atlantic Ocean based on: (A) sea level pressure below 966 hPa, (B) 10-meter wind above 84 km/h, (C) mean velocity above 78 km/h. The panel (D) shows intense events based on the three criteria, while the panel (E) shows intense events based on the criteria (A) and (B). Finally, the panel (F) is similar to (E), but for events generated just on the purple box. Cyclones generated north of 35° S are in green and generated south of 35° S are in blue. The red points are the beginning of the track of each event.

Figure 6.6 shows the spatial and temporal distribution of cyclones on the position where they reach the higher intensity, separated by season. In general, the more intense position of the events agrees with the results of higher intensity based on the 850 hPa relative vorticity of all the events of the 41-years dataset (Figure 6.3) and with the theoretical definition of baroclinic zones. In terms of time of the year, there is a clear decrease in the number of events during austral autumn (Figure 6.6D and Figure 6.6H) and the position of spring intense events are slightly further from the continent and at latitudes south of 45° S. Only during winter (Figure 6.6A and Figure 6.6E) more intense events occur near the coast. Figures 6.6I, 6.6J, 6K and 6.6L point out that some of the intense cases identified by the pressure criterion exhibit their most intense period farther pole ward compared to those identified by the 10-meter wind criterion. Comparing these results with Figures 6.5A and 6.5B, where the whole year tracks are presented, we can suggest that the intense events separated according to maximum winds are generally more displaced towards the equator than intense events separated according to minimum pressure. This difference may result from the distinct nature of the variables, with the sea level pressure more extensive and persistent, while the 10-meter winds are in essence more turbulent.

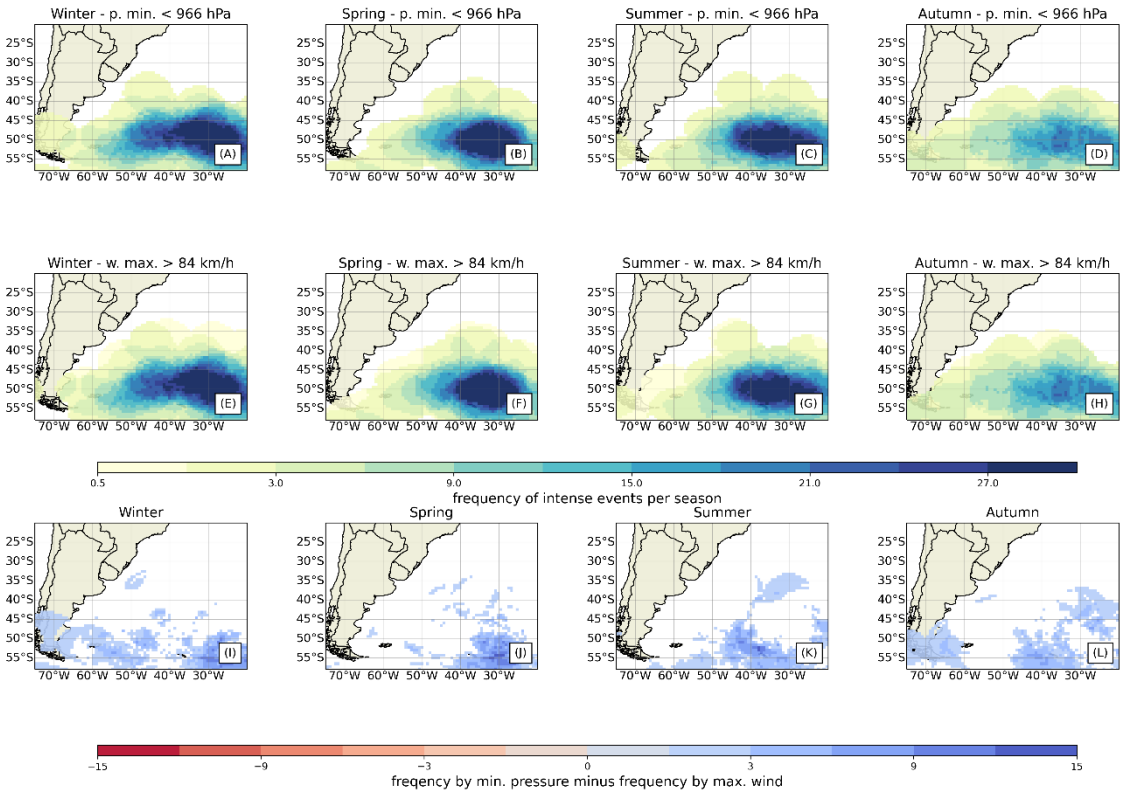


Figure 6.6. Positions where the extratropical cyclones of Southwest Atlantic Ocean reach the higher intensity. The upper (middle) line of panels shows the position of intense events per season based on sea level pressure below 966 hPa (10-meter winds above 84 km/h). The lower line of panels shows the difference in results based on these criteria.

6.3.4. Interannual variability

Figure 6.7 shows the annual count of extratropical cyclones and the respective linear and cubic polynomial regression of the whole study area (Figure 6.7A), northern part of the area (north of 35°S, Figure 6.7B) and southern part of the area (south of 35°S, Figure 6.7C). Overall, there is a large interannual variability and a slight increase trend in the three regions. By using the linear regression, the increase slopes are 0.19, 0.04 and 0.15 to the whole area, northern part, and southern part, respectively. However, using Mann-Kendall test, the linear regression has no statistically significant monotonic trend at the 90% level (Table 6.2). Analyzing the cubic polynomial regression, a greater positive trend was observed from 1980's to 2010's decades, while a negative trend was present after 2010. The cubic polynomial regression has a coefficient of determination of 0.32, 0.13 and 0.22, for the total, northern and southern parts of the area, respectively. On average, there are 97 events per year on the whole area, 13 on the northern part and 83 on the southern part, respectively. The largest yearly

count of extratropical cyclones occurred in 2013, considering the entire area (122 events). Depicting the north and south areas, 105 events were observed in the south in 2013, and 21 events in the northern part in 1999 and 2008. Performing a Pearson's correlation, the count of extratropical cyclones over the two parts of the area has no significant correlation, with a coefficient of -0.14, using the statistical significance of 95% level.

Table 6.2. Slope of the linear trends in the 1982–2022 period, p-value according to the Mann–Kendal test and coefficient of determination (R^2) of extratropical cyclones of total, northern and southern parts of the study area.

Area	Mann-Kendall p-value	Slope	R^2
Whole area	0.26	0.19	0.05
Northern part	0.35	0.04	0.02
Southern part	0.33	0.15	0.03

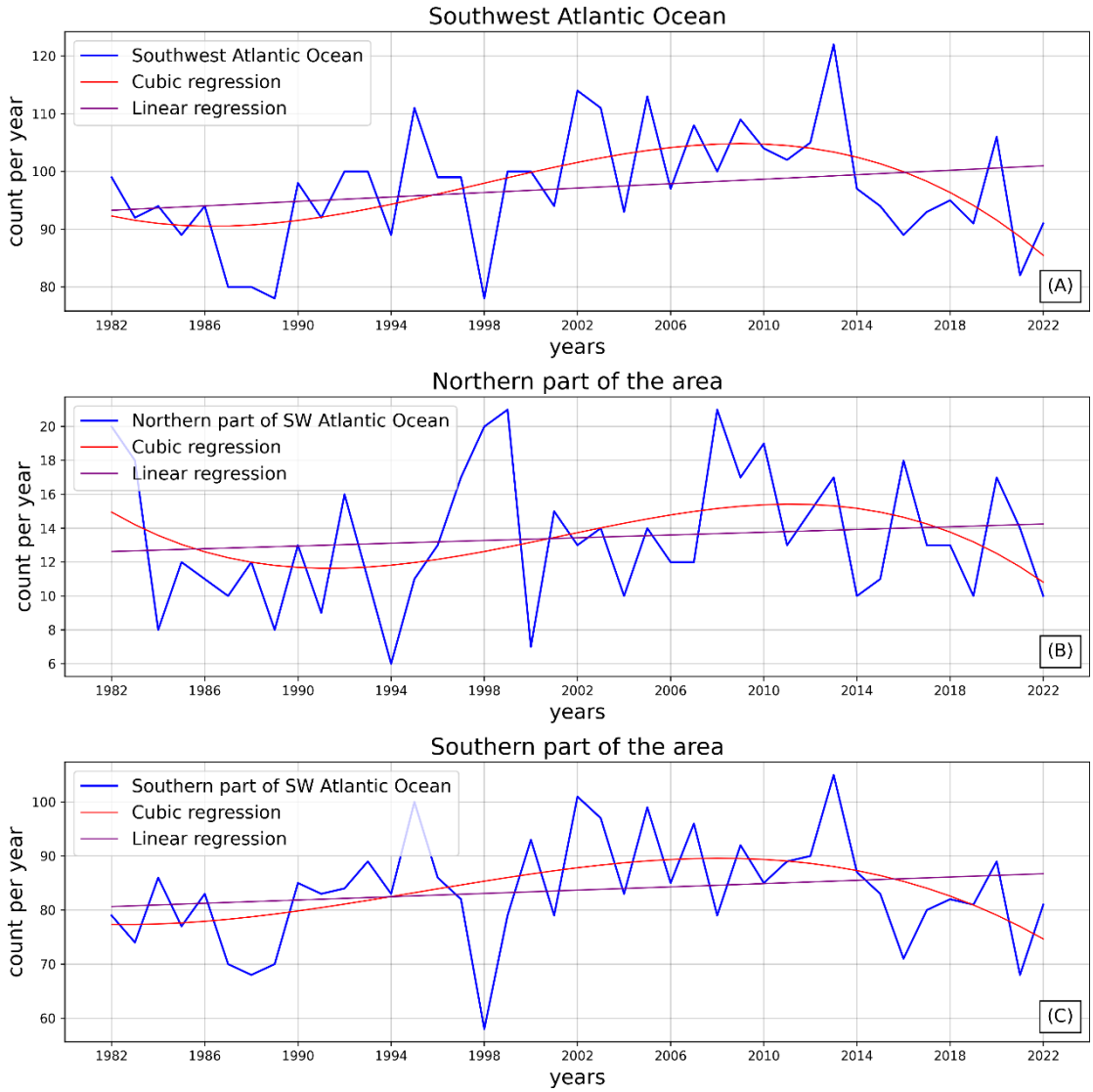


Figure 6.7. Annual count of extratropical cyclones (blue), and respective linear regression (red) and cubic polynomial regression (purple). The upper panel shows the results for the Southwest Atlantic Ocean while the middle (lower) panel shows the same for the northern (southern) part of the whole area.

Figure 6.8 shows the annual count of intense cyclones, based in the minimum sea level pressure (blue line), maximum 10-meter winds (red line) and higher mean velocity (purple line) criteria. Comparing the variability of these events, the number of intense events decreased between 1995 and 2000 and increased between 2005 and 2010, in the three series. This pattern suggests an important interannual variability in the count of intense and fast events in the region. The correlations between fast events and intense events, according to minimum pressure and 10-meter winds, exhibit positive associations. Specifically, there is a moderate correlation between intensity as determined by

minimum pressure and as determined by 10-meter winds, whereas a strong correlation between fast and intense events. (see left upper corner of Figure 6.8).

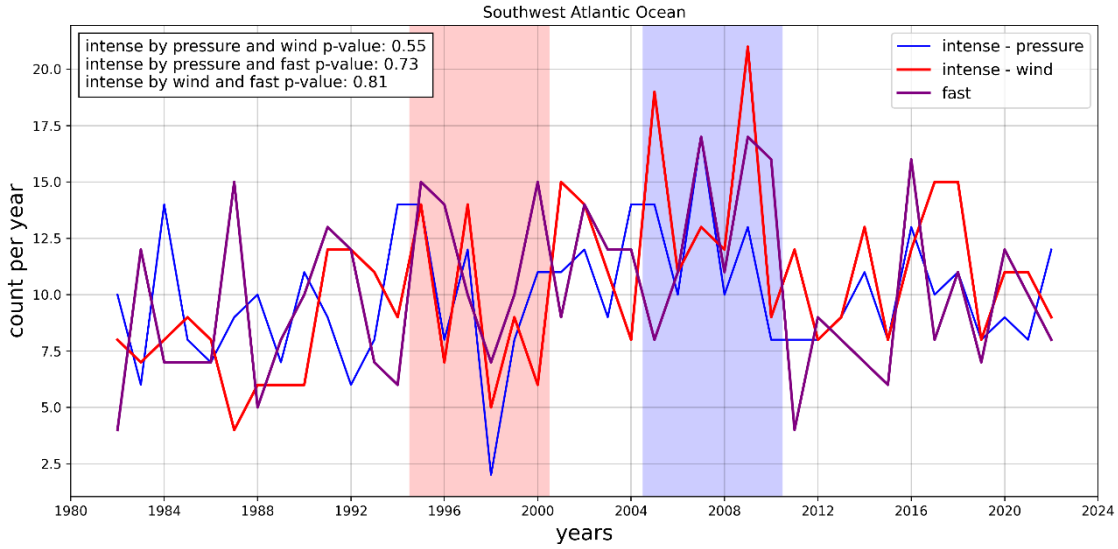


Figure 6.8. Annual count of intense extratropical cyclones in the Southwestern Atlantic Ocean based in minimum sea level pressure below 966 hPa (blue), maximum 10-meter winds above 84 km/h (red) and faster events (velocity greater than 78 km/h, purple) criteria. At the left upper corner of the figure some correlations are presented.

In the context of seasonal trends, Figure 6.9 shows the annual count and the respective linear regression for each season. In the northern part, a slight positive trend was observed in summer (slope of 0.03) and autumn (slope of 0.02), and an even smaller trend was found during winter and spring. However, the p-values of the Mann-Kendall test of all the seasons are higher than the 0.05, which suggests that the trends are not significant in a 95% level. Using the same test for each season in southern part, only the trend of summer (slope of 0.17) was significant (95% level). Visually, a slight negative trend in the cyclone count was observed during the autumn and a slight positive trend in the winter. However, these trends were not significant by Mann-Kendall test (95% level).

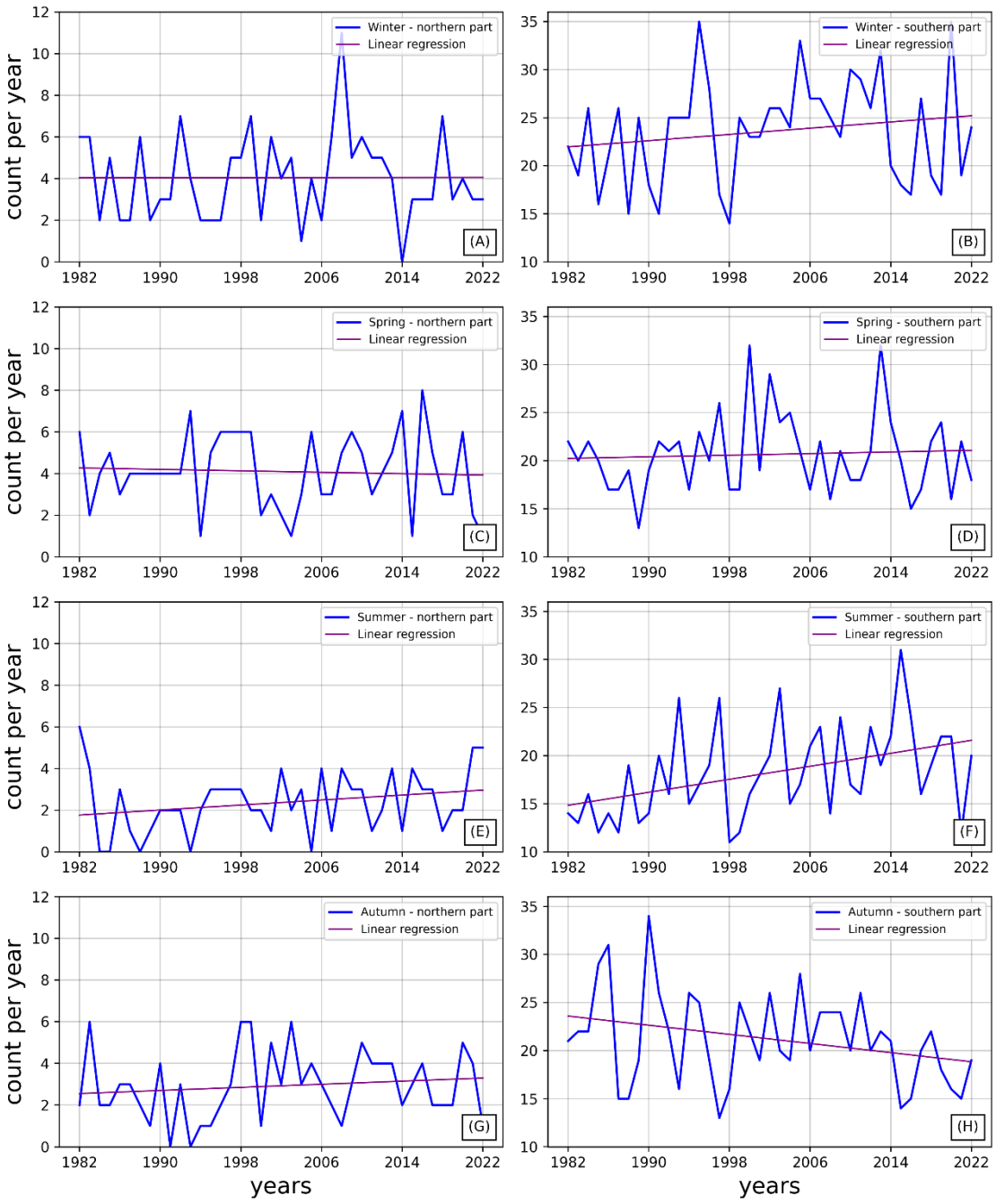


Figure 6.9. The left (right) column shows the annual count of extratropical cyclones in blue, and respective linear regression in purple for the northern (southern) part of the study area. From top to bottom the results are presented for winter, spring, summer and autumn seasons.

Figure 6.10 shows the power spectrum of the yearly count of extratropical cyclones and the associated red noise, with the lines of 99% significance and 95% significance, computed by the F-test. There is a significant energy at the 2-3 years period, during winter (in northern part), summer, spring and autumn (in both areas). This energy peak could be related to El-Nino South Oscillation (ENSO) that modifies the precipitation regime in the region [Barreiro, 2010]. The

5-years period presented an energy peak in winter northern part and autumn southern part. A significant peak at the 6-year period was found in the winter southern and summer northern area. Decadal oscillations can be suggested by peaks at 8 and 10 years period over spring and winter. However, further analysis should be made to understand the underlying mechanisms responsible for these energy peaks.

6.3.5. Composite of intense events

In meteorology, the composite analysis is a useful technique that can express the basic structural characteristics of a phenomenon. Therefore, we constructed composites for the 14 events of Figure 6.5E, selected based on their intensity criteria in terms of mean sea level pressure and 10-meter winds. Table 6.3 shows the description of the extratropical cyclones evolved in this analysis. There are 2 events during autumn, 1 in spring, 2 in summer and 9 during winter. Composite analysis inhibits the case-to-case variability; therefore, it cannot be compared to the case studies (e.g., [Li and Dolman, 2023]). Figure 6.11 shows the spatio-temporal evolution of composite atmospheric circulation 24 hours before to 12 hours after the cyclogenesis of the 14 intense events in coastal area of south of Brazil and Uruguay (purple box in Figure 6.1).

The composite of 24 hours before cyclogenesis shows a moving trough aligned to the western part of South America centered near 70° W, stretching from 20° S to 50° S (Figure 6.11A) at 300 hPa. The 12 hours before composite shows the deepening of the trough (Figure 6.12B) and the 0 hours field has a marked divergence (not shown) east of the trough in the wind field. The enhanced intensity of the wind velocity suggests that, on average, intense events form in the equatorial entrance of the jet, and the displacement of the cyclone is related to the moving trough and displacement of the jet, which agrees with the results of Crespo et al. [2020]. Case 1 and case 13 of Table 6.3 formed a cyclonic vortex at 300 hPa (not shown).

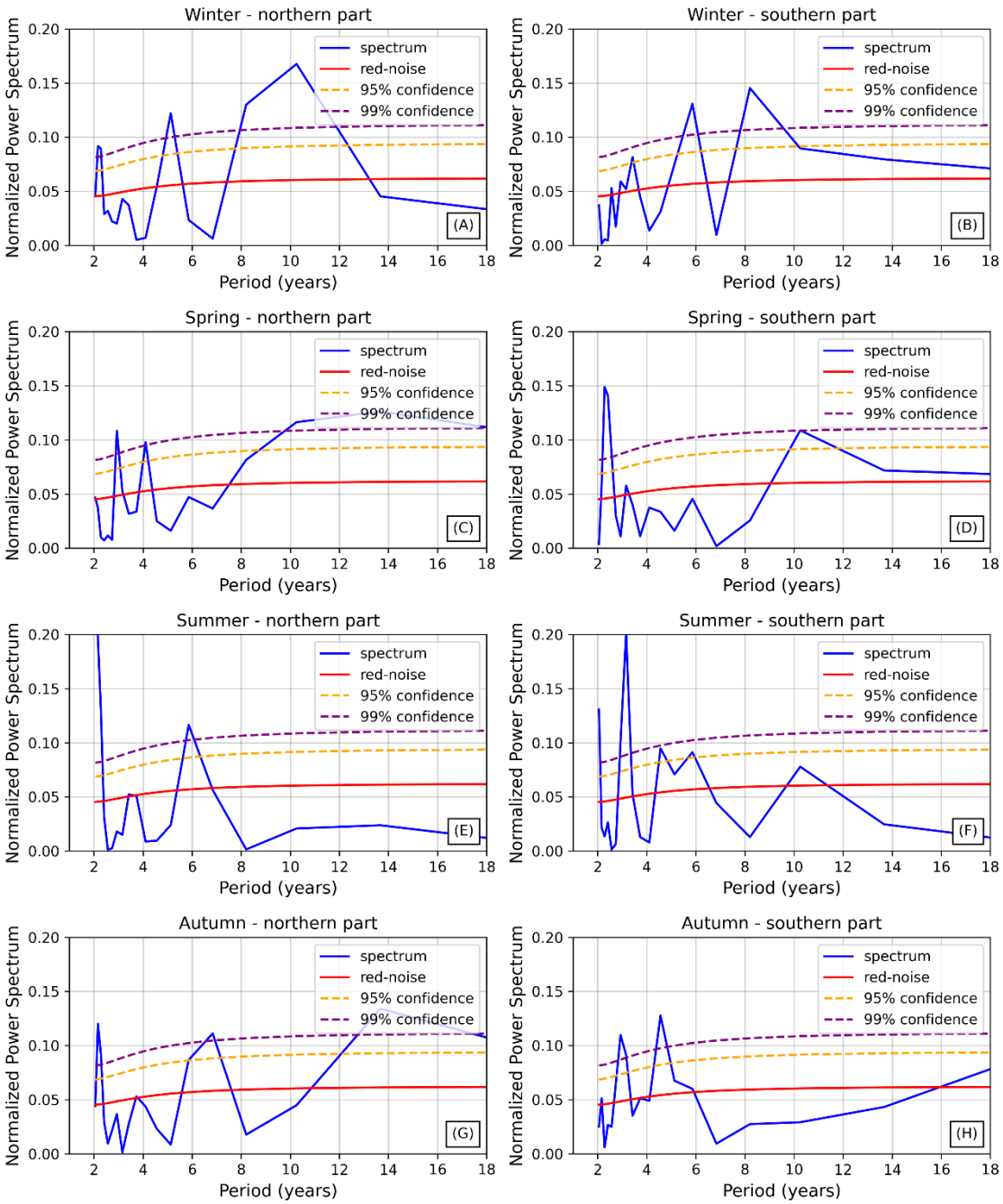


Figure 6.10. Normalized power spectrum of extratropical cyclones count (blue) with 20 realizations, red-noise fit (red) and F-test confidence level of 95% (orange) and 99% (purple) for northern (left column) and southern (right column) parts of the study area. From top to bottom the results are presented for winter, spring, summer and autumn seasons.

Composites of 500 hPa geopotential height and temperature (Figures 6.11E, 6.11F, 6.11G and 6.11H) revealed that the extent of the moving eastward trough goes between 20° S and 50° S at middle troposphere, 24 hours before and 12 hours before the cyclogenesis. Mendes et al. [2007] studied the

precursors of South America cyclogenesis and explained that the transient trough coming from the South Pacific in middle troposphere generally extent within the 40°S-50°S band.

Table 6.3. Extratropical cyclone events that reach the intense threshold of mean sea level pressure and 10-meter winds and with cyclogenesis under the coastal area (purple box of Figure 1).

First Date	Last Date	Duration (hours)	Speed (km/h)	Min. Pressure (hPa)	Max. Wind (km/h)
1983/Jun/4	1983/Jun/6	67	62	952.9	84.9
1983/Sep/28	1983/Oct/1	57	72	958.6	85.9
1984/Jun/26	1984/Jun/27	33	54	965.3	96.8
1990/Apr/17	1990/Apr/18	19	93	962.9	94.8
1990/Jun/8	1990/Jun/10	36	77	958.4	88.6
1990/Dec/11	1990/Dec/13	48	63	961.0	93.8
1991/Jun/3	1991/Jun/4	27	67	957.5	98.5
1992/Jun/5	1992/Jun/8	63	75	953.5	113.2
1997/May/22	1997/May/23	41	68	957.3	96.3
2002/Jun/10	2002/Jun/11	22	91	943.7	102.5
2002/Jun/18	2002/Jun/19	25	100	963.4	93.3
2003/Dec/9	2003/Dec/10	31	75	962.9	90.8
2007/Jul/23	2007/Jul/23	14	44	965.5	94.1
2022/Jul/16	2022/Jul/18	34	71	959.8	94.8

Figures 6.11I, 6.11J, 6.11K and 6.11L show the composites of geopotential height, relative humidity and wind at 700 hPa for the 14 intense events. The connection between the incursion of warm and wet tropical air from the tropics and mid-latitude transient trough is a typical feature observed by Garreou and Wallace [1998] and Mendes et al. [2007]. The cyclogenesis of intense events is favored by intense humid northwesterly winds. This low-level jet is an important conduit of moisture transport that modulates the South America precipitation [Marengo et al., 2002; Vera et al., 2006; Montini et al., 2019; Jones et al., 2023]. The wind field at 850 hPa detached a close circulation 12 hours before the

cyclogenesis and the transport of humidity from the tropics is pointed to the coastal area during the process of formation and intensification of the cyclone. As the cyclone moves eastward, the connection with the continental transport of moisture from the tropics is interrupted, and the processes of ocean-atmosphere interaction become more important [Sutil et al., 2019]. An expected pattern is the inclination of the cyclonic disturbance between the upper and lower troposphere. Figure 6.12 shows the same fields to the 9 events of winter. The characteristics are similar to those of the Figure 6.11, however the intensity of the stream jet at 300 hPa is more pronounced.

6.4. Summary and conclusions

This study investigates the characteristics of extratropical cyclones in the Southwest Atlantic Ocean, focusing on their interannual variability. Special attention is given to the formation positions related to 35°S latitude, as well as cyclone intensity.

The spatial distribution showed the well-known most favorable region of cyclogenesis in the eastern part of the South America, which is influenced by the Andes Mountains. The most favorable region for intensification of the extratropical cyclones was shifted to the ocean, which agrees with the baroclinic zone concept. The frequency distribution showed that when comparing to the whole South Hemisphere, Atlantic Ocean events proved to be faster, in average. Evaluating the intensity of the events, the 10th percentile of minimum mean sea level pressure was of around 966 hPa and the 90th percentile of maximum 10-meter wind was of about 84 km/h.

The intense events with respect to the minimum sea level pressure are further south, comparing to the intense events with respect to the maximum 10-meter winds. On the other hand, the faster events are shifted far from the continent. Relating the intense events with respect to the two variables and the faster events, 56 cyclones reached the three parameters threshold in the 41 years, with a track mainly shifted far from the continent. If considering the cyclones that reached both intensity parameters (minimum pressure and maximum wind), some of the 166 intense events of the 41 years are shifted

toward the coastal region, and thus have a greater potential to impact the population.

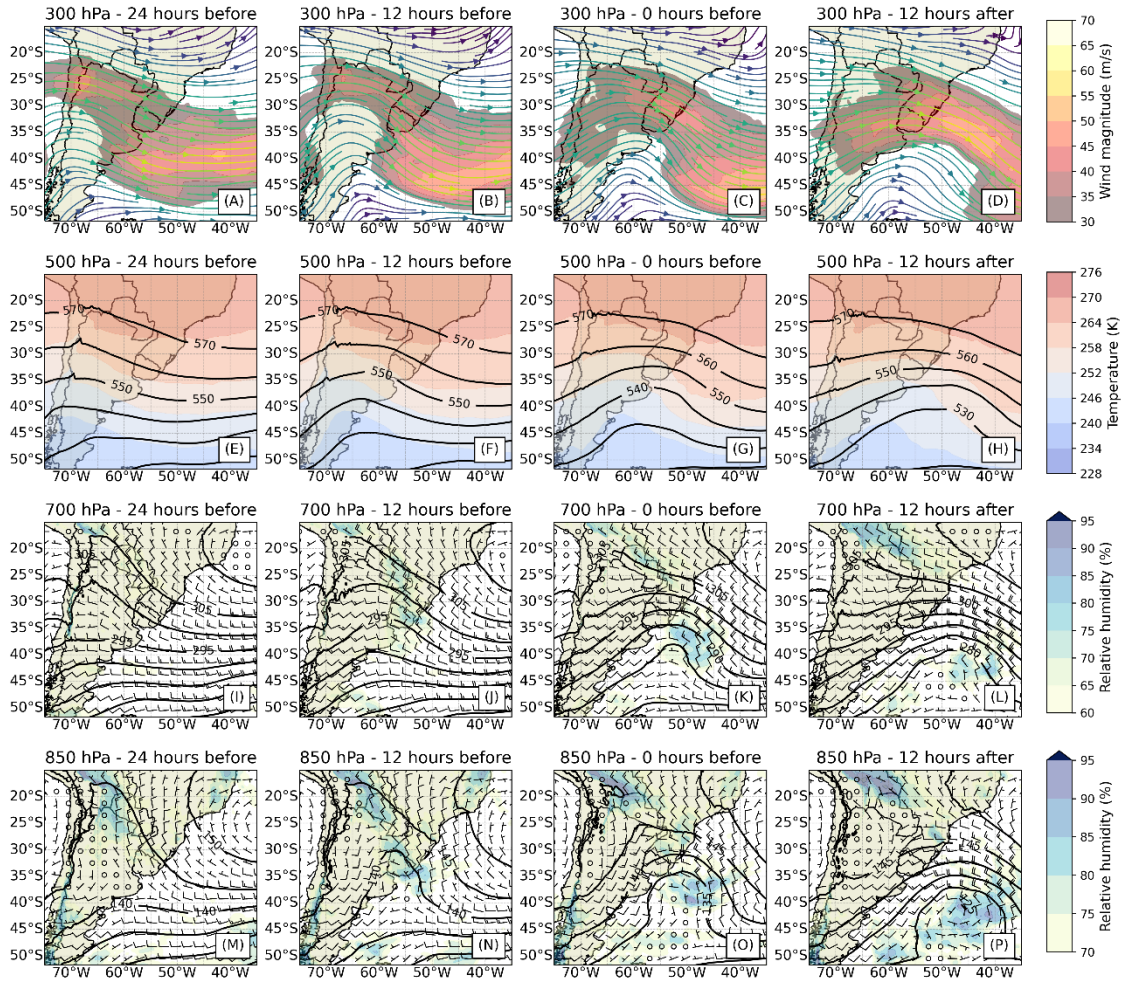


Figure 6.11. Composites of the 14 intense events of Table 3 on 24 hours before (A, E, I and M), 12 hours before (B, F, J and N), the time (C, G, K and O) and 12 hours after (D, H, L and P) the cyclogenesis. (A to D) 300 hPa streamlines with magnitude up to 60 m/s shaded, (E to H) 500 hPa geopotential height (dams) and air temperature (K), (I to L) 700 hPa wind (barb), geopotential height (dams) and relative humidity, shading magnitude above 60% and (M to P) 850 hPa wind (barb), geopotential height (dams) and relative humidity, shading magnitude above 70%.

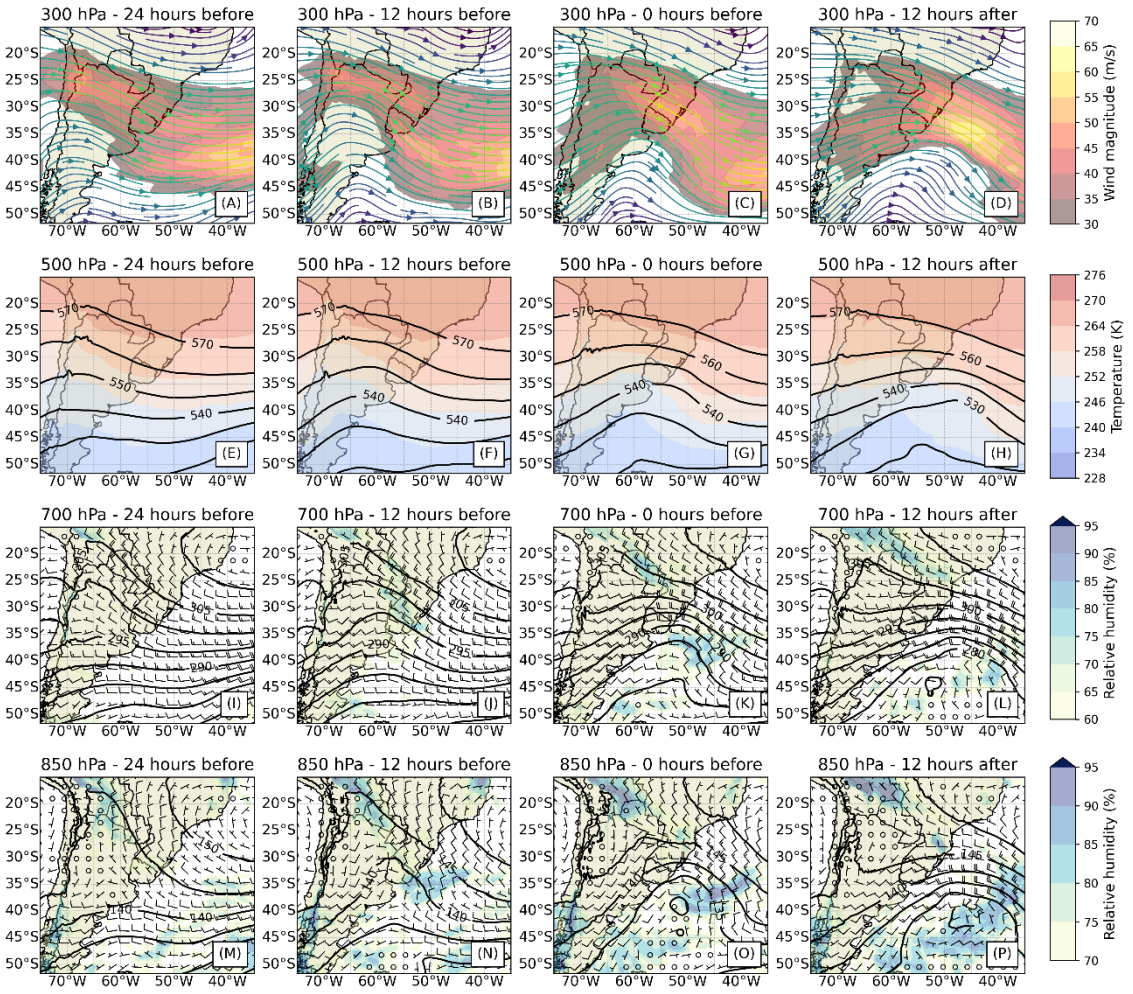


Figure 6.12. Composites of the 9 winter intense events of Table 3 on 24 hours before (A, E, I and M), 12 hours before (B, F, J and N), the time (C, G, K and O) and 12 hours after (D, H, L and P) the cyclogenesis. (A to D) 300 hPa streamlines, color shading magnitude above 60 m/s, (E to H) 500 hPa geapotential height (dams) and air temperature (K), (I to L) 700 hPa wind (barb), geopotential height (dams) and relative humidity, shading magnitude above 60% and (M to P) 850 hPa wind (barb), geopotential height (dams) and relative humidity, shading magnitude above 70%.

A closer visual inspection of cyclone count time series for the total, northern and southern parts of the study area, according to 35°S of latitude, revealed a slight increase trend, although Mann-Kendall test showed that this is not statistically significant for the three time-series. The cubic polynomial model performed a better fit of the data for the three areas, meaning that the count of cyclones has an oscillatory pattern. The Pearson correlation of the two segments of the area exhibited very weak association.

The count of intense events, measured by the minimum sea level pressure and by the maximum 10-meter winds, and the fast events showed an important interannual variability, similar to the total count of events. The greater quantity of

intense cyclones occurred between 2005 and 2010. The Pearson´s correlation is moderate between intense events with respect to sea level pressure and 10-meter winds criteria and strong between faster cyclones and intense ones by the two criteria.

We explored the cyclones analysis in another perspective: seasonal count of the two parts of the study area. While the trend in the northern part of the area proved insignificant across all seasons, a notable trend emerged in the southern part during summer, with an increasing slope of 1.7 per decade, as determined by the Mann Kendall test at a 95% confidence level. The variability analysis revealed the significance of oscillations with periods of 2-3 years in the northern part during winter, as well as in both parts during spring, summer, and autumn. Additionally, a peak of energy in the 5-year period was observed in the northern part during winter, and in the southern part during autumn. Peaks between 8 and 10 years, present in winter and spring, may be linked to decadal oscillations. The origin of these peaks warrants further investigation in future studies.

To understand the meteorological characteristics associated with intense events formed in the coastal area of south of Brazil and Uruguay, the composite of meteorological variables of upper, middle and lower levels of the troposphere was constructed. Even knowing that each event presents a particular meteorological condition, the composites helped to understand the preferential pattern of evolution, such as the equatorial entrance of the jet stream in upper-levels, the deep trough in upper and mid-levels and the importance of the moisture transport, directed from the tropics to the coastal area, in the lower troposphere. These patterns are consistent with previous studies of Mendes et al. [2007] on the precursors of South America cyclogenesis, and Montini et al. [2019] regarding the role of the low level jet in transport moisture and in enhancing the instability at the end of its path, promoting cyclone intensification.

This study offers a significant new perspective on intense extratropical cyclones within the Southwest Atlantic Ocean, contributing to the broader understanding of variability analysis and the distinct characteristics of systems that significantly affect both coastal communities and the natural environment. Our findings shed light on the prevailing synoptic conditions conducive to the

development of intense cyclones, aligning with prior research by Vera et al. [2002], Gan and Rao [1994] and Mendes et al. [2007]. Such insights are relevant for informing and preparing for future events, particularly those with the potential to significantly impact coastal regions. The provided results about energy peaks yield valuable insights; however, it also brings inquiries into the underlying mechanisms accountable for the observed patterns of variability.

Further investigation on link between the variability of cyclone counts and key oceanic parameters such as sea level temperature and upper ocean heat content (UOHC), as well as established large-scale modes of variability, like Atlantic Multidecadal Oscilation (AMO), Southern Annular Mode (SAM), may be useful in understanding the factors that contribute to the oscillatory pattern observed in annual cyclone counts. The influence of oceanic eddies and oceanic fronts in the atmosphere also needs further investigations. Some recent studies focused on these features and their role in the sea-air interactions (e.g. [Orselli et al., 2019; Pezzi et al., 2022 and Ginis and Kang, 2024]). In the scope of this study, special attention must be given to climate change and their impacts. Considering the change of heat and humidity air-sea fluxes in a condition of higher sea surface temperature, it would be interesting to study the relationship between marine heatwaves events and the occurrence of cyclones, especially the more intense ones.

Capítulo VII: Artigo sobre a Relação entre Ciclones e Ondas de Calor Marinhas

O terceiro manuscrito apresenta uma descrição das características das ondas de calor marinhas no Sudoeste do Oceano Atlântico e sua relação com os ciclones extratropicais. Os resultados sobre intensidade e duração das ondas de calor marinhas lançam novas perguntas para trabalhos futuros. De autoria de Carina K. Padilha Reinke e Jeferson P. Machado, é intitulado **"*Marine Heatwaves in the Southwest Atlantic Ocean and their Relationships with Extratropical Cyclones*"** e será submetido ao periódico ***"Ocean and Coastal Research"***.

Marine Heatwaves in the Southwest Atlantic Ocean and their Relationships with Extratropical Cyclones

Abstract

Marine heatwaves (MHWs) are periods of anomalously warm ocean temperatures, that can significantly impact the ecological balance and disrupt surrounding societies. Given the limited research on these conditions in the southwestern Atlantic Ocean, this study aims to explore the MHW characteristics and trends in the area. Our findings indicate a frequency of 1.5 to 3 events per year and greater duration and intensity within a region bounded by 37.5°S and 45°S latitude and 50°W and 55°W longitude. Another outcome of the present

study is the greater increase in MHW days per year during the last two decades, even when considering only the most intense events. Additionally, this study reveals a statistical correlation between MHWs and extratropical cyclones, since MHWs are generally linked to atmospheric conditions, particularly with atmospheric blockings. Moreover, the increase in sea surface temperature (SST) could favor the intensification of extratropical cyclones locally. Our results challenge the hypothesis that cyclones are suppressed during MHWs and that the incursion of extratropical cyclones usually promotes the end of MHW events. Furthermore, analysis of the SST during the intensification of the most intense extratropical cyclone events reveals that positive SST anomalies were unlikely in those events, ruling out the probable influence of positive SST anomalies on the intensification of these events.

Keywords

Extratropical cyclone, marine heatwave, correlation, trend.

7.1. Introduction

Marine heatwaves (MHW) are extended periods of anomalously warm ocean temperatures over considerable areas that impact the marine ecosystems [Hobday et al. 2016; Hoolbrok et al. 2019; Oliver et al. 2021]. The term was first introduced by Pearce et al. [2011], to describe an event on the southwestern coast of Western Australia, during February and March of 2011. Throughout this period, the sea surface temperature (SST) reached 3°C above the monthly mean over a large area and biological effects, such as fish and invertebrate deaths, extensions and contractions in species distributions and variations in recruitment and growth-rates, were reported. From that point forward, the scientific community's interest in the subject has increased, mainly due to the rising SST trends and the fact that these events have become longer and more intense over the years [Frölicher et al. 2018, Oliver et al. 2019; Smale et al. 2019]. The events can last from several days to several months and can cover areas ranging from tens to hundreds of kilometers.

Discrete events in local areas and their ecological and socioeconomic impacts have been identified and documented. According to Pershing et al.

[2013] and Mills et al. [2013], an MHW event occurred in the northwestern Atlantic, with a peak occurring during the boreal summer of 2012, which caused changes in the lobster fishery, the movement of squid and the distribution of species, such as cods. Several studies have addressed the 2013-2015 event in the northeastern Pacific Ocean, discussing the link between atmospheric events over North America [Seager et al. 2015; Di Lorenzo e Mantua 2016] and changes in the composition of the zooplankton community resulting in major disturbances in the marine ecosystem [Gentemann et al. 2016]. In the Mediterranean Sea, the rapid warming trend observed in recent decades has been associated with a strong increase in MHWs, both at the surface and in the subsurface, increasingly impacting the local marine ecosystem [Sparnocchia 2006; Garrabou et al. 2009; Marba and Duarte 2010; Garrabou et al. 2019; IPCC 2022; Simon et al. 2023; Dayan et al. 2023].

Studies revealed that MHWs are often caused by compounding influences of atmospheric forcing and/or oceanic processes [Oliver et al. 2021; Carrasco et al. 2023]. In regions such as the Tasman Sea and the Mediterranean Sea, atmospheric heatwaves have been linked to alterations in air–sea heat fluxes, which, in turn, increase the surface oceanic temperature, leading to MHW events [Oliver et al. 2017; Garrabou et al. 2022]. Over the North Pacific region, the atmospheric driver that significantly influences the MHW occurrence is the weakening of the North Pacific high-pressure system [Amaya et al. 2020]. In addition, anomalous ocean heat transport has been considered an important local process for the development of MHW events, such as those occurring over the Angola Benguela upwelling system [Rouault 2007] and western Australia [Benthuysen et al. 2014]. Holbrook et al. [2019] provided a global assessment of MHW and identified key local process and large-scale climate modes, such as the El Niño-Southern Oscillation (ENSO), that influence the occurrence of MHW events. The study also examined teleconnections, which are climate anomalies related to each other at large distances, and their regional associations with MHWs. These authors highlighted that few studies have explained the mechanisms of southwestern Atlantic Ocean MHW and they suggested that more studies can clarify the importance of increased poleward transport, which potentially results in MHW events.

Manta et al. [2018] studied MHWs in the Southwestern Atlantic shelf, near the Rio de la Plata River water plume between 1988 and 2017 and verified an increase in MHW days before 2014. This research focused on the austral summer extreme event of 2017, when the blocking atmospheric configuration was responsible for low wind speed and persistent extremely high air temperature, leading to heat gain in surface waters. Rodrigues et al. [2019] analyzed the local processes involved in the extreme MHW that occurred in the austral summer of 2013/2014 near the southern region of Brazil, where severe drought occurred. They reported that the Madden-Julian oscillation ultimately led to atmospheric blocking conditions over the western South Atlantic, affecting the local heat fluxes, winds, and cloud coverage, and increasing the degree of anomalous heating of surface waters. To understand the perspective for the next few decades, Costa and Rodrigues [2021] used observations and CMIP6 simulations for two different scenarios and reported that the frequency and characteristics are likely to change in the near and far future, confirming the link between MHWs and atmospheric blocking near the southeastern region of Brazil.

In addition to correlations with high air temperatures and blocking atmospheric conditions during MHWs, some studies have identified a link between these events and tropical cyclones. Pun et al. [2023] explored the dominant role of the MHW in the rare event of Typhoon Bavi in the East China Sea, in which the total heat flux was enhanced, which intensified the typhoon event. Choi et al. [2024] analyzed a group of tropical cyclones that intensified during MHWs. Their study revealed a notable increase in the intensity of these cyclonic events coinciding with MHW occurrences. Additionally, they reported increased precipitation intensity associated with these cyclones compared to those occurring outside of MHW periods. Therefore, the amplified total heat flux during MHWs is a key factor to strengthening the intensity of tropical cyclones.

On the other hand, the linkages between MHWs and individual extratropical cyclones are less studied, although determining and understanding the nature of these linkages is challenging [Schulz et al. 2019]. Concerning the influence of sea surface temperature distributions on the development of extratropical cyclones, Bui and Spengler [2021] concluded that the surface latent heat flux associated with a high absolute sea surface temperature plays a key

role in enhancing moist baroclinic development, which is conducive to explosive cyclone development, causing intense and rapidly developing events. Over the Northeast Pacific, Phillips and O'Neill [2020] explained the emergence of a positive sea surface temperature anomaly during a period of diminished storm activity spanning from 2013 to 2016. However, they observed that events that did not follow this pattern emerged with a significant surface heat flux, swiftly and temporarily contributing to the decrease in sea surface temperature. Sutil et al. [2019] presented an air-sea interaction analysis of an extratropical cyclone event in 2006 near the southern coast of Brazil and verified that the ocean-atmosphere numerical modeling system had a greater ability to simulate the intensity and trajectory of the cyclone, than the simulation of the sole atmospheric model. However, no studies investigated the linkage between extratropical cyclones and the occurrence of MHWs in the southwestern Atlantic Ocean.

Thus, studies underscore the importance of enhancing the understanding of MHWs and their relationships with local atmospheric conditions. Moreover, the contribution of anomalously warm ocean environments during the formation of intense extratropical cyclones in the coastal southwestern Atlantic Ocean remains unclear. Therefore, this study aims to investigate the spatial variability of MHW characteristics in the southwestern Atlantic Ocean, analyze the interannual variability and trends of MHWs and perform a statistical correlation of MHW events and extratropical cyclones. The results are divided into three aspects: the MHW characteristics and trends in the area; interannual variability of MHW; the correlation between MHWs and extratropical cyclones; and the analysis of the surface sea temperature (SST) during the formation of the most intense extratropical cyclones that reach the coastal area. Following these results, the main conclusions drawn from this study are presented.

7.2. Data and Methods

7.2.1. Data

To the MHW analysis, we used the National Oceanic and Atmospheric Optimum Interpolation Sea Surface Temperature dataset (NOAA OI SST V2) [Reynolds et al. 2007; Huang et al. 2021]. With a horizontal global regular grid resolution of 1/4°, the data are retrieved from the multisatellite sensor Advanced Very High-

Resolution Radiometer imager (AVHRR) and Visible Infrared Imaging Radiometer Suite (NIIRS). The sea surface temperature daily dataset was searched from 1° January 1982 to 31 December 2023.

The European Centre for Medium Range Weather Forecast ERA5 reanalysis dataset (ERA5/ECMWF) [Hersbach et al. 2020] was used to understand the meteorological conditions. The horizontal resolution is 31 km, and there are 137 vertical levels from the surface up to 80 km, in average. In the previous generations, the ERA5 reanalysis improved the spatial and temporal resolutions and enhanced the assimilation of the reprocessed dataset. The hourly data of the 850 hPa relative vorticity were retrieved from 1 January 1982 to 31 December 2023.

Additionally, the current bathymetric dataset of the General Bathymetric Chart of the Oceans (GEBCO-2023) was used. This international effort provides a global terrain model, with heterogeneous bathymetric data sources and oceanic depths mainly measured by acoustic measuring systems, such as multibeam echosounders [Hell and Jakobsson 2011].

7.2.2. Study Area

The Southwestern Atlantic Ocean is marked by a narrower continental shelf in its northern part, at approximately 70 km, and wider, up to 860 km in width, in its southern part (Figure 7.1). The coastline's geometry is characterized by the irregular indentations of several gulfs in the south and the expansive estuary of the La Plata in the center (approximately 35°S). The study area comprises latitudes of 25°S to 45°S and longitudes of 40°W to 65°W, with a maximum depth of approximately 6600 in the southern part, between 50°W and 55°W.

Near the western coast, there are currents of opposite directions: the northern part is dominated by a southward flow of warm salty waters (Brazil current) and the southern part is dominated by a northward flow of cold and nutrient-rich waters (Malvinas Current) [Matano et al. 2010; Piola et al. 2018]. The confluence of the Brazil and Malvinas currents, commonly referred to in the literature as the Brazil/Malvinas Confluence, takes place near the mouth of the

La Plata River. This region is distinguished by pronounced mesoscale variability. Moreover, the intense property contrast found there, makes this region one of the highest frontal systems of the world ocean and its modifications have key implications for the global climate system [Telesca et al. 2017].

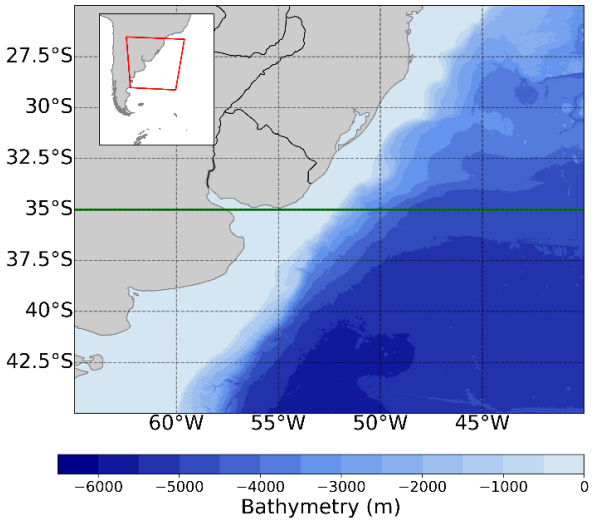


Figure 7.1. Bathymetry map of the Southwestern Atlantic Ocean (GEBCO bathymetry dataset - www.gebco.net). The green line divides two bands of the area.

7.2.3. Methods

We use the method developed and described by Hobday et al. [2016] to identify MHWs in the study area. This method is widely utilized and involves the use of local daily data series. The upper-percentile climatology of each day of the year serves as the threshold above which the MHWs were detected, drawing a parallel with definitions of atmospheric heatwaves. As discussed by Pisano et al. [2020] and Marullo et al. [2023], the determination and characterization of MHW events are sensitive to the presence of underlying trends, leading to differences according to the baseline period. Considering the positive trend in SST, climatology based on earlier years has resulted in longer and more intense MHWs in the last decade, compared to climatology based on more recent years. This study used the entire period to generate the baseline period (1982 to 2023), resulting in slightly smoother results than those of older studies. We used the 90th-percentile threshold, and a minimum duration of 5 days. Similar to Hobday et al. [2016], two periods of extreme temperature with a gap of two days or fewer days were considered one event. The events were identified at each point of the

study area, in the same grid size as the NOAA OI SST V2 data. Three intensity parameters were developed by Hobday et al. [2016] and were used in our area and period: the mean intensity, which is the mean anomaly of the SST during the entire period of the MHW event; the maximum intensity, which is the peak SST anomaly that occurred on the maximum intensity day of the event and the cumulative intensity, that is the sum of all the SST anomalies of the entire period of the event.

Following Hobday et al. [2018], we categorized the events of MHW, according to the Table 7.1. The characterization was based on the maximum intensity, which was calculated from the SST anomaly, using long-term climatology for a location (Equation 1). $SST_{d,lat,lon}$ is the temperature of a day *d* at a point located by a latitude and longitude and the $SST_{cld,lat,lon}$ is the long-term climatology for a day of the year at a point located by a latitude and longitude. The temperature difference between the historical mean and the historical 90th percentile is the basis for the definition of the categories. It means that the maximum intensity reached in one day of the event is the metric to categorize the event.

Table 7.1. The threshold created by Hobday et al. (2018) to categorize a local event based on long-term climatology. DBH90 is the temperature difference between the historical mean and the historical 90th percentile.

Category	Threshold
Moderate (category I)	I_{max}> DBH90
Strong (category II)	I_{max}> Twice DBH90
Severe (category III)	I_{max}> Three times DBH90
Extreme (category IV)	I_{max}> Four times DBH90

$$I_{max} = \max\left(SST_{d,lat,lon} - SST_{cld,lat,lon}\right) \text{(Equation 1)}$$

To better understand the variability in the days of MHW per year, we performed a time series of the mean number of days per year with MHW events. The Strong, Severe and Extreme events were counted for each position and year, and the number of days of these events was calculated for each year. To observe the different characteristic of the increase in the number of days per year according to decade, a linear regression was performed for two 21-year periods, with the statistical significance determined by the Mann-Kendall test [Kendall 1975].

To identify and track the extratropical cyclones over the study area, we used a recent lagrangian approach technique, described by Padilha Reinke et al. [2024]. The identification method used the connected component labeling technique to group surface areas meeting the relative vorticity threshold, treating them as a unique labeled field, similar to Inatsu [2009]. Each label is identified by a geographic point (longitude, latitude), via a simple center of mass [Bay and Breen 2008]. The program searches for enclosed areas at the next time frame with a maximum displacement of 150 km, similar to Crawford et al. [2021]. The minimum lifetime of events, such as Padilha Reinke et al. [2024], was 12 hours. The list of cyclones of the area used ERA5/ECMWF reanalysis hourly data between 1 January 1982 and 31 December 2023, totaling 42 years.

The relationships between the occurrence of MHW and extratropical cyclones in the area during the last 42 years was performed via maps of Pearson correlation coefficient (r), which is the most common method for measuring linear correlations [Patten and Newhart 2017]. The significance of the correlation was tested by a two-sided t-test. [Wilks 2006].

7.3. Results

7.3.1. MHW characteristics in the Southwest Atlantic Ocean between 1982 and 2023

In recent years, improvements of satellite sensors have increased of spatiotemporal resolution of SST information. Figure 7.2 shows the spatial distribution of the mean southwestern Atlantic Ocean SST (°C) and trends from 1982 to 2023 throughout the year, during the winter and summer. A very marked annual cycle can be observed, with the lowest values occurring in the winter, between 5.5°C and 22.8°C, and the highest values between 10.8°C and 26.0°C in the summer. The trend is stronger in the winter, between 50°W-55°W, and 40°S-45°S, with a maximum value of 0.9°C per decade. The positive trend observed in the annual, winter and summer SSTs and the marked cycle agrees with the studies of Rivas [2010] and Risaro et al. [2022]. According to these previous studies, the trend is strongly correlated with a decrease in the local zonal wind from a decrease in the strength of westerly winds, which is also suggested by numerical simulations. The area of the maximum trend matches the Brazil-

Malvinas Confluence and can be related to the displacement of this discontinuity region. Combes and Matano [2014] searched the drivers of positive trends related to a southward shift in the Brazil-Malvinas Confluence and reported that the weakening of the Antarctic Circumpolar Current led to a weakening of the Malvinas Current transport between the years of the study, which caused a southward drift of the confluence. The characteristics of climatological SST and trends are important features to consider in MHW analysis.

Figure 7.3 shows the spatial distribution of mean southwestern Atlantic Ocean MHW characteristics between 1982 and 2023. The MHW frequency (Figure 7.3A) ranged from 1.5 to 3 events per year, with the higher frequencies in the southern band of the area and mainly between 45°W and 55°W. In terms of coastal area, the Rio De La Plata estuary had relatively high values of frequency. With respect to the number of MHW days per year (Figure 7.3B), greater values were found between 37.5°S-45°S of latitude and 50°W-55°W of longitude, with more than 31 days of MHW per year in average. The mean duration of the events (Figure 7.3C), mean intensity (Figure 7.3D), maximum intensity (Figure 7.3E) and cumulative intensity (Figure 7.3F) peaked between 37.5°S-45°S of latitude and 50°W-55°W. Outside of this area, the mean duration rangeed from 6 to 16 days, while the greatest value within it was 24 days. The same uniformity of the area outside the above latitude/longitude limits was observed for the intensity parameters, with the mean intensity ranging between 1.1°C and 3.0°C, the maximum intensity ranging from 1.4°C to 3.6°C and the cumulative intensity ranging from 13.0°C to 45.8°C. On the other hand, within the box these parameters have values of 4.6°C, 5.6°C and 102.3°C for the mean, maximum and cumulative intensities, respectively. The displacement of the Brazil-Malvinas Confluence is the most likely factor in determining this peak in intensity and duration. The two currents have different characteristics, and the movement of their frontier can change the superficial sea temperature locally into a longer period. If this hypothesis is correct, oceanic process drives the MHW within this peak area. Further studies are necessary to confirm this hypothesis.

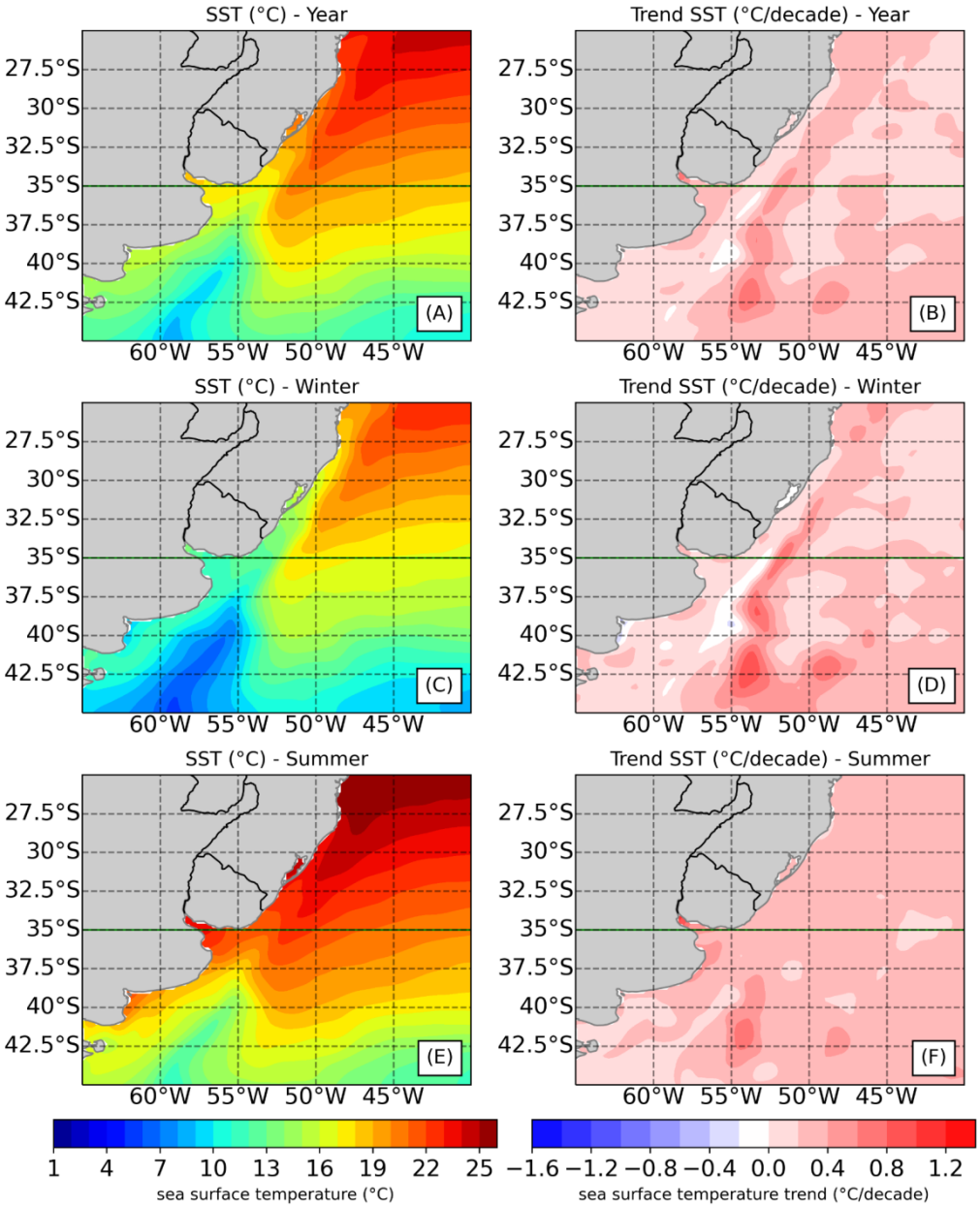


Figure 7.2. Spatial distribution of the mean southwestern Atlantic Ocean SST (°C) (A, C and E) and SST trends (°C/decade) (B, D and F) from 1982 to 2023 over the entire study period (A and B), winter (December, January and February) (C and D), and summer (June, July and August) (E and F).

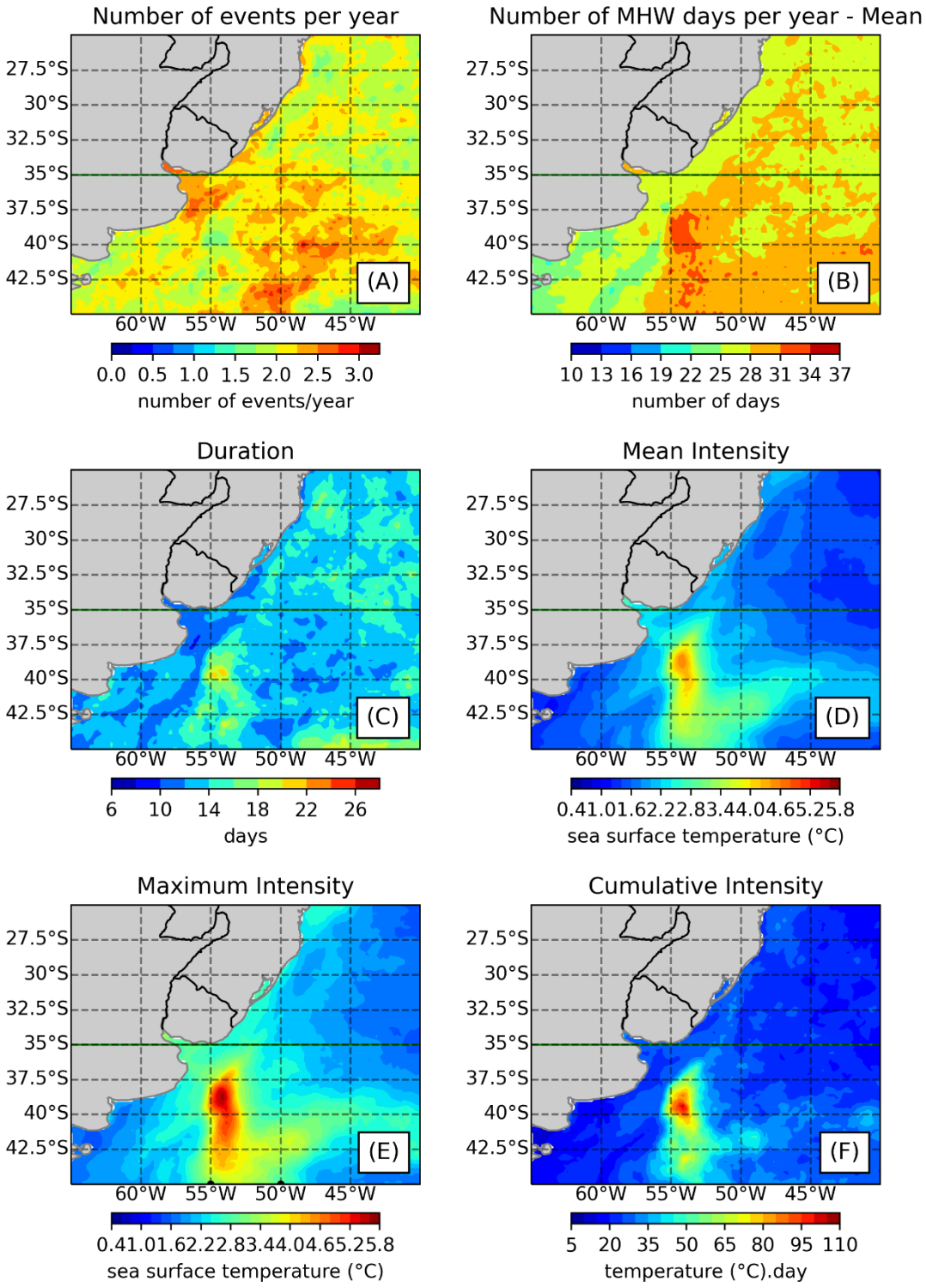


Figure 7.3. Spatial distribution of the mean southwestern Atlantic Ocean MHW characteristics from 1982 to 2023: (A) frequency (events/year), (B) number of day with MHWs (days/year), (C) mean intensity (°C), (D) maximum intensity (°C) and cumulative intensity (°C.day).

7.3.2. Interannual Variability and Trends of MHW days per year in the Southwestern Atlantic Ocean

The variability and trend of the number of MHWs days per year is important to better understanding the conditions associated with changes in SST and oceanographic process, which can impact marine ecosystems. Figure 7.4 shows the MHW days per year (blue line) mean for the entire area. Visually, two periods behave differently. While the first 21-year period had a mean of 14.7 days and a standard deviation of 6.5, the last 21-year period have mean of 37.1 days and 14.2 of standard deviation, considering the entire area. This different behavior motivated us to separate the linear regression into two periods. The slopes of each period are in the top of the figure. Verifying the monotonic trend via the Mann-Kendall test, the second period has a statistically significant upward trend across the entire area (95% confidence).

Considering the events classified as strong, severe and extreme, the total number of MHW days per year has increased during recent decades, with slopes of 4.77 days per decade. This analysis allowed the separation of days with more intense temperature anomalies and conditions that covered a large area since the increase in intense MHW days was calculated under an area. These results are important because intense events that cover a considerable area can cause greater impacts on marine ecosystems. The spatial trend of MHW days is presented in Figure 7.5, for both periods. In the first period (Figure 7.5A and 7.5C), there was a stable condition in terms of trends in almost the entire band. However, the last period presents a weak trend in areas near the South America coast and a strong trend in areas far from the continent. The longest MHW of the whole period occurred between 22 September 2022 and 19 August 2023. The highest maximum intensity event occurred from 29 April 2017 to 16 July 2017, with 11.14°C. The event with the highest mean intensity occurred between 20 June 2015 and 21 September 2015, with a 7.18°C temperature anomaly.

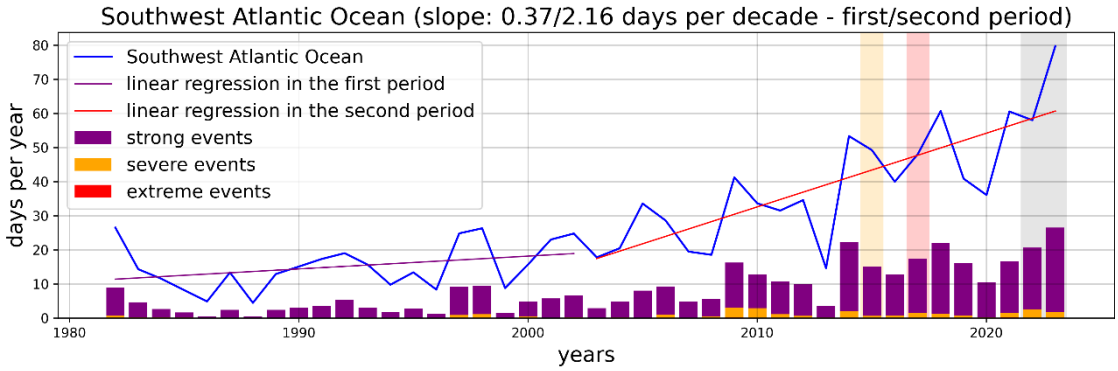


Figure 7.4. Temporal evolution and trend of days with MHW per year in the entire study area between 1982 and 2023. The year with the longest MHW is shown in grey, and the year with the highest maximum (mean) intensity is shown in red (yellow).

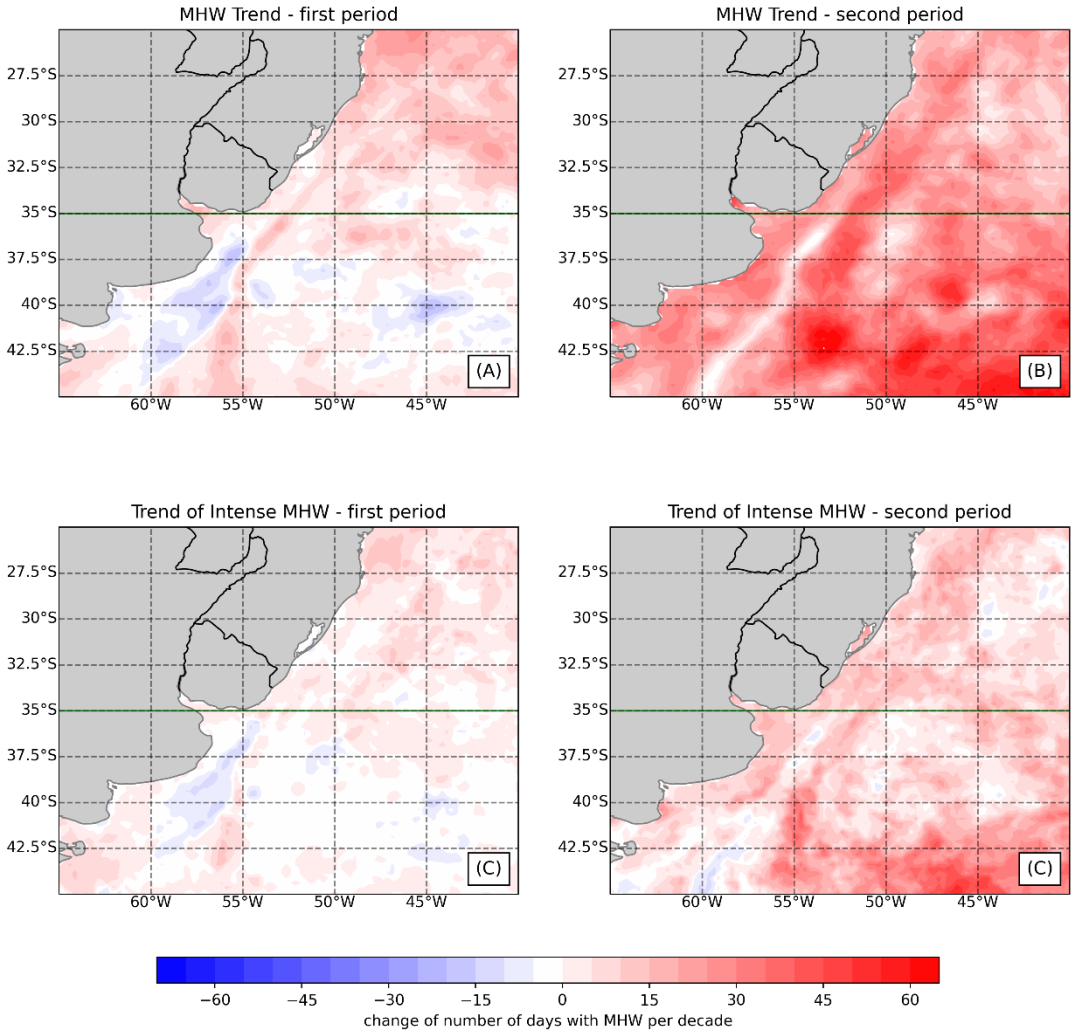


Figure 7.5. Map of trend of days with MHW first period (A) and second period (B). Maps of trend of days with strong, severe and extreme MHW in the first period (C) and in the second period (D).

7.3.3. Relationship between MHW and extratropical cyclones on the southwestern Atlantic Ocean

This analysis explained by the Pearson correlation coefficient between MHWs and extratropical cyclones, evaluated how often the co-occurrence occurred over the southwestern Atlantic Ocean. Figure 7.6 presents four aspects of the analysis. Figure 7.6A correlates days with MHW and days with extratropical cyclone covering every day of the 42 years of data. Cloud cover and precipitation over the ocean associated with storms could intuitively indicate a negative correlation between the two events. Another reason for the contrary correlation is that atmospheric blocking conditions often inhibit the meteorological conditions required for cyclone formation for a long period. However, the result for the entire study area indicates no significant correlation. Considering that the cooling caused by the extratropical cyclone could terminate an MHW, the Figure 7.6B, correlates the last day of the MHW to extratropical cyclones, and we found an inconclusive correlation. Figure 7.6C and 7.6D shows the same correlation coefficient, although MHW events were excluded, and the results demonstrated a lack of linear relationships between the variables. These analysis correlated events that occurred in the same part of the area. Compounding the last day of MHWs and extratropical cyclones events in some part of the southwestern Atlantic area, approximately 30% of the events of MHW ended with extratropical cyclones. The same analysis separating only events of the “Strong”, “Severe” and “Extreme” categories revealed that 30% of compounding events occurred.

Another aspect of the relationship between MHWs and extratropical cyclones is that the higher-than-expected sea surface temperature might enhance the total heat flux, mainly the latent heat flux, and contribute to intensifying extratropical cyclone events. Figure 7.7 shows the sea surface temperature anomaly mean during the first day of the most intense extratropical cyclones that occurred from 1982 to 2022 near the coastal part of Uruguay and south of Brazil (purple box of Figure 7.7), according to Padilha Reinke et al. (in revision). This map indicates that many of the region's most intense events did not occur under conditions of positive sea surface temperature anomalies.

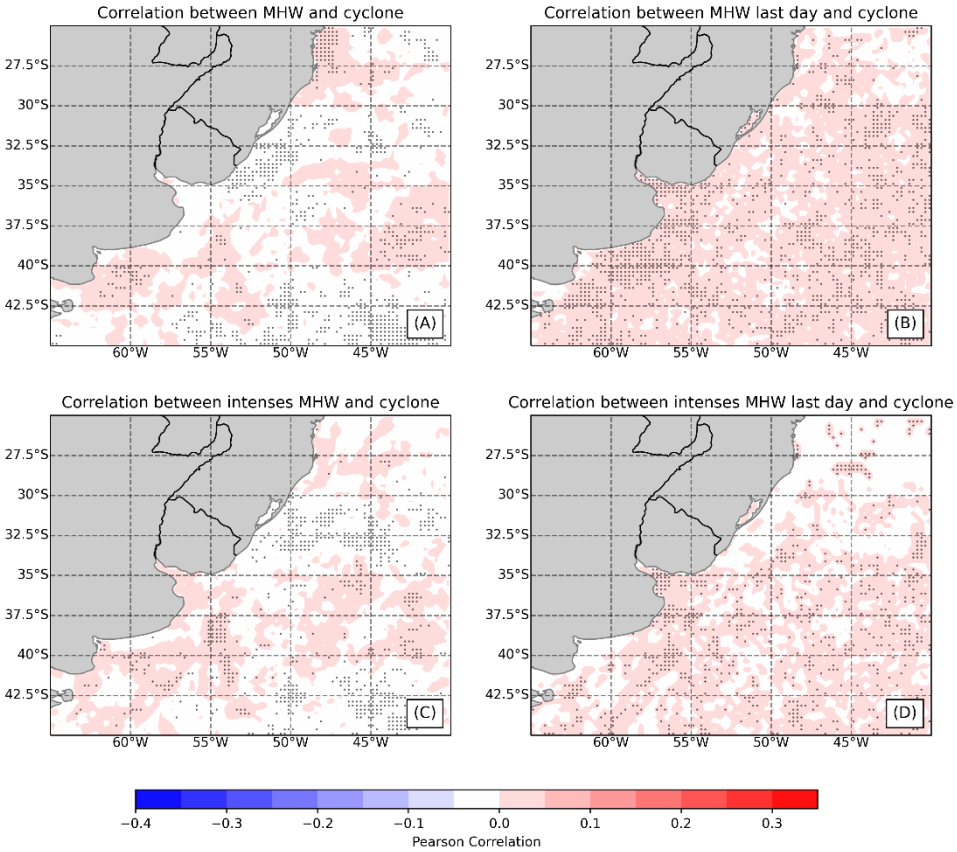


Figure 7.6. Correlation map of (A) days with cyclone and days with MHW in the study area and (B) last day of MHW and cyclone events, (C) days with intense MHW and cyclone and (D) last day of intense MHW and cyclone events.

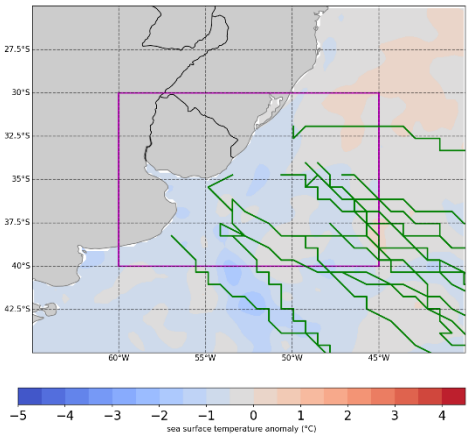


Figure 7.7. Sea surface temperature anomaly (°C) during the first day of the 14 most intense events near the coast of southern region of Brazil and Uruguay (purple box), selected by a study of Padilha Reinke et al. (in revision). The green lines are the tracks of these extratropical cyclones.

7.4. Conclusion

This study characterized and examined the spatiotemporal variability of MHWs in the southwestern Atlantic Ocean, via daily interpolated satellite data spanning from 1982 to 2023. Another analysis explored in this study is the relationship between MHWs and extratropical cyclones in the southwestern Atlantic Ocean.

The southwestern Atlantic Ocean had a positive trend in the SST anomaly during the period between 1982 and 2023. These results are consistent with those of other studies, which correlated the change with a local decline in the intensity of westerly winds and the displacement of the Brazil-Malvinas Confluence, under global warming condition [Combes and Matano 2014; Risaro et al. 2022].

When the characteristics of MHW across the area were analyzed, the number of MHW events per year ranged from 1.5 to 3 events per year, with the highest values occurring in the southern band of the area. The southwestern Atlantic shelf near the Rio de la Plata River is a coastal area that had more events per year, which is in agreement with a study by Manta et al. [2018]. The number of days with MHW, duration and intensity of the events had a different pattern within the area between 37.5°S and 45°S of latitude and between 50° W and 55° W of longitude, compared to the sea surface ocean outside this box. Within the box, the mean duration of MHWs was 24 days, outside the region the duration varies between 6 and 16 days. Moreover, the intensity was 124% greater in the box (considering mean and maximum intensities). This different pattern may be related to the displacement of the Confluence Brazil-Malvinas, similar to the SST anomaly pattern. When the Brazil Current moves anomalously southward, with salty and warm water, the SST presents a positive anomaly over a vast area. In addition to the greater intensity and duration of MHWs within the particular region, we cannot state that the ecological impacts are greater, as the ecosystem may be more adapted to this temperature variation in that region.

We found a positive trend in the number of days with MHW per year. The mean number of days with MHWs was computed to the entire area and for the northern and southern band related to 35°S latitude. From this analysis, we found that in the more recent 21 years, the number of days with MHWs has increased

more significantly than it did in the first 21 years of the study, in the three areas. Intense MHW events, categorized as strong, severe and extreme, also showed an increase in the number of days per year. Xu et al [2022] demonstrated that the long-term SST warming trend has accelerated in recent decades and suggested carefully distinguishing between the long-term warming trend and externally forced changes, as well as understanding their impacts on MHWs. From this perspective, our analysis may be affected by the general SST trend over the area; however, separating the increase in variability, with increasing MHW, from the positive SST trend is an approach for further studies.

When the most intense cyclones that hit the coast near Uruguay and southern Brazil were analyzed, the SST did not show a general pattern of positive anomalies during the intensification process. In some cases, warmer water could have been an additional factor for cyclone intensification, but this study demostrated that it is not a limiting condition for cyclone intensification.

The correlation between cyclone days and MHW days, as well as between cyclone days and the last day of MHW in the study area, were very weak and generally insignificant. Even when focusing exclusively on the most intense MHW events, the correlations for extratropical cyclones and both days with events and last-days occurrence remained weak.

The results presented in this study provide a solid basis for further research into the relationship between the Brazil-Malvinas Confluence and the preferred region for more intense and longer-lasting MHW events in the southwestern Atlantic Ocean. Regarding to the study of MHWs that occurred with extratropical cyclone, the analysis of air-sea heat fluxes and the evaluation of the performance of regional models during the events would be good subjects for further studies.

Capítulo VIII: Síntese da Discussão

Como primeiro resultado, foi apresentado um algoritmo para identificação e rastreamento de ciclones extratropicais, utilizando técnicas reconhecidas na literatura. Uma análise dos parâmetros do programa foi realizada com base nos dados horários de alta resolução de reanálise do ERA5/ECMWF. O campo de vorticidade relativa em 850 hPa foi utilizado, aplicando a técnica de componentes conectados, que identifica áreas com valores abaixo de um limite de vorticidade relativa. O encadeamento destas áreas em campos de horários subsequentes, obedecendo uma velocidade máxima de deslocamento e tempo de vida mínimo, gerou uma lista de eventos de ciclone extratropical, para os quais foram investigadas as suas características.

Foi utilizado o filtro gaussiano, para diminuir a condição ruidosa do campo de vorticidade relativa e eliminar efeitos relacionados ao relevo no continente. O grau de filtragem ideal foi determinado comparando os resultados obtidos a partir de três testes do desvio padrão da gaussiana. Além disso, foram mostrados testes de valores limites a partir dos quais a vorticidade relativa em 850 hPa foi selecionada no programa e um teste de sensibilidade para áreas mínimas abaixo do limite de vorticidade relativa em 850 hPa, para a identificação dos ciclones extratropicais. Com essas análises, os parâmetros adequados e utilizados no restante dos resultados foram os seguintes: desvio padrão da gaussiana de 0,5;

limite de vorticidade relativa em 850 hPa para a identificação dos ciclones extratropicais de -10^{-4} s^{-1}, e área mínima de 15 pixels.

Dois casos de ciclones extratropicais foram discutidos, comparando a identificação por inspeção visual e dados de estação automática com a identificação obtida pelo programa. O primeiro caso foi reconhecidamente intenso para a região costeira do sul do Brasil, com efeitos descritos em trabalhos anteriores. Já o segundo caso apresentou uma intensidade e tempo de vida dentro da média e deslocou-se sem chegar próximo ao continente. Ambos os casos apresentaram uma boa acurácia em detectar a ciclogênese e o período mais intenso dos eventos. No segundo caso, a subdivisão do ciclone extratropical em dois centros diferentes também foi identificada. No entanto, a posição dos ciclones extratropicais durante o processo de enfraquecimento não apresentou uma boa performance. Apesar disso, o programa se mostrou útil para a análise das características dos eventos.

Ao comparar a aplicação do algoritmo em dados com resoluções temporais de 1 hora e de 6 horas, observou-se que a resolução de 1 hora resultou em um número médio maior de eventos por ano. Esse resultado pode ser explicado pela inclusão de eventos de menor duração e pela maior precisão na identificação do deslocamento dos sistemas meteorológicos em dados horários. No entanto, ambas as resoluções temporais apresentaram uma tendência de número de eventos por ano similar. A duração dos eventos foi ligeiramente maior com a utilização de dados a cada 6 horas, o que concorda com Neu et al. (2013), que comparou diversas metodologias em dados do ERA-interim/ECMWF com a resolução temporal de 6 horas. Em termos de distância percorrida, a resolução temporal de 6 horas apresentou maiores valores. Já em relação à velocidade de deslocamento, os resultados com resolução temporal de 6 horas foram similares a estudos prévios que utilizaram essa resolução, enquanto a resolução temporal de 1 hora apresentou valores em média maiores.

Foi mostrada a distribuição espacial de frequência de ciclogênese para o Hemisfério Sul, para cada estação do ano. Os resultados foram similares a outros estudos, com relação as áreas mais favoráveis ao desenvolvimento ou à supressão de ciclones extratropicais no Hemisfério Sul.

Posteriormente, em uma abordagem voltada ao Sudoeste do Oceano Atlântico, este estudo investigou as características e variabilidade interanual de ciclones extratropicais. Comparando com a região de formação dos ciclones extratropicais no Sudoeste do Atlântico, as áreas de intensificação destes eventos se mostraram deslocadas em direção ao oceano, o que concorda com os estudos teóricos sobre zonas baroclínicas. Analisando a distribuição de frequência de velocidade de deslocamento de ciclones extratropicais, os eventos do Sudoeste do Oceano Atlântico se mostraram mais rápidos do que a média para todo o Hemisfério Sul. Os eventos mais intensos foram identificados pelo percentil 10% da menor pressão ao nível médio do mar dos eventos da área, em torno de 966 hPa, e pelo percentil 90% do maior vento em 10 metros dos eventos da área, de aproximadamente 84 km/h. Além disso, os ciclones extratropicais mais rápidos foram obtidos pelo percentil 90% da velocidade de deslocamento dos eventos da área, em torno de 78 km/h.

Como resultado, observou-se que eventos intensos com respeito a menor pressão ao nível médio do mar estão posicionados à sul, em relação aos eventos intensos com respeito aos maiores ventos em 10 metros. Por outro lado, os ciclones extratropicais mais rápidos em geral estão posicionados longe do continente. Dos eventos identificados entre 1982 e 2022, 56 atingiram os dois limites de intensidade e o limite de rapidez, simultaneamente. Considerando somente os eventos intensos, 166 ciclones extratropicais foram identificados, sendo alguns destes posicionados na área costeira, com maior potencial de impactar a população.

Séries temporais de contagem anual de ciclones extratropicais no Sudoeste do Oceano Atlântico e nas partes norte e sul, de acordo com 35°S de latitude revelaram uma leve tendência de aumento, no entanto, o teste Mann-Kendall mostrou que a tendência positiva não apresentou significância estatística. Um desempenho melhor foi obtido pela utilização de um modelo de regressão cúbica, o que significa que a contagem de ciclones extratropicais, tanto na área total como em seus segmentos sul e norte, tem um comportamento oscilatório. A correlação entre as séries temporais das partes norte e sul exibiram uma associação fraca, utilizando o coeficiente de correlação de Pearson.

Uma variabilidade interanual importante foi mostrada nas séries de contagem de eventos intensos e rápidos. O período que se destacou por apresentar maiores contagens de eventos intensos foi de 2005 a 2010. A correlação de Pearson mostrou-se moderada entre eventos intensos com respeito à menor pressão ao nível médio do mar e ao maior vento em 10 metros e forte entre eventos rápidos e intensos conforme os dois critérios.

Em uma perspectiva sazonal, a tendência de contagem de ciclones na faixa norte mostrou-se sem significância estatística em todas as estações, pelo teste de Mann-Kendall (nível de confiança de 95%). Na faixa sul, uma tendência de aumento de 1,7 ciclones por década foi encontrada durante o verão. A análise da variabilidade revelou significância oscilatória de 2-3 anos na parte norte durante o inverno, assim como em ambas as partes na primavera, verão e outono. Um pico de energia no período de 5 anos foi observado na parte norte durante o inverno e na parte sul durante o outono. Destacam-se os picos de energia entre 8 e 10 anos no inverno e primavera, que podem estar relacionados à oscilação decadal.

Focando nos eventos mais intensos encontrados para a área costeira entre o sul do Brasil e o Uruguai, compostos de variáveis meteorológicas em níveis altos, médios e baixos da troposfera foram construídos, para compreender melhor as características que os destacam. Em altos níveis, os compostos mostraram que a entrada equatorial do jato subtropical foi o padrão preferencial para o desenvolvimento destes eventos. Nos níveis médios e altos, um cavado profundo alinhado à Cordilheira dos Andes foi a configuração observada, contribuindo para o direcionamento de umidade da região tropical para a área costeira de estudo em níveis baixos da troposfera. Esse padrão é consistente com estudos anteriores como de Mendes et al. [2007] e Montini et al. [2019].

Finalmente, as características e tendências de ocorrência de MHW foram estudadas. A compreensão de que a TSM apresentou uma tendência positiva nas últimas décadas é base para esse trabalho, considerando os eventos no Sudoeste do Oceano Atlântico. Estudos prévios [Risaro et al. 2022 e Combes e Matano, 2014] sugerem que as mudanças na SST podem estar relacionadas a

uma diminuição dos ventos de oeste e ao deslocamento para sul da Confluência Brasil-Malvinas.

Em média, o número de eventos de MHW por ano varia entre 1,5 e 3, com uma condição de maior quantidade de eventos na faixa sul do Sudoeste do Oceano Atlântico e na área costeira próxima à pluma do Rio da La Plata, o que concorda com o estudo de Manta et al. [2018]. Na área limitada pelas latitudes de 37,5°S e 45°S e longitudes de 50°W e 55°W o número de dias por ano com MHW e a intensidade, medida pela intensidade média, máxima e cumulativa, apresentou valores maiores do que no restante da região Sudoeste do Oceano Atlântico. Dentro da área limitada pelas latitudes e longitudes acima, a duração média dos eventos foi de 24 dias, enquanto fora dela variou entre 6 e 16 dias. Em termos de intensidade, nas três formas de quantificação, os valores foram 124% maiores dentro da área limitada. Uma hipótese levantada para essa diferença em relação ao restante da região é o deslocamento da Confluência Brasil-Malvinas, já que o deslocamento anômalo para sul da Corrente do Brasil durante o período de alguns dias ou meses, com águas mais quentes e salgadas, pode ser o fator gerador de episódios de MHWs naquela região. Apesar da maior intensidade e duração dos eventos ocorridos na área, limitada pelas latitudes e longitudes acima expostas, não se pode afirmar que os impactos ecológicos das MHWs dentro da área são maiores, já que o ecossistema pode estar melhor adaptado às variações de temperatura.

Similar à tendência de anomalia de SST, foi encontrada uma tendência positiva de número de dias com MHW por ano, computando médias para toda a área de estudo. A tendência se mostrou mais intensa nos últimos 21 anos, com aumento de 2,16 dias por década. Os eventos categorizados como fortes, severos e extremos também apresentaram uma tendência de aumento de número de dias por ano. Xu et al. [2022] demostrou que a tendência de aquecimento da SST tem acelerado nos anos recentes e sugere cuidado ao distinguir entre a tendência de longo prazo e mudanças externamente forçadas, bem como a compreensão dos impactos das MHWs.

Capítulo IX: Conclusões

O presente documento de tese propôs avançar no conhecimento sobre ciclones extratropicais e a relação destes com MHWs. Esse tema é emergente porque tanto as variações de intensidade e quantidade de ciclones extratropicais como de MHWs tem implicações significativas para o ecossistema marinho, para o clima global e para a população que vive nas áreas próximas ao Oceano Atlântico Sudoeste.

Como resultado da tese, foi disponibilizado para a comunidade científica um programa de identificação e rastreamento de ciclones extratropicais. Este programa permite ajustes nos parâmetros de área mínima e vorticidade relativa, possibilitando sua aplicação em diferentes regiões e períodos. A análise focou em ciclones extratropicais utilizando dados do ERA5/ECMWF no Hemisfério Sul, por meio de mapas de frequência de ciclones extratropicais para o Hemisfério Sul, para cada estação do ano. Os dois estudos de caso apresentados indicaram que o programa possui um bom desempenho na detecção da ciclogênese e do período mais intenso dos ciclones. No entanto, em alguns casos o processo de ciclólise pode não ser identificado com a mesma precisão. Apesar disso, o programa apresenta resultados consistentes com estudos prévios. Além disso, utiliza uma linguagem de programação amplamente adotada atualmente e

oferece facilidade para realizar testes com diferentes parâmetros. Esse programa foi utilizado nos artigos da tese.

A tese também contribuiu para um entendimento mais profundo das características, variabilidade e tendência de ocorrência de ciclones extratropicais que se desenvolveram no sudoeste do Oceano Atlântico, nas últimas quatro décadas. Os resultados relacionados aos períodos de variabilidade com picos de energia são importantes, porém trazem questionamentos a respeito dos fatores e mecanismos que determinam esses picos de variabilidade. Além disso, o trabalho contribuiu para a melhor compreensão das condições e variabilidade dos eventos intensos de ciclone extratropical na área, evidenciando as condições sinóticas que prevaleceram no desenvolvimento dos eventos intensos, concordando com estudos como Gan and Rao [1994], Vera et al. [2002] e Mendes et al. [2007]. Estes resultados são relevantes para a preparação e tomada de decisão em futuros eventos intensos, particularmente para aqueles da área costeira, com potenciais impactos para a sociedade local.

Paralelamente, a identificação das MHWs ocorridas no Sudoeste do Oceano Atlântico nos últimos 42 anos trouxe insights sobre as características desses eventos e sobre o aumento de número de dias com MHW, especialmente nos últimos 21 anos. Além da área costeira no entorno da pluma do Rio de La Plata se destacar pela maior frequência de eventos de MHW por ano, uma região em alto mar, entre 37,5°S e 45°S de latitude e entre 50°W e 55°W de longitude apresentou condições médias maiores de intensidade e número de dias com MHW por ano, comparado ao restante da área. Esse resultado parece estar relacionado a expansão para sul da Convergência Brasil-Malvinas, porém necessita de estudos mais aprofundados.

Finalmente, como resultado deste trabalho observou-se que, de forma geral, a relação entre dias com ciclones extratropicais e MHWs na área de estudo não é relevante. Outra lacuna científica abordada na hipótese da tese é a suposição de que eventos de MHWs geralmente terminam com a chegada de ciclones extratropicais na região. No entanto, a análise estatística demostrou que essa relação é pouco significativa. Mesmo ao correlacionar apenas os eventos de MHW mais intensos, os resultados para dias com eventos e dias de término

também apresentaram uma relação fraca. Um campo médio de anomalia de TSM no primeiro dia dos 14 ciclones extratropicais mais intensos ocorridos próximos à costa do Uruguai e sul do Brasil, mostrou que a condição de anomalia positiva de TSM não é provável durante o desenvolvimento de eventos intensos de ciclones extratropicais. Portanto, a hipótese de que existe uma relação estatística significativa entre ciclones extratropicais intensos e eventos de MHW mostrou-se incorreta. No entanto, essa condição geral não exclui a possibilidade de que em casos isolados o fluxo na interface ar-mar desempenhe um papel fundamental para a intensificação de ciclones extratropicais. Estudos de caso como os apresentados por Dal Piva et al. [2008] e Sutil et al. [2019] exemplificam essa influência.

9.1. Perspectivas Futuras

Aprimoramentos do algoritmo apresentado neste trabalho podem ser realizados no futuro, como a inclusão de parâmetros em diferentes níveis de altitude, para a identificação e caracterização dos ciclones extratropicais. Uma abordagem de comparação entre eventos identificados em outras áreas do mundo pode também enriquecer a compreensão dos ciclones extratropicais identificados nas últimas décadas.

O conhecimento dos fatores que influenciam os picos de variabilidade na contagem de ciclones extratropicais por estação do ano, tanto para as faixas sul quanto norte do Sudoeste do Oceano Atlântico, é uma sugestão importante para estudos futuros. Além disso, investigar a ligação entre a variabilidade na contagem de ciclones extratropicais e parâmetros oceânicos chave, como conteúdo de calor no oceano superior (UOHC), modos de grande escala como a Oscilação Multidecadal do Atlântico (AMO), Modo Anular Sul (SAM) pode ser útil para compreender os fatores que contribuem para os padrões de oscilação, observados na contagem anual de ciclones extratropicais.

Embora este trabalho esteja limitado às últimas quatro décadas, as tendências de ciclones extratropicais encontradas sugerem a necessidade de uma compreensão mais aprofundada das mudanças na frequência de ciclones, sob a perspectiva das mudanças climáticas e seus impactos no Sudoeste do Oceano Atlântico.

Os resultados apresentados neste estudo fornecem uma base sólida para o aprofundamento da investigação sobre a relação entre a Confluência Brasil-Malvinas e a região preferencial para eventos de MHW mais intensos e de maior duração no Sudoeste do Oceano Atlântico. Outro aspecto que necessita de maior aprofundamento é a distinção entre o impacto da tendência de aumento em longo prazo da TSM e o aumento da variabilidade da TSM no crescimento do número de dias com MHW por ano. O aumento dos dias com MHW está associado ao crescimento da variabilidade da TSM e não necessariamente ao aumento de longo prazo da TSM.

O estudo de casos de MHWs que terminaram com a ocorrência de um ciclone extratropical em suas imediações, analisando os fluxos de calor na interface ar-mar e avaliando o desempenho de modelos regionais durante os eventos pode ser assunto para estudos subsequentes.

Referências Bibliográficas

Ahrens, CD (2001) Essentials of Meteorology: an invitation to the atmosphere, Australia; Pacific Grove, CA: Brooks/Cole/Thomson Learning, 3rd ed., p. 438.

Albuquerque MDG, Leal Alves DC, Espinoza JMDA, Oliveira UR, Simões RS (2018) Determining Shoreline Res-ponse to Meteo-oceanographic Events Using Remote Sensing and Unmanned Aerial Vehicle (UAV): Case Study in Southern Brazil. J Coast Res, 85, 766–770. Doi: 10.2112/SI85-154.1

Almeida LP, Ferreira Ó, Pacheco A. (2011) Thresholds for morphological changes on an exposed sandy beach as a function of wave height. Earth Surf Proces Landf, 36(4), 523-532. Doi: 10.1002/esp.2072

Amaya DJ, Miller AJ, Xie SP, Yu K (2020) Physical drivers of the summer 2019 North Pacific marine heatwave. Nat Commun, 11(1903), 1-9. Doi: 10.1038/s41467-020-15820-w

Andrade HN, Quadro MFL, Nunes AB, Oliveira FSC Ávila VD, Teixeira MS, Alves RCM (2024) Explosive cyclones occurred between 2010 and 2020 in the South Atlantic under the perspective of two detection schems. Geosc, 96, 1-19. Doi: 10.1590/0001-3765202420231051

Bai L, Breen D (2008) Calculating Center of Mass in an Unbounded 2D Environment. J. Graph. Tools, 13, 53–60. Doi: 10.1080/2151237X.2008.10129266

Barreiro M (2010) Influence of ENSO and the South Atlantic Ocean on climate predictability over Southeastern South America. Clim Dyn, 35(7), 1493-1508. Doi: 10.1007/s00382-009-0666-9

Benthuysen J, Feng M, Zhong L (2014) Spatial patterns of warming off Western Australia during the 2011 Ningaloo Niño: Quantifying impacts of remote and local forcing. Cont. Shelf Res, 91, 232-246. Doi: 10.1016/j.csr.2014.09.014

Bitencourt DP, Gan M, Acevedo OC, Fuentes MV, Muza MN, Rodrigues ML, Quadro MF (2011) Relating winds along the Southern Brazilian coast to extratropical cyclones. Meteorol Appl, 18, 223-229. Doi: 10.1002/met.232

Bjerknes J (1919) On the structure of moving cyclones. Geqfys Publ, Norske Videnskaps-Akademi, Oslo, 8. Doi: 10.1175/1520-0493(1919)47<95:OTSOMC>2.0.CO;2

Bjerknes e Holmboe (1944) On the theory of cyclones. J Atmo Sci, 1 (1), 1-22. Doi: 10.1175/1520-0469(1944)001<0001:OTTOC>2.0.CO;2

Bjerknes J, Solberg H (1922) Life cycle of cyclones and the polar front theory of atmospheric circulation.

Blender R, Shubert M (2000) Cyclone Tracking in Different Spatial and Temporal Resolutions. Mon. Weather Rev. 2000, 128, 377–384. Doi: 10.1175/1520-0493(2000)128<0377:CTIDSA>2.0.CO;2

Bluestein HB (1993) Synoptic-Dynamic Meteorology in Midlatitudes: Observations and Theory of Weather Systems, Oxford University Press, v. 1, p. 431.

Bui H and Spengler T (2021) On the influence of Sea Surface Temperature Distributions on the Development of extratropical cyclones J Atmos Sci 78:1173-1188. Doi: 10.1175/JAS-D-20-0137.1

Campos RM, Gramcianinov CB, de Camargo R, Silva Dias PL (2022) Assessment and calibration of ERA5 severe winds in the Atlantic Ocean using satellite data. Rem Sens, 14 (4918). Doi: 10.3390/rs14194918

Carlson T N (1991) Mid-latitude Weather Systems, Routledge, p. 507.

Carrasco D, Pizarro O, Jacques-Coper M, Narváez DA (2023) Main drivers of marine heatwaves in the eastern South Pacific. Front Mar Sci 10(1129276):1-16. Doi: 10.3389/fmars.2023.1129276

Castello JP e Krug LC org. (2017) Introdução às Ciências do Mar. Pelotas: Editora Textos, p. 602.

Catto JL, Ackerley D, Booth JF, Champion AJ, Colle BA, Pfahl S, Pinto JG, Quinting JF, Seiler S (2019) The Future of Midlatitude Cyclones. Curr Clim Change Rep, 5, 407–420. Doi: 10.1007/s40641-019-00149-4

Choi HY, Park MS, Kim HS, Lee S (2024) Marine heatwave events strengthen the intensity of tropical cyclones. Commun Earth Environ, 5(69):1-8. Doi: 10.1038/s43247-024-01239-4

Combes V, Matano RP (2014) Trends in the Brazil/Malvinas Confluence region, Geophys Res Lett, 41(24), 8971–8977. Doi: 10.1002/2014GL062523.

Costa NV and Rodrigues RR (2021) Future summer marine heatwaves in the western South Atlantic. Geophys Res Lett, 48(22), 1-10. Doi: 10.1029/2021GL094509

Crawford AD, Serreze MC (2016) Does the Summer Arctic Frontal Zone Influence Arctic Ocean Cyclone Activity? J Clim, 29(13), 4977–4993. Doi: 10.1175/JCLI-D-15-0755.1

Crawford AD, Alley KE, Cooke AM, Serreze MC (2020) Synoptic climatology of rain-on-snow events in Alaska. Mon Weather Rev, 148(3), 1275–1295. Doi: 10.1175/MWR-D-19-0311.1

Crawford AD, Schreiber EAP, Sommer N, Serreze MC, Stroeve JC; Barber DG (2021) Sensitivity of Northern Hemisphere Cyclone Detection and Tracking Results to Fine Spatial and Temporal Resolution Using ERA5. Mon Weather Rev, 149(8), 2581–2598. Doi: 10.1175/MWR-D-20-0417.1

Crespo NM, da Rocha RP, Sprenger M, Wernli H (2020) A potential vorticity perspective on cyclogenesis over centre-eastern South America. International Journal of Climatology, 41(1), 663–678. Doi: 10.1002/joc.6644

Cronin MF, Gentemann CL, Edson J, Ueki I, Bourassa M, Brown S, Clayson CA, Fairall CW, Farrar JT, Gille ST, Gulev S, Josey SA, Kato S, Katsumata M, Kent E, Krug M, Minnett PJ, Parfitt R, Pinker RT, Stackhouse PW, Swart S, Tomita H, Vandemark D, Weller RA, Yoneyama K, Yu L, Zhag D (2019) Air-sea fluxes with a focus on heat and momentum. Front Mar Sci, 6(430),1-30. Doi: 10.3389/fmars.2019.00430

Dacre HF (2020) A review of extratropical cyclones: observations and conceptual models over the past 100 years. Weather, 75(1), 4-7. Doi: 10.1002/wea.3653

Dal Piva E, Moscati M. C. L., Gan, M. A. (2008) Papel dos fluxos de calor latent e sensível em superfície associado a um caso de ciclogênese na costa leste da América do Sul. Revista Brasileira de Meteorologia, 23(4),450-476.

Dal Piva E, Gan MA, Moscati MCL (2011) The role of latent and sensible heat fluxes in an explosive cyclogenesis over the South American East Coast. J Meteorol Soc JPN, 89(6), 637-663. Doi: 10.2151/jmsj.2011-604

Dalanhese L, Stuivenvolt-Allen J, LaPlante M, Wang S, Costa T, Da Silva H, Belem AL (2023) A new climatology of South American extratropical cyclogenesis with an inter-comparison among ERA5, JRA55, and the Brazilian Navy. Int J Climatol, 43, 1-41. Doi: 10.1002/joc.8251

Dayan H, McAdam R, Juza M, Masina S, Speich S (2023) Marine heat waves in the Mediterranean Sea: An assessment from the surface to the subsurface to meet national needs. Front Mar Sci,10,1-21. Doi: 10.3389/fmars.2023.1045138

Di Lorenzo E, Mantua N (2016) Multi-year persistence of the 2014/15 North Pacific marine heatwave. Nature Clim Change, 6, 1042–1047. Doi: 10.1038/nclimate3082

Dos Santos JD, Machado JP, Saraiva JMB, (2023) The Response of Southwest Atlantic Storm Tracks to Climate Change in the Brazilian Earth System Model. Atmosphere, 14(7), 1-21. Doi: 10.3390/atmos14071055

Eakin CM, Morgan JA, Heron SF, Smith TB, Liu G, et al. (2010) Caribbean Corals in Crisis: Record Thermal Stress, Bleaching, and Mortality in 2005. PLoS ONE 5(11). doi:10.1371/journal.pone.0013969

Eichler TP, Gottschalck J (2018) A Comparison of Southern Hemisphere Cyclone Track Climatology and Interannual Variability in Coarse-Gridded Reanalysis Datasets. Adv Meteorol, 2013(19), 1-16. Doi: 10.1155/2013/891260

Emery WJ, Thomson RE (2001) Data Analysis Methods in Physical Oceanography, Elsevier Science, 2nd revised edition, New York, USA, 658p. ISBN 0-444-50757-4

Everitt B, Hothorn T (2011) An introduction to applied multivariate analysis with R. Springer, New York, USA, 273p. Doi: 10.1007/978-1-4419-9650-3

Eyring V, Bony S, Meehl GA, Senior CA, Stevens B, Stouffer RJ, Taylor KE (2016) Overview of the coupled model intercomparison project phase 6 (CMIP6) experimental design and organization. Geosci Model Dev, 9, 1937-1958. Doi: 10.5194/gmd-9-1937-2016

Flaounas E, Kotroni V, Lagouvardos K, Flaounas I (2014) CycloTRACK (v1.0)-tracking winter extratropical cyclones based on relative vorticity: Sensitivity to data filtering and other relevant parameters. Geosci Model Dev, 7, 1841–1853. Doi: 10.5194/gmd-7-1841-2014

Fordyce AJ, Ainsworth TD, Heron SF, Leggat W (2019) Marine Heatwave hotspots in coral reef environments: physical drivers, ecophysiological outcomes, and impact upon structural complexity. Front Mar Sci, 6 (498), 1-17. Doi: 10.3389/fmars.2019.00498.

Frölicher TL e Laufkötter C (2018) Emerging risks from marine heat waves. Nat Commun, 9(650),1-4. Doi: 10.1038/s41467-018-03163-6

Frölicher TL, Fischer EM, Gruber N (2018) Marine heatwaves under global warming. Nature, 560, 360–364. Doi: 10.1038/s41586-018-0383-9

Fyfe JC (2003) Extratropical Southern Hemisphere cyclones: Harbingers of climate change? J Clim, 16 (17), 2802-2805. Doi: 10.1175/1520-0442(2003)016_2802_eshcho_2.0.co_2

Gan MA e Rao VB (1991) Surface cyclogenesis over South America. Mon Weather Rev, 119 (5), 1293-1302. Doi: 10.1175/1520-0493(1991)119<1293:SCOSA>2.0.CO;2

Gan MA, Rao VB (1994) The influence of the Andes Cordillera on transient disturbances. Mon Weather Rev, 122, 1141–1157. Doi: 10.1175/1520-0493(1994)122<1141:TIOTAC>2.0.CO;2

Garrabou J, Coma R, Bensoussan M, Bally P, Chevaldonné P, Cigliano M, Diaz D, Harmelin JG, Gambi MC, Kersting DK, Ledoux JB, Lejeusne C, Linares C, Marschal C, Pérez T, Ribes M, Romano JC, Serrano E, Teixido N, Torrents O, Zabala M, Zuberer F, Cerrano C *(*2009) Mass mortality in Northwestern Mediterranean rocky benthic communities: effects of the 2003 heat wave. Glob Change Biol, 15(5), 1090-1103. Doi: 10.1111/j.1365-2486.2008.01823.x

Garrabou J, Gómez-Gras D, Ledoux J-B, Linares C, Bensoussan N, López-Sendino P, Bazairi H, Espinosa F, Ramdani M, Grimes S, Benabdi M, Souissi JB, Soufi E, Khamassi F, Ghanem R, Ocaña O, Ramos-Esplà A, Izquierdo A, Anton I, Rubio-Portillo E, Barbera C, Cebrian E, Marbà N, Hendriks IE, Duarte CM, Deudero S, Díaz D, Vázquez-Luis M, Alvarez E, Hereu B, Kersting DK, Gori A, Viladrich N, Sartoretto S, Pairaud I, Ruitton S, Pergent G, Pergent-Martini C, Rouanet E, Teixidó N, Gattuso J-P, Fraschetti S, Rivetti I, Azzurro E, Cerrano C, Ponti M, Turicchia E, Bavestrello G, Cattaneo-Vietti R, Bo M, Bertolino M, Montefalcone M, Chimienti G, Grech D, Rilov G, TuneyKizilkaya I, Kizilkaya Z, EdaTopçu N, Gerovasileiou V, Sini M, Bakran-Petricioli T, Kipson S, Harmelin JG (2019) Collaborative Database to Track Mass Mortality Events in the Mediterranean Sea. Front Mar Sci, 6(707), 1-5. Doi: 10.3389/fmars.2019.00707

Garrabou J, Gómez-Gras D, Medrano A, Cerrano C, Ponti, M, Schlegel R, Bensoussan N, Turicchia E, Sini M, Gerovasileiou V, Teixido N, Mirasole A, Tamburello L, Cebrian E, Rilov G, Ledoux J-B, Souissi JB, Khamassi F, Ghanem R, Benabdi M, Grimes S, Ocaña O, Bazairi H, Hereu B, Linares C, Kersting DK, Rovira G, Ortega J, Casals D, Pagès-Escolà M, Margarit N Capdevila P, Rubio-Portillo E, Anton I, López-Sendino P, Díaz D, Vázquez-Luis M, Duarte C, Marbà N, Aspillaga E, Espinosa F, Grech D, Guala I, Azzurro E, Farina S, Gambi MC, Chimienti G, Fraschetti S, Ceccherelli G Kipson S, Bakran-Petricioli T, Petricioli D, Jimenez C, Katsanevakis S, Kizilkaya IT, Kizilkaya Z, Sartoretto S, Elodie R, Ruitton S, Comeau S, Gattuso J-P, HarmelinJ-G (2022) Marine heatwaves drive

recurrent mass mortalities in the Mediterranean Sea. Glob Change Biol, 28(19), 5708-5725. Doi: 10.1111/gcb.16301

Garreaud RD e Wallace JM (1998) Summertime incursions of Midlatitude air into Subtropical and Tropical South America. Mon Weather Rev, 126(10), 2713-2733. Doi: 10.1175/1520-0493(1998)126<2713:SIOMAI>2.0.CO;2

Gentemann CL, Fewings MR, García-Reyes M (2017) Satellite sea surface temperatures along the West Coast of the United States during the 2014–2016 northeast Pacific marine heatwave. Geophys Res Lett 44, 312–319. Doi: 10.1002/2016GL071039.

Gilman DL, Fuglister FJ e Mitchell Jr JM (1963) On the Power Spectrum of Red Noise. J Atmos Sci, 20(2), 182–184. Doi: 10.1175/1520-0469(1963)020<0182:OTPSON>2.0.CO;2

Giorgi F, Coppola E, Solmon F, Mariotti L, Sylla MB, Bi X, Elguindi N, Diro GT, Nair V, Giuliani G, Turuncoglu UU, Cozzini S, Güttler I, O'Brien TA, Tawfik AB, Shalaby A, Zakey AS, Steiner AL, Stordal F, Sloan LC, Brankovic C (2012) RegCM4: model description and preliminary tests over multiple CORDEX domains. Clim Res, 52, 7-29. Doi: 10.3354/cr01018

Glitzenhirn E (2015) Relevância do acoplamento oceano-atmosfera na representação do ciclone Catarina. Dissertação (mestrado), Universidade de São Paulo, São Paulo.

Gonzales RC, Woods RE (1992) Digital Image Processing, 3rd ed.; Pearson International Edition; Pearson Education: London, UK

Gramcianinov CB (2018). Changes in South Atlantic cyclones due climate change. Tese (doutorado) Instituto de Astronomia, Geofísica e Ciências Atmosféricas, Universidade de São Paulo, São Paulo. Doi: 10.11606/T.14.2019.tde-03122018-151737.

Gramcianinov CB, Hodges KI e Camargo R (2019) The properties and genesis environments of South Atlantic cyclones. Clim Dyn**,** 53, 4115–4140. Doi: 10.1007/s00382-019-04778-1

Gramcianinov CB, Campos RM, Camargo R, Hodges KI, Soares CG, da Silva Dias PL (2020) Analysis of Atlantic extratropical storm tracks characteristics in 41 years of ERA5 and CFSR/CFSv2 databases. Ocean Eng, 216, 108111, 1-15. Doi: 10.1016/j.oceaneng.2020.108111

Gramcianinov CB, Campos RM, Guedes Soares C, de Camargo R (2020) Extreme waves generated by cyclonic winds in the western portion of the South Atlantic Ocean, Ocean Eng, 213 (107745), 1-14. Doi: 10.1016/j.oceaneng.2020.107745.

Gramcianinov CB, Camargo R de, Campos RM, Soares CG, Silva Dias PL (2023) Impacto f extratropical Cyclone intensity and speed on the extreme wave trends in the Atlantic Ocean. Clim. Dynam, 60, 1447-1466. Doi: 10.1007/s00382-022-06390-2.

Hanley J, Caballero R (2012) Objective identification and tracking of multicentre cyclones in the ERA-Interim reanalysis dataset. Q J R Meteorol Soc, 138, 612–625. Doi: 10.1002/qj.948

Harvey JG (1976) Atmosphere and Ocean: Our Fluid Environments, Artemis Press, 143p.

Haskim GJ (2015) Synoptic Meteorology – Cyclogenesis. Encyclopedia of Atmospheric Sciences, 2nd ed., Academic Press, 299-303p.

Hell B and Jakobsson M (2011) Gridding heterogeneous bathymetric data sets with stacked continuous curvature splines in tension. Mar Geophys Res, 32, 493-501. Doi: 10.1007/s11001-011-9141-1

Hersbach H, Bell B, Berrisford P, Hirahara S, Horányi A, Muñoz-Sabater J, Nicolas J, Peubey C, Radu R, Schepers D, et al. (2020) The ERA5 global reanalysis. Q J R Meteorol Soc 146, 1999–2049. Doi: 10.1002/qj.3803

Hewson TD e Neu U (2015) Cyclones, windstorms and the IMILAST project. Tellus A: Dynamic Meteorology and Oceanography, 67, 1-33. Doi: 10.3402/tellusa.v67.27128

Hewson TD, Titley HA (2009) Objective identification, typing and tracking of the complete life-cycles of cyclonic features at high spatial resolution. Meteorol Appl, 17, 355–381. Doi: 10.1002/met.204

Hobday AJ, Alexander LV, Perkins SE, Smale DA, Straub SC, Oliver ECJ, Benthuysen J, Burrows MT, Donat MG, Feng M, Holbrook NJ, Moore PJ, Scannell HA, Sen Gupta A, Wernberg T (2016) A hierarchical approach to defining marine heatwaves. Prog Oceanogr, 141, 227-238. Doi: 10.1016/j.pocean.2015.12.014

Hobday AJ, Oliver ECJ, Sen Gupta A, Benthuysen JA, Burrows MT, Donat MG, Holbrook NJ, Moore PJ, Thomsen MS, Wernberg T, Smale DA (2018) Categorizing and naming marine heatwaves. Oceanography 31(2), 162–173. Doi: 10.5670/oceanog.2018.205.

Hodges KI (1994) A general method for tracking analysis and its application to meteorological data. Mon Weather Rev, 12, 2573–2586. Doi: 10.1175/1520-0493(1994)122<2573:AGMFTA>2.0.CO;2

Hodges KI (1995) Feature tracking on the unit sphere. Mon Weather Rev, 123, 3458–3465. Doi: 10.1175/1520-0493(1995)123<3458:FTOTUS>2.0.CO;2

Hodges KI, Hoskins BJ, Boyle J (2003) A Comparison of Recent Reanalysis Datasets Using Objective Feature Tracking: Storm Tracks and Tropical Easterly Waves. Mon Weather Rev, 131, 2012–2037. Doi: 10.1175/1520-0493(2003)131<2012:ACORRD>2.0.CO;2

Hoolbrock NJ, Scanell HA, Sen Gupta A, Benthuysen JA, Feng M, Oliver ECJ, Alexander LV, Burrows MT, Donat MG, Hobday AJ, Moore PJ, Perkins-Kiskpatrick SE, Smale DA, Straub SC, Wernberg T (2019) A global assessment of marine heatwaves and their drivers. Nat Commun, 10(2624), 1-13. Doi: 10.1038/s41467-019-10206-z

Holton JR (2004) An Introduction to Dynamic Meteorology, 4th ed.; Elsevier, Amsterdam, The Netherlands, 535p.

Hoskins BJ, Hodges KI (2002) New Perspectives on the Northern Hemisphere winter storm tracks. J Atmos Sci, 59, 1041–1061. Doi: 10.1175/1520-0469(2002)059<1041:NPOTNH>2.0.CO;2

Hoskins BJ, Hodges KI (2005) A new perspective on Southern Hemisphere storm tracks. J Clim, 18, 4108–4129. Doi: 10.1175/JCLI3570.1

Huang B, Liu C, Banzon V, Freeman E, Graham G, Hankins B, Smith T, Zhang H-M (2021) Improvements of the Daily Optimum Interpolation Sea Surface Temperature (DOISST) version 2.1. J Clim, 34(8), 2923-2939. Doi: 10.1175/JCLI-D-20-0166.1

Inatsu M (2009) The neighbor enclosed area tracking algorithm for extratropical wintertime cyclones. Atmos Sci Lett, 10, 267–272. Doi: 10.1002/asl.238

Inatsu M, Amada S (2013) Dynamics and geometry of extratropical cyclones in the upper troposphere by a neighbor enclosed area tracking algorithm. J Clim, 26, 8641–8653. Doi: 10.1175/JCLI-D-12-00379.1

IPCC (2023) Climate Change 2023: Synthesis Report, Contribution of Working Groups I, II and III to the Sixth Assessment Report of the Intergovernmental Panel on Climate Change [Core Writing Team, H. Lee and J. Romero (eds.)], IPCC, Geneva, Switzerland, pp. 35-115. Doi: 10.59327/IPCC/AR6-9789291691647

Jones C, Mu Y, Carvalho LMV e Ding Q (2023) The South America Low-Level Jet: form, variability and large-scale forcing. Clim Atmos Sci, 6(175), 1-11. Doi: 10.1038/s41612-023-00501-4

Kendall MG (1975) Rank Correlation Methods. 4th Edition, Griffin, London, UK, 202 p.

Kunkel KE, Easterling DR, Kristovich DAR, Gleason B, L. Stoecker L e Smith R (2012) Meteorological Causes of the Secular Variations in Observed Extreme Precipitation Events for the Conterminous United States. J Hydrometeorol, 13(3), 1131–1141. Doi: 10.1175/JHM-D-11-0108.1

Lambert SJ (1988) A cyclone climatology of the Canadian climate centre general circulation. J Clim, 1, 109–115. Doi: 10.1175/1520-0442(1988)001<0109:ACCOTC>2.0.CO;2

Lambert SJ e Fyfe JC (2006) Changes in winter cyclone frequencies and strengths simulated in enhanced greenhouse warming experiments: results from the models participating in the IPCC diagnostic exercise. Clim Dyn, 26, 713–728. Doi: 10.1007/s00382-006-0110-3

Laurila TK, Gregow H, Cornér J e Sinclair VA (2021) Characteristics of extratropical cyclones and precursors to windstorms in northern Europe. Weather Clim Dyn, 2, 1111–1130. Doi: 10.5194/wcd-2-1111-2021

Li L e Dolman AJ (2023) On the reliability of composite analysis: an example of wet summers in North China. Atmos Res, 292(106881), 1-10. Doi: 10.1016/j.atmosres.2023.106881

Lim EP, Simmonds I (2007) Southern hemisphere winter extratropical cyclone characteristics and vertical organization observed with the ERA-40 data in 1979–2001. J Clim, 20, 2675–2690. Doi: 10.1175/JCLI4135.1

Lionello P, Dalan F, Elvini E (2002) Cyclones in the Mediterranean region: The present and the doubled CO_2 climate scenarios. Clim Res, 22, 147–159. http://www.jstor.org/stable/24868314

Lu C (2017) A modified algorithm for identifying and tracking extratropical cyclones. Adv Atmos Sci, 34, 909–924. Doi: 10.1007/s00376-017-6231-2

Ma I, Ginis I, Kang SK (2024) Numerical Study of Effects of Warm Ocean Eddies on Tropical Cyclones Intensity in Northwest Pacific. Atmosphere, 15(445), 1-22. Doi: 10.3390/atmos15040445

Manta G, de Mello S, Trinchin R, Badagian J, Barreiro M (2018) The 2017 record marine heatwave in the Southwestern Atlantic shelf. Geoph Res Let, 45(12), 449–456. Doi: 10.1029/2018GL081070

Marbà N, Duarte CM (2010) Mediterranean warming triggers seagrass (Posidonia oceanica) shoot mortality. Global Change Biology, 16, 2366-2375. Doi: 10.1111/j.1365-2486.2009.02130.x

Marengo JA, Douglas MW, Silva Dias PL (2002) The South American low-level jet east of the Andes during the 1999 LBA-TRMM and LBA-WET AMC campaign. J Geophys Res, 107(D20), 1-11. Doi: 10.1029/2001JD001188

Marullo S, Artale V, Santoleri R (2011) The SST multidecadal variability in the Atlantic-Mediterranean Region and its relation to AMO. J Clim 24, 4385-4401. Doi: 10.1175/2011JCLI3884.1

Matano RP, Palma ED, Piola AR (2010) The influence of the Brazil and Malvinas Currents on the Southwestern Atlantic Shelf circulation. Ocean Sci, 6, 983–995. Doi: 10.5194/os-6-983-2010

McErlich C, McDonald A, Renwick J, Schuddeboom A (2023) An assessment of Southern Hemisphere extratropical cyclones in ERA5 using WindSat. J Geophy Res, 128 (e2023JD038554). Doi: 10.1029/2023JD038554

Medeiros B, Williamson DL, Olson JG (2016) Reference aquaplanet climate in the Community Atmosphere Model Version 5. J Adv Model Earth Sy, 8, 406–424. Doi: 10.1002/2015MS000593

Mendes D, Souza EP, Trigo IF, Miranda PMA (2007) On precursors of South American cyclogenesis. Tellus A, 59, 114-121. Doi: 10.1111/j.1600-0870.2006.00215.x

Mendes D, Souza EP, Marengo JA, Mendes MCD (2009) Climatology of extratropical cyclones over the South American–southern oceans sector. Theor Appl Climatol, 100, 239–250. Doi: 10.1007/s00704-009-0161-6

Mills KE, Pershing AJ, Brown CJ, Chen Y, Chiang F-S, Holland DS, Lehuta S, Nye JA, Sun JC, Thomas AC, Wahle RA (2013) Fisheries management in a changing climate: Lessons from the 2012 ocean heatwave in the Northwest Atlantic. Oceanography 26(2), 191–195. Doi: 10.5670/oceanog.2013.27.

Montini TL, Jones C, Carvalho LMV (2019) The South American Low-Level Jet: A New Climatology, Variability, and Changes. J Geophys Res: Atmospheres, 124, 1200-1218. Doi: 10.1029/2018JD029634

Murray RJ, Simmonds I (1991) A numerical scheme for tracking cyclone centres from digital data. Part I: Development and operation of the scheme. Aust Meteorol Mag, 39, 155–166.

Neu U, Akperov MG, Bellenbaum N, Benestad R, Blender R, Caballero R, Cocozza A, Dacre HF, Feng Y, Fraedrich K et al. (2013) IMILAST: A community effort to inter-compare extratropical cyclone detection and tracking algorithms. Bull Am Meteorol Soc, 94, 529–547. Doi: 10.1175/BAMS-D-11-00154.1

Oliveira UR, Simões RS, Calliari LJ (2019) Dunes erosion under an extreme high wave energy event on the central and southern coast of Rio Grande do Sul state, Brazil. Rev Bras Geomorfol, 20, 137–158. Doi: 10.1016/j.ocecoaman.2022.106373

Oliver E, Benthuysen J, Bindoff N (2017) The unprecedented 2015/16 Tasman Sea marine heatwave. Nat Commun 8(16101), 1-12. Doi: 10.1038/ncomms16101

Oliver ECJ, Donat MG, Burrows MT, Moore PJ, Smale DA, Alexander LV, Benthuysen JÁ, Feng M, Gupta AS, Hobday AJ, Holbrook NJ, Perkins-Kirkpatrick SE, Scannell A, Straub SC, Wernberg T (2018) Longer and more frequent marine heatwaves over the past century. Nat Commun 9(1324), 1-12. Doi: 10.1038/s41467-018-03732-9

Oliver ECJ, Burrows MT, Donat MG, Gupta AS, Alexander LV, Perkins-Kirkpatrick SE, Benthuysen JA, Hobday AJ, Holbrook NJ, Moore PJ, Thomsen MS, Wernberg T, Smale DA (2019) Projected marine heatwaves in the 21st century and the potential for ecological impact. Front Mar Sci, 6(734), 1-12. Doi: 10.3389/fmars.2019.00734

Oliver ECJ, Banthuysen JA, Darmaraki S, Donat MG, Hobday AJ, Holbrook NJ, Schlegel RW, Sen Gupta A (2021) Marine heatwaves. Ann Re Mar Sci 13, 313-342. Doi: 10.1146/annurev-marine-032720-095144

Orselli IBM, Rodrigo K, de Azevedo JLL, Galdino F, Araujo M, Garcia CAE (2019) The sea-air CO_2 net fluxes in the South Atlantic Ocean and the role played by Agulhas eddies. Progr Oceanogr, 170, 40-52. Doi: 10.1016/j.pocean.2018.10.006

Padilha Reinke CK, Machado JP, Mata MM, de Azevedo JLL, Saraiva JMB, Rodrigues RR (2024) Objective Algorithm for Detection and Tracking of Extratropical Cyclones in the Southern Hemisphere. Atmosphere, 15(230), 1- 19. Doi: 10.3390/atmos15020230

Palmén E (1931) Die beziehung zwischen troposphärischen und stratosphärischen temperatur-und luftdruckschwankungen. Beitr Phys fr Atmos, 17, 102–116.

Parise CK, Calliari LJ, Krusche N (2009) Extreme Storm Surges in the South of Brazil: Atmospheric Conditions and Shore Erosion. Braz J Oceanogr, 57(3), 175-188. Doi: 10.1590/S1679-87592009000300002

Patten ML, Newhart M (2017) Understanding Research Methods: An Overview of the Essentials. 10th ed. Tenth edition. | New York, NY. Routledge, Routledge. doi: 10.4324/9781315213033

Pearce A, Lenanton R, Jackson G, Moore J, Feng M, Gaughan D (2011) The “marine heat wave” off Western Australia during the summer of 2010/11. Fish Res Rep No. 222. Department of Fisheries, Western Australia. 40p.

Peixoto JP, Oort AH (1992) Physics of Climate; American Institute of Physics: College Park, ML, USA, 520p

Pérez-Alarcón A, Coll-Hidalgo P, Trigo RM, Nieto R, Gimeno L (2024) CyTRACK: An open-source and user-friendly python toolbox for detecting and tracking cyclones. Environ Model Softw, 176 (106027). Doi: 10.1016/j.envsoft.2024.106027

Pershing AJ, Mills KE, Thomas AC, Wahle RA (2013) Impacts of the 2012 Ocean Heat Wave on fish and fisheries. 2013 ICES Annual Science Conference, Reykjavik, Iceland. CM 2013/B:35. Doi: 10.17895/ices.pub.24753087

Pezzi LP, Souza RB, Quadro MFL (2016) Uma revisão dos processos de interação oceano-atmosfera em regiões de intense gradiente termal do Oceano Atlântico Sul baseada em dados observacionais. Revista Brasileira de Meteorologia, 31 (4), 428-453. Doi: 10.1590/0102-778631231420150032

Pezzi LP, Quadro MFL, Lorenzzetti JA, Miller AJ, Rosa EB, Lima LN, Sutil UA (2022) The effect of Oceanic South Atlantic Convergence Zone episodes on regional SST anomalies: the roles of heat fluxes and upper-ocean dynamics. Clim Dyn, 59, 2041-2065. Doi: 10.1007/s00382-022-06195-3

Phillips B, O´Neill L (2020) Observational analysis of extratropical cyclone interactions with Northeast Pacific sea surface temperature anomalies. J Clim 33(15), 6745-6763. Doi: 10.1175/JCLI-D-19-0853.1

Pinto JG, Spangehl T, Ulbrich U, Speth P (2005) Sensitivities of a cyclone detection and tracking algorithm: Individual tracks and climatology. Meteorol Z, 14, 823‑838. Doi: 10.1127/0941-2948/2005/0068

Piola AR, Palma ED, Bianchi AA, Belmiro MC, Castro BM, Dottori M, Guerrero RA, Marrari M, Matano RP, Möller OO, Saraceno M (2018). Physical Oceanography of the SW Atlantic Shelf: A Review. In: Hoffmeyer M, Sabatini M, Brandini F, Calliari D, Santinelli N (eds) Plankton Ecology of the Southwestern Atlantic. Springer, Cham:37-56. Doi: 10.1007/978-3-319-77869-3_2

Pisano A, Marullo S, Artale V, Falcini F, Yang C, Leonelli FE, Santoleri R, Nardelli BB (2020) New evidence of Mediterranean climate change and variability from sea surface temperature observations. Remote Sens 12(132), 1-18. Doi: 10.3390/rs12010132

Prieto GA (2007) Improving earthquake source spectrum estimation using multitaper techniques. Ph.D. Dissertation, University of California, 1–141.

Pun IF, Hsu HH, Moon IJ, Lin I-I, Jeong J-Y (2023) Marine heatwave as a supercharger for the strongest typhoon in the East China Sea. Npj Clim Atmos Sci 6(128),1-12. Doi: 10.1038/s41612-023-00449-5

Raible CC, Della-Marta PM, Schwierz C, Wernli H, Blender R (2008) Northern Hemisphere extratropical cyclones: A comparison of detection and tracking

methods and different reanalyses. Mon Weather Rev, 136, 880–897. Doi: 10.1175/2007MWR2143.1

Reale M, Margarida LR, Liberato LR, Lionello P, Pinto JG, Salon S, Ulbrich SA (2019) Global Climatology of Explosive Cyclones using a Multi-Tracking Approach. Tellus Dyn Meteorol Oceanogr, 71(1611340), 1-19. Doi: 10.1080/16000870.2019.1611340

Reboita MS, da Rocha RP, Ambrizzi T, Sugahara S (2010) South Atlantic Ocean cyclogenesis climatology simulated by regional climate model (RegCM3). Clim Dyn, 35, 1331–1347. Doi: 10.1007/s00382-009-0668-7

Reboita MS, da Rocha RP, Ambrizzi T (2012) Dynamic and climatological features of cyclonic developments over southwestern South Atlantic Ocean. In: Horizons in Earth Science Research. Hauppauge: Nova Science Publishers.

Reboita MS (2017) Ciclones em superfície nas latitudes austrais: parte I – Revisão Bibliográfica. Revista Brasileira de Meteorologia, 32(2), 1-16. Doi: 10.1590/0102-77863220010

Reboita MS, da Rocha RP, Souza MR, Llopart M (2018) Extratropical cyclones over the southwestern South Atlantic Ocean: HadGEM2-ES and RegCM4 projections. Int J Climatol, 38, 2866–2879. Doi: 10.1002/joc.5468

Reboita MS, Giuliani G, Reale M, Coppola E (2020) Future changes in the wintertime cyclonic activity over the CORDEX-CORE southern hemisphere domains in a multi-model approach. Clim Dyn, 57, 1533-1549. Doi: 10.1007/s00382-020-05317-z

Reboita MS, Reale M, da Rocha RP, Giorgi F, Giuliani G, Coppola E, Nino RBL, Llopart M, Torres JA, Cavazos T (2021) Future changes in the wintertime cyclonic activity over the CORDEXCORE southern hemisphere domains in a multimodel approach. Clim Dyn, 57, 1533–1549. Doi: 10.1007/s00382-020-05317-z

Reynolds, Smith TM, Liu C, Chelton DB, Casey KS (2007) Daily High-Resolution-Blended Analyses for Sea Surface Temperature. J Clim 20, 5473-5496. Doi: 10.1175/2007JCLI1824.1

Risaro DB, Chidichimo MP, Piola AR (2022) Interannual Variability and Trends of Sea Surface Temperature Around Southern South America. Front Mar Sci 9(829144), 1-20. Doi: 10.3389/fmars.2022.829144

Rivas AL (2010) Spatial and temporal variability of satellite-derived sea surface temperature in the southwestern Atlantic Ocean. Cont Shelf Res 30(7), 752-760. Doi: 10.1016/j.csr.2010.01.009

Rodrigues RR, Taschetto AS, Sen Gupta A, Foltz GR (2019) Common cause for severe droughts in South America and marine heatwaves in the South Atlantic. Nat Geosci, 12, 620–626. Doi: 10.1038/s41561-019-0393-8

Rouault M, Illig S, Bartholomae C, Reason CJC, Bentamy A (2007) Propagation and origin of warm anomalies in the Angola Benguela upwelling system in 2001. J Mar Syst, 68 (3-4), 473-488. Doi: 10.1016/j.jmarsys.2006.11.010

Rudeva I, Gulev SK (2007) Climatology of cyclone size characteristics and their changes during the cyclone life cycle. Mon Weather Rev, 135, 2568–2587. Doi: 10.1175/MWR3420.1

Salinger MJ, Renwick J, Behrens E, Mullan AB, Diamond HJ, Sirguey P, Smith RO, Trought MCT, Alexander VL, Cullen NJ, Fitzharris BB, Hepburn CD, Parker AK, Sutton PJ (2019) The unprecedented coupled ocean-atmosphere summer heatwave in the New Zealand region 2017/18: drivers, mechanisms and impacts. Environ Res Lett 14(044023), 1-18. Doi: 10.1088/1748-9326/ab012a

Samet H (1989) Applications of Special Data Structures: Computer Graphics, Image Processing and GIS. Addison-Wesley: Boston, MA, USA, 507p.

Satake Y, Inatsu M, Mori M, Hasegawa A (2013) Tropical cyclone tracking using a neighbor enclosed area tracking algorithm. Mon Weather Rev, 141, 3539–3555. Doi: 10.1175/MWR-D-12-00092.1

Schultz DM, Keyser D, Bosart LF (1998) The effect of large-scale flow on low-level frontal structure and evolution in midlatitude cyclones. Mon Weather Rev, 126, 1767-1791. Doi: 10.1175/1520-0493(1998)126<1767:TEOLSF>2.0.CO;2

Schulz DM, Bosart LF, Colle BA, Davies HC, Dearden C, Keyser D, Martius O, Roebber P, Steenburgh WJ, Volkert H, Winters AC (2019) Extratropical Cyclones: A century of research on Meteorology´s Center piece. Meteorol Monogr 59(16), 1-56. Doi: 10.1175/AMSMONOGRAPHS-D-18-0015.1

Seager R, Hoerling M, Schubert S, Wang H, Lyon B, Kumar A, Nakamura J, Henderson N (2015) Causes of the 2011-14 California Drought. J Clim, 28(18), 6997-7024. Doi: 10.1175/JCLI-D-14-00860.1

Shimkus CE, Ting M, Booth JF, Adamo SB, Madajewicz M, Kushnir Y, Rieder HE (2017) Winter storm intensity hazards and property losses in the New York tristate area. Ann N Y Acad Sci, 1400 (1), 65-80. Doi: 10.1111/nyas.13396

Shapiro MA, Keyser D (1990) Fronts, jet streams and the tropopause. In: Newton C, Holopainen EO, eds, Extratropical Cyclones. American Meteorological Society & Springer, Boston, MA, 167–191. Doi: 10.1007/978-1-944970-33-8_10

Shaw TA, Baldwin M, Barnes EA, Caballero R, Garfinkel CI, Hwang Y-T, Li C, O'Gorman PA, Rivière G, Simpson IR, Voigt A (2016) Storm track processes and the opposing influences of climate change. Nat Geosci, 9, 656–664. Doi: 10.1038/ngeo2783

Simmonds I, Keay K (2000) Variability of Southern Hemisphere Extratropical Cyclone Behavior, 1958-97. J Clim, 13, 550–561. Doi: 10.1175/1520-0442(2000)013<0550:VOSHEC>2.0.CO;2

Simões RS, Calliari LJ, Figueiredo SA, Oliveira UR, Almeida LPM (2022) Coastline dynamics in the extreme south of Brazil and their socio-environmental impacts. Ocean Coast Manag, 230(106373), 1-9. Doi: 10.1016/j.ocecoaman.2022.106373

Simon A, Pires C, Frölicher TL, Russo A (2023) Long-term warming and interannual variability contributions' to marine heatwaves in the Mediterranean. Weather Clim Extrem 42(100619), 2212-0947. Doi: 10.1016/j.wace.2023.100619.

Sinclair MR (1994) An objective cyclone climatology for the Southern Hemisphere. Mon Weather Rev, 122, 2239–2256. Doi: 10.1175/1520-0493(1994)122<2239:AOCCFT>2.0.CO;2

Sinclair MR (1997) Objective Identification of Cyclones and their Circulation Intensity and Climatology. Wea. Forecast, 12(3), 595-612. Doi: 10.1175/1520-0434(1997)012<0595:OIOCAT>2.0.CO;2

Sinclair M, Watterson IG (1999) Objective assessment of extratropical weather systems in simulated climates. J Clim, 12(12), 3467-3485. Doi: 10.1175/1520-0442(1999)012<3467:OAOEWS>2.0.CO;2

Sinclair VA, Rantanen M, Haapanala P, Räisänen J, Järvinen H (2020) The characteristics and structure of extra-tropical cyclones in a warmer climate. Weather Clim Dynam, 1, 1-25. Doi: 10.5194/wcd-1-1-2020

Smale DA, Wernberg T, Oliver ECJ, Thomsen M, Harvey BP, Straub SC, Burrows MT, Alexander LV, Benthuysen JA, Donat MG, Feng M, Hobday AJ, Holbrook NJ, Perkpatrick SE, Scannell HA, Sen Gupta A, Payne BL, Moore PJ (2019) Marine heatwaves threaten global biodiversity and the provision of ecosystem services. Nat Clim Chang 9, 306–312. Doi: 10.1038/s41558-019-0412-1

Sparnocchia S, Schiano ME, Picco P, Bozzano R, Cappelletti A (2006) The anomalous warming of summer 2003 in the surface layer of the Central Ligurian Sea (Western Mediterranean). Ann Geophys 24, 443-452. Doi: 10.5194/angeo-24-443-2006

Sutil UA, Pezzi LP, Alves RCM, Nunes AB (2019) Ocean-Atmosphere Interactions in an Extratropical Cyclone in the Southwest Atlantic. J Geophys Res: Atmospheres, 42(1), 525-535. Doi: 10.11137/2019_1_525_535

Telesca L, Pierini JO, Lovallo M, Santamaría-del-Angel E (2017) Spatio-temporal variability in the Brazil-Malvinas Confluence Zone (BMCZ), based on spectroradiometric MODIS-AQUA chlorophyll-a observations. Oceanologia 60(1), 1-10. Doi: 10.1016/j.oceano.2017.08.002

Treut HL, Kalnay E (1990) Comparison of observed and simulated cyclone frequency distribution as determined by an objective method. Atmósfera, 3, 57–71.

Trigo IF (2006) Climatology and interannual variability of storm-tracks in the Euro-Atlantic sector: A comparison between ERA-40 and NCEP/NCAR reanalyses. Clim Dyn, 26, 127–143. Doi: 10.1007/s00382-005-0065-9

Ulbrich U, Leckebusch GC, Pinto JG (2009) Extra-tropical cyclones in the present and future climate: A review. Theor Appl Climatol, 96, 117–131. Doi: 10.1007/s00704-008-0083-8

Valsangkar A, Monteiro JM, Narayanan V, Hotz I, Natarajan V (2019) An Exploratory Framework for Cyclone Identification and Tracking. IEEE Trans Vis Comput Graph, 10, 1–14. Doi: 10.1109/TVCG.2018.2810068

Vera CS, Vigliarolo PK, Berbry EH (2002) Cold season synoptic-scale waves over subtropical South America. Mon Weather Rev, 130, 684–699. Doi: 10.1175/1520-0493(2002)130<0684:CSSSWO>2.0.CO;2

Vianna ML, Menezes VV, Pezza AB, Simmonds I (2010) Interactions between Hurricane Catarina (2004) and warm core rings in the South Atlantic Ocean. J Geophys Res, 115 (C07002), 1-19. Doi: 10.1029/2009JC005974

Wallace JM, Hobbs PV (2006) The General Circulation. In An Introductory Survey, 2nd ed.; Elsevier: Amsterdam, The Netherlands; Academic Press: Boston, MA, USA, 412–450.

Wang XL, Swail VR, Zwiers FW (2006) Climatology and Changes of Extratropical Cyclone Activity: Comparison of ERA-40 with NCEP-NCAR Reanalysis for 1958–2001. J Clim, 19, 3145–3166. Doi: 10.1175/JCLI3781.1

Wells NC (2011) The Atmosphere and Ocean: A Physical Introduction, John Wiley and Sons, 3rd edition. University of Southampton, UK, 432 p.

Wernberg T, Smale DA, Tuya F, Thomsen MS, Langlois TJ, de Bettignies T, Bennett S, Rousseaux CS (2013) An extreme climatic event alters marine

ecosystem structure in a global biodiversity hotspot. Nat Clim Change, 3(1), 78-82. Doi: 10.1038/nclimate1627

Wilks DS (2006) Statistical Methods in the atmospheric sciences, second edition. Academic Press, USA, 648 p.

Williamson DL (1981) Storm track representation and verification. Tellus, 33**,** 513-530. Doi: 10.1111/j.2153-3490.1981.tb01778.x

Xu Y, Li J, Fu H (2022) The role of sea surface temperature variability in changes to global surface air temperature related to two periods of warming slowdown since 1940. Clim Dynam, 59, 499-517. Doi: 10.1007/s00382-022-06139-x

Yang Y, Wu L, Cai W, Jia F, Ng B, Wang G, Geng T (2022) Suppressed Atlantic Niño/Niña variability under greenhouse warming. Nat Clim Change, 12, 814-821. Doi: 10.1038/s41558-022-01444-z

Yue S, Pilon P (2019) A comparison of the power of the t-test, Mann-Kendall and bootstrap tests for trend detection. Hydrolog Sci J, 49 (1), 21-37. Doi: 10.1623/hysj.49.1.21.53996

Zhang C (2005) Madden-Julian Oscillation. Rev Geophys, 43, RG2003, 1-36. Doi: 10.1029/2004RG000158

Zhang J, Xu H, Ma J, Deng J (2019) Interannual Variability of Spring Extratropical Cyclones over the Yellow, Bohai, and East China Seas and Possible Causes. Atmosphere, 10(40), 1-19. Doi: 10.3390/atmos10010040